

Flight Control Design using Mixed H_2/μ Optimization

THESIS

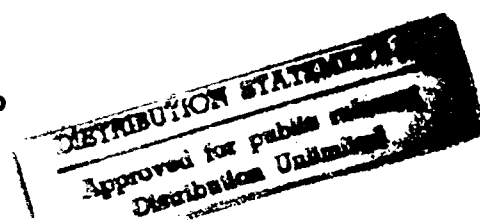
Douglas D. Decker
Captain, USAF

AFIT/GA/ENY/94D-8

19941228 076

DEPARTMENT OF THE AIR
AIR UNIVERSITY
AIR FORCE INSTITUTE OF TECHNOLOGY

Wright-Patterson Air Force Base, Ohio



AFIT/GA/ENY/94D-8

Flight Control Design using Mixed H_2/μ Optimization

THESIS

Douglas D. Decker
Captain, USAF

AFIT/GA/ENY/94D-8

THIS THESIS IS UNCLASSIFIED

Approved for public release; distribution unlimited

REPORT DOCUMENTATION PAGE			Form Approved OMB No. 0704-0188	
Public reporting burden for this collection of information is estimated to average 1 hour per response, including the time for reviewing instructions, searching existing data sources, gathering and maintaining the data needed, and completing and reviewing the collection of information. Send comments regarding this burden estimate or any other aspect of this collection of information, including suggestions for reducing this burden, to Washington Headquarters Services, Directorate for Information Operations and Reports, 1215 Jefferson Davis Highway, Suite 1204, Arlington, VA 22202-4302, and to the Office of Management and Budget, Paperwork Reduction Project (0704-0188), Washington, DC 20503.				
1. AGENCY USE ONLY (Leave blank)	2. REPORT DATE December 1994	3. REPORT TYPE AND DATES COVERED Master's Thesis		
4. TITLE AND SUBTITLE FLIGHT CONTROL DESIGN USING MIXED H_2/μ OPTIMIZATION			5. FUNDING NUMBERS	
6. AUTHOR(S) Douglas D. Decker, Captain, USAF				
7. PERFORMING ORGANIZATION NAME(S) AND ADDRESS(ES) Air Force Institute of Technology, WPAFB OH 45433-6583			8. PERFORMING ORGANIZATION REPORT NUMBER AFIT/GA/ENY/94D-8	
9. SPONSORING/MONITORING AGENCY NAME(S) AND ADDRESS(ES) Dr Marc Jacobs AFOSR/NM Bolling AFB DC 20332-0001			10. SPONSORING/MONITORING AGENCY REPORT NUMBER	
11. SUPPLEMENTARY NOTES				
12a. DISTRIBUTION/AVAILABILITY STATEMENT Approved For Public Release; Distribution Unlimited			12b. DISTRIBUTION CODE	
13. ABSTRACT (Maximum 200 words) This thesis examines the use of the mixed H_2/μ optimal control synthesis method in the design of a flight control system for the lateral/directional axes of the F-16 Variable Stability In-Flight Simulator Test Aircraft (VISTA). The method is designed to minimize the H_2 norm (two-norm) for a given value of μ . This should provide adequate noise and disturbance rejection while maintaining robustness against several types of uncertainties in the system. This thesis finds that, for this problem, the two-norm is not an accurate representation of the outputs of interest. When the two-norm is broken up into its constituent parts an appropriate solution can be found. This thesis also finds that it is possible to use an H_2 controller which is destabilizing to the evaluation model as the starting point in the mixed H_2/μ curve and still get an acceptable answer. A numerical approach was used, utilizing a recently improved computer algorithm.				
14. SUBJECT TERMS Control Theory, H_2 Optimization, H_∞ Optimization, μ -Synthesis, Multiobjective Optimal Control			15. NUMBER OF PAGES 158	
			16. PRICE CODE	
17. SECURITY CLASSIFICATION UNCLASSIFIED	18. SECURITY CLASSIFICATION OF THIS PAGE UNCLASSIFIED	19. SECURITY CLASSIFICATION OF ABSTRACT UNCLASSIFIED	20. LIMITATION OF ABSTRACT UL	

The views expressed in this thesis are those of the author and do not reflect the official policy or position of the Department of Defense or the U. S. Government.

Accession For	
NTIS GRA&I	<input checked="checked" type="checkbox"/>
DTIC TAB	<input type="checkbox"/>
Unannounced	<input type="checkbox"/>
Justification	
By	
Distribution	
Availability Codes	
Dist	Avail and/or Special
A-1	

AFIT/GA/ENY/94D-8

Flight Control Design using Mixed H_2/μ Optimization

THESIS

Presented to the Faculty of the School of Engineering
of the Air Force Institute of Technology

Air University

In Partial Fulfillment of the
Requirements for the Degree of
Master of Science

Douglas D. Decker, B.S.

Captain, USAF

December 1994

Approved for public release; distribution unlimited

Acknowledgements

I would first like to thank my advisor, Dr. Brett Ridgely, for all his help in getting this thesis done; from answering my questions to editorial comments and proofreading. Thanks also go to Dave Jacques and Linda Smith for programming new optimization schemes and letting me bounce ideas off of them.

A very big debt of gratitude goes to my wife, Celia. Thank you honey for your patience and understanding. It's been a long haul and you've been great. Thanks also to Daniel and Drew, you guys and your Mom were always there to bring me back to earth and show me what's truly important.

Most of all, I would like to give thanks to God for showing me the way to get around the roadblocks that held me at bay for so long. He makes all things possible.

Douglas D. Decker

Table of Contents

	Page
Acknowledgements	ii
List of Figures	vi
List of Tables	ix
Abstract	x
 I. Introduction	 1-1
1.1 Background/Motivation	1-1
1.2 Thesis Outline	1-2
 II. Preliminaries	 2-1
2.1 Mathematical Preliminaries	2-1
2.1.1 H_2 Optimal Control	2-1
2.1.2 H_∞ Optimal Control	2-6
2.1.3 Mixed H_2/H_∞ Control	2-12
2.1.4 μ Analysis and Synthesis	2-26
2.1.5 Mixed H_2/μ Control	2-36
2.2 Control Preliminaries	2-37
2.2.1 Dynamic Inversion	2-37
2.2.2 Control Selector	2-38
 III. F-16 Design Example	 3-1
3.1 Overview	3-1
3.2 Details	3-3
3.2.1 Lateral/Directional Equations of Motion	3-3
3.2.2 Control Selector	3-4

	Page
3.2.3 Inner Loop Design	3-5
3.2.4 Actuator	3-9
3.2.5 T1 and T2	3-9
3.2.6 The Ideal Model	3-10
3.2.7 Noises	3-11
3.3 Evaluation Model	3-12
3.4 Robust Analysis Model	3-16
3.4.1 Structured Uncertainty	3-16
3.4.2 Unstructured Uncertainty	3-19
3.4.3 Robust Performance	3-19
IV. μ Design	4-1
4.1 Outer Loop Design	4-1
4.2 μ design	4-1
4.2.1 The Ideal Model and the Performance Weighting	4-1
4.2.2 Actuator	4-2
4.2.3 Parameter Uncertainty Weighting	4-4
4.2.4 State space formulation	4-5
4.2.5 Results	4-8
V. H_2 and Mixed H_2/μ Design A	5-1
5.1 H_2 Design	5-1
5.1.1 State Space	5-2
5.1.2 Results	5-12
5.2 Mixed H_2/μ using H_2 Controller A	5-14
5.2.1 More Definitions	5-14
5.2.2 The Mix	5-15

	Page
VI. H_2 Revisited	6-1
6.1 Another Look at the Two-norm	6-1
6.2 Mixed H_2/μ Design B	6-4
6.3 Yet Another Look at the Two-norm	6-8
6.4 Mixed H_2/μ Design C	6-13
VII. Conclusions and Recommendations	7-1
7.1 Summary and Conclusions	7-1
7.2 Recommendations	7-2
Appendix A. Model Data	A-1
A.1 Design Model Data	A-1
A.1.1 Central Flight Condition	A-1
A.1.2 Design Actuator	A-1
A.1.3 Ideal Model	A-2
A.2 Evaluation Model Data	A-2
Appendix B. μ Optimal Controller	B-1
Appendix C. State Space Representation of H_2 Problem on the Evaluation Model .	C-1
Bibliography	BIB-1
Vita	VITA-1

List of Figures

Figure	Page
2.1. Basic Block Diagram for the H_2 problem	2-2
2.2. H_2 system with parameterized controller	2-4
2.3. Basic Block Diagram for the H_∞ problem	2-9
2.4. Example of an H_∞ problem	2-13
2.5. Basic Block Diagram for the mixed H_2/H_∞ problem	2-14
2.6. Possible regions for γ	2-25
2.7. Typical mixed H_2/H_∞ γ vs. α curve	2-26
2.8. System with uncertainty	2-27
2.9. P-K version of the system with uncertainty	2-28
2.10. M- Δ version of a matrix with uncertainty	2-29
2.11. M- Δ version of a matrix with two uncertainties	2-31
2.12. M- Δ version of the system for robust stability and robust performance	2-33
2.13. LFT system with uncertainty and exogenous inputs and outputs	2-33
2.14. Mixed H_2/μ curve	2-36
3.1. Basic Design Model of the VISTA F-16	3-2
3.2. Design Block Diagram of the Inner Loop	3-8
3.3. Design Block Diagram of the VISTA F-16 with Noise	3-12
3.4. Evaluation Model for the VISTA F-16	3-13
3.5. Wind Gust (solid) compared to Sensor Noise (dashed)	3-14
3.6. Open Outer Loop Response to Wind Gust and Sensor Noise, angles in degrees	3-15
3.7. Robust Analysis Model for the VISTA F-16	3-16
3.8. Singular Value plot of W_{perf}^{-1}	3-20
4.1. Design Model for μ -synthesis	4-2
4.2. Singular Value plot of $W_{\Delta ACT}$	4-3

Figure	Page
4.3. Singular Value plot for the optimal μ controller	4-9
4.4. Noiseless Tracking Capability of the μ controller (solid line) compared to the ideal response (dashed) for a step in β and a step in $\dot{\mu}$	4-10
4.5. Noisy Tracking Capability of the μ controller (solid line) compared to the ideal response (dashed) for a step in β and a step in $\dot{\mu}$	4-11
4.6. μ bounds for the μ controller	4-12
4.7. Robust Analysis of the μ controller	4-13
4.8. System's Response to Wind Gust and Sensor noise, μ Controller	4-14
4.9. System's Response to Sensor Noise only, μ Controller	4-16
5.1. Design Model for H_2 -synthesis	5-2
5.2. System's Response to Wind Gust and Sensor Noise, $K = I$	5-6
5.3. FFT of the state responses to noise	5-7
5.4. Closed loop SV plots for Z_{states} vs. wind gust and sensor noise, $K = I$	5-9
5.5. Effect of varying one design weight, k_m , on closed loop gain of Z_{states} for wind gust and noise input at $\omega \approx 3.8$ rad/sec	5-10
5.6. System's Response to Wind Gust and Sensor Noise, 1st controller	5-11
5.7. Closed loop SV plots for Z_{states} vs. wind gust and sensor noise for the 1st controller	5-12
5.8. System's Response to Wind Gust and Sensor Noise, H_2 Controller A	5-13
5.9. Closed loop SV plots for Z_{states} vs. wind gust and sensor noise for H_2 Controller A	5-14
5.10. γ vs. α curve using Design A	5-16
5.11. "Knee" of the γ vs. α curve using Design A	5-17
5.12. System's Response to Wind Gust and Sensor Noise, Mixed Controller A	5-18
5.13. γ vs. α for 23rd order based on Mixed Design A, μ controller shown by *	5-19
6.1. P-K version of the H_2 part of the H_2/H_∞ problem	6-1
6.2. γ vs. α curves for the various two-norms using Design A (x), and the μ Controller(*)	6-3
6.3. γ vs. α curves for the various two-norms using Design B (x) and the μ Controller(*)	6-6

Figure	Page
6.4. System's Response to Steps in β and $\dot{\mu}$, Mixed Controller B	6-7
6.5. System's Response to Wind Gust and Sensor Noise, Mixed Controller B	6-10
6.6. System's Response to Sensor Noise only, Mixed Controller B	6-11
6.7. System's Response to Wind Gust and Sensor noise, Controller C	6-15
6.8. System's Response to Sensor noise only, Controller C	6-16
6.9. Closed loop SV plots for Z_{states} vs. wind gust and sensor noise for Controller C	6-17
6.10. Mu bounds plot of Controller C	6-18
6.11. γ vs. α curve for the various two-norms using Design C (x) and the μ controller (*)	6-19
6.12. System's Response to Wind Gust and Sensor noise, Mixed Controller C	6-21
6.13. System's Response to Sensor noise only, Mixed Controller C	6-22
6.14. Step Response plot of Mixed Controller C	6-23
6.15. Mu bounds plot of Mixed Controller C	6-24
6.16. Noisy Step Response plot of Mixed Controller C	6-25
6.17. Noisy Step Response plot of the μ controller	6-26
C.1. H_2 Problem on the Evaluation Model	C-2

List of Tables

Table	Page
3.1. Structured Uncertainty Levels	3-18
4.1. Reduction in Open Loop Noise and Wind Effects using μ Controller	4-15
5.1. Design Weights for the 1st controller	5-9
5.2. Design Weights for H_2 Controller A	5-12
5.3. Change in μ Controller Noise and Wind Effects using H_2 Controller A	5-14
5.4. Change in μ Controller Noise and Wind Effects using Mixed Design A	5-17
6.1. Various two-norms for the μ Controller and Mixed Controller A	6-3
6.2. Various two-norms for the μ Controller and H_2 Controller B	6-4
6.3. Change in μ Controller Noise and Wind Effects using H_2 Controller B	6-4
6.4. Various two-norms for the μ Controller, H_2 Controller B and Mixed Controller B	6-5
6.5. Change in μ Controller Noise and Wind Effects using Mixed Controller B	6-5
6.6. Various two-norms for the μ Controller and Mixed Controller B	6-9
6.7. Change in μ Controller Noise Effects Only using Mixed Controller B	6-9
6.8. Various two-norms for the μ Controller and H_2 Controller C	6-14
6.9. Change in μ Controller Noise and Wind Effects using H_2 Controller C	6-14
6.10. Change in μ Controller Noise Effects Only using H_2 Controller C	6-17
6.11. Various two-norms for the μ Controller and Mixed and H_2 Controller C	6-20
6.12. Change in μ Controller Noise and Wind Effects using Mixed Controller C	6-20
6.13. Change in μ Controller Noise Effects Only using Mixed Controller C	6-20

Abstract

This thesis examines the use of the mixed H_2/μ optimal control synthesis method in the design of a flight control system for the lateral/directional axes of the F-16 Variable Stability In-Flight Simulator Test Aircraft (VISTA). The method is designed to minimize the H_2 norm (two-norm) for a given value of μ . This should provide adequate noise and disturbance rejection while maintaining robustness against several types of uncertainties in the system. This thesis finds that, for this problem, the two-norm is not an accurate representation of the outputs of interest. When the two-norm is broken up into its constituent parts an appropriate solution can be found. This thesis also finds that it is possible to use an H_2 controller which is destabilizing to the evaluation model as the starting point in the mixed H_2/μ curve and still get an acceptable answer. A numerical approach was used, utilizing a recently improved computer algorithm.

Flight Control Design using Mixed H_2/μ Optimization

I. Introduction

1.1 Background/Motivation

To design a controller, the designer must use a model of the system he or she wishes to control. Usually, however, the model is not perfect. In general, there will be many underlying assumptions made in developing the model. These assumptions could include linearizations, simplifying assumptions, approximations, etc. The end result is a model which could be far from perfect. Sometimes the imperfection can be characterized well — for example, a parameter which is plus or minus a known amount. Sometimes the imperfection cannot be characterized very well.

Any controller developed from this model is then suspect. It may work well on the design model but perform poorly when tested on the actual system or an accurate evaluation model. If we could somehow incorporate this unknown uncertainty into the design model and design for it, we should be able to get a more capable controller, in terms of working well in the face of uncertainty. That is, a controller that is more robust.

H_∞ optimal control is capable of designing for uncertainty. To be specific, it minimizes the output energy of a system with unknown, but bounded energy inputs. This method is also useful in designing a good tracker (minimize the energy of an error signal due to a pulse command).

Unfortunately, H_∞ is limited in that it can only handle one uncertainty. It is probable that a real system would have multiple uncertainties occurring at different locations. H_∞ by itself is incapable of handling this problem.

Doyle developed a method which would eliminate this limitation. His work centered on the complex structured singular value, μ , which allows for these multiple uncertainties. See [PD93] for an excellent summary.

If unknown, but bounded energy inputs were all we had to worry about in a system, H_∞ and μ would take care of everything. Unfortunately, there are other concerns. One of them is the response to noise entering the system. Noise is not bounded energy. It is usually characterized as white Gaussian (constant power at all frequencies, random). H_∞ and μ are incapable of handling this type of input. However, H_2 optimization is designed to minimize the energy of a system's output when the system is faced with white Gaussian noise inputs. Note that the objectives in H_∞ and μ compete with the objective of H_2 . However, we can trade off these objectives in an optimal fashion using mixed H_2/H_∞ optimization.

To date, only a numerical solution is available for mixed H_2/H_∞ . Ridgely [Rid91] was the first to develop a numerical optimization approach to find a general mixed H_2/H_∞ controller. Walker [Wal94] has improved upon this method by eliminating several assumptions made by Ridgely and producing a computationally more efficient solution to the problem. Further improvements have been made to the efficiency and robustness of the numerical computation by Smith [Smi94].

Madiwale [Mad89] first proposed adding robustness to the mixed control problem. Walker incorporated μ into the mixed H_2/H_∞ format described above and completed a SISO example and a 2×2 MIMO example.

The purpose of this thesis is to extend the work by Walker to a more rigorous example using H_2/μ and the improved numerical algorithm.

1.2 Thesis Outline

This thesis is divided into seven chapters, including this introductory chapter. The next two chapters provide the groundwork on which the controller is based. The development of mixed H_2/H_∞ design theory is described in Chapter II. This chapter also describes the complex structured singular value, μ , in terms of analysis and synthesis. This chapter ends with a discussion of several

controller design topics necessary for the development of the design and analysis models described in Chapter III.

Chapter III presents the mathematical state space model used in our MIMO VISTA F-16 example. Also, in this chapter, the basic design model is described as well as the evaluation model for analyzing the time responses. To evaluate robustness, a robust analysis model is developed for the μ analysis.

The μ design model is constructed by adding certain inputs and outputs associated with the uncertainties to the basic design model. This model is then used to develop the μ controller. Chapter IV describes this process and the subsequent analysis of that controller.

Chapter V shows the development of an H_2 controller from the basic design. The controller is evaluated and mixed with the μ controller. The resulting mixed controller is evaluated and found to be deficient.

In Chapter VI, the deficiency is analyzed and a correction is made. Another H_2 controller is developed which, again, is mixed with the μ controller. This mixed controller exhibits another deficiency which is analyzed and corrected. This final correction will prove to be sufficient and the resulting H_2 controller is then mixed with the μ controller. This final mixed controller is then analyzed.

Chapter VII then summarizes the results of this study, presents some conclusions and provides recommendations for further study.

II. Preliminaries

Before we can begin, we must discuss some of the basic theory. The majority of this chapter will discuss the optimization methods used: H_2 , H_∞ and μ . The final section will discuss a few control design topics.

2.1 Mathematical Preliminaries

2.1.1 H_2 Optimal Control.

2.1.1.1 The H_2 space. H_2 is defined as the space of all transfer function matrices which are stable (eigenvalues in the open left-half complex plane) and have a bounded two-norm. The two-norm (designated α) is defined as

$$\alpha^2 = \|T_{zw}\|_2^2 := \frac{1}{2\pi} \int_{-\infty}^{+\infty} \text{tr} [T_{zw}^*(j\omega) T_{zw}(j\omega)] d\omega \quad (2.1)$$

The subspace $\Re H_2$ is defined as the space of *real-rational* functions (rational functions with real coefficients) in H_2 . An easier way to compute (2.1) is found in [DFT92] and is summarized here.

Consider the transfer function

$$G(s) = \left[\begin{array}{c|c} A & B \\ \hline C & 0 \end{array} \right] \in \Re H_2 \quad (2.2)$$

Note that (2.2) makes use of the following notation.

$$\left[\begin{array}{c|c} A & B \\ \hline C & D \end{array} \right] := C(sI - A)^{-1}B + D \quad (2.3)$$

The two-norm is determined from the following algorithm:

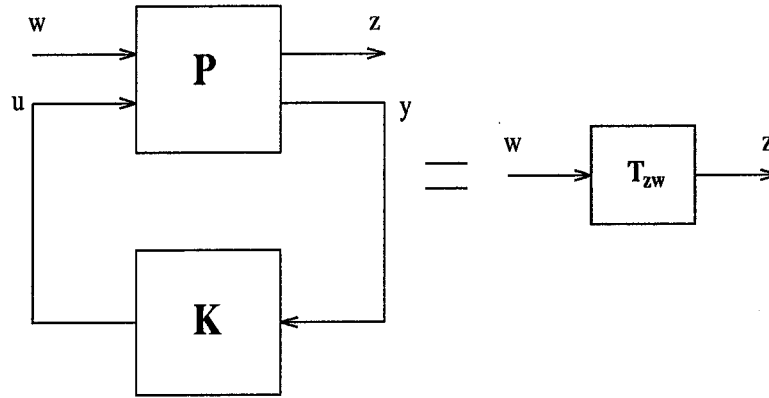


Figure 2.1 Basic Block Diagram for the H_2 problem

Step 1 Find the positive semidefinite solutions to the following Lyapunov equations.

$$AL_c + L_c A^T + BB^T = 0 \quad (2.4)$$

$$L_o A + A^T L_o + C^T C = 0 \quad (2.5)$$

L_c and L_o are the *controllability* and *observability gramians* of $G(s)$, respectively.

Step 2 Now the two-norm can be calculated by

$$\alpha^2 = \|G(s)\|_2^2 = \text{tr}(L_c C^T C) = \text{tr}(L_o B B^T) \quad (2.6)$$

2.1.1.2 H_2 optimization. Consider the H_2 block diagram in Figure 2.1. The input to the system is w , a zero-mean, unit intensity, white Gaussian noise type input (typically, for aircraft, wind gusts and sensor noise). The output z is whatever quantities we wish to have minimally affected by w . The plant is designated P . For design purposes, P will include the design weights which can be used to emphasize or de-emphasize the importance of a certain frequency range. K is the feedback controller which will be found using the method described in this section. The measurements from the plant, y , are input into the controller. The control, u , is the output of the controller which is fed back into P .

The objective of H_2 optimization is to find the stabilizing controller K which minimizes the energy of z with w being a white Gaussian noise input. This is the same thing as minimizing the two-norm of the closed loop transfer function, T_{zw} . The solution is obtained by solving 2 Algebraic Riccati Equations (ARE) and is actually a generalization of the LQG problem. LQG requires that there only be two white noises entered at specific locations and that the outputs be statically weighted states and controls. H_2 allows the white noise inputs to be placed anywhere, and the outputs to be anything and placed anywhere. Dynamic weightings are also allowed.

The minimal value of the two-norm, $\underline{\alpha}$, is defined as

$$\underline{\alpha} = \inf_{K(s) \text{ Stabilizing}} \|z\|_2 \quad (2.7)$$

$$= \inf_{K(s) \text{ Stabilizing}} \|T_{zw}\|_2 \quad (2.8)$$

A state space realization of P is given by

$$\dot{x}_2 = A_2 x_2 + B_w w + B_{u_2} u \quad (2.9)$$

$$z = C_z x_2 + D_{zw} w + D_{zu} u \quad (2.10)$$

$$y = C_{y_2} x_2 + D_{yw} w + D_{yu} u \quad (2.11)$$

The 2 subscript indicates that this representation is for H_2 optimization.

To find K, the following assumptions are made:

- (i) $D_{zw} = 0$
- (ii) $D_{yu} = 0$
- (iii) (A_2, B_{u_2}) is stabilizable and (C_{y_2}, A_2) is detectable
- (iv) $D_{zu}^T D_{zu} = I$ and $D_{yw} D_{yw}^T = I$

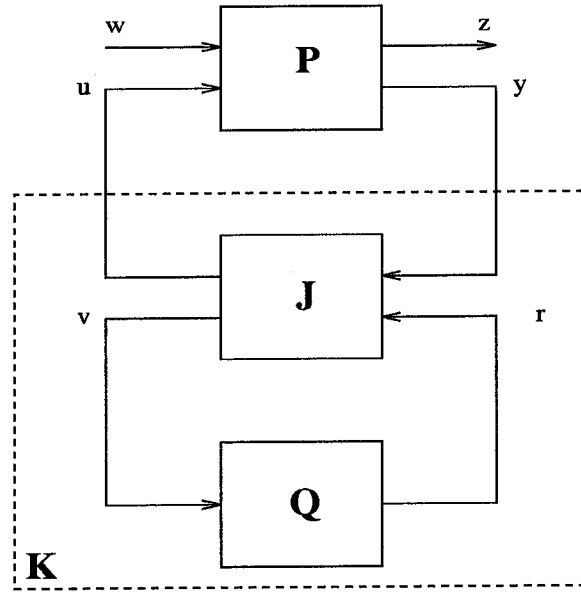


Figure 2.2 H_2 system with parameterized controller

$$\begin{aligned}
 \text{(v)} \quad & \begin{bmatrix} A_2 - j\omega I & B_{u_2} \\ C_z & D_{zu} \end{bmatrix} \text{ has full column rank for all } \omega \\
 \text{(vi)} \quad & \begin{bmatrix} A_2 - j\omega I & B_w \\ C_{y_2} & D_{yw} \end{bmatrix} \text{ has full row rank for all } \omega
 \end{aligned}$$

Condition (i) is necessary for the two-norm to be finite. Condition (ii) is made to simplify the problem (it is not necessary). Condition (iii) is necessary for a stabilizing compensator to exist. Condition (iv) is actually a simplifying assumption; the underlying necessary condition of (iv) is that the products be full rank to avoid a singular control problem (we must have a penalty on all controls and no perfect measurements). This simplifying assumption can be relaxed to the necessary full-rank condition through scaling [Dai90]. Finally, conditions (v) and (vi) are required to ensure the existence of stabilizing solutions to the two AREs in the H_2 solution.

For any given α , the family of all stabilizing controllers, K , that satisfies $\underline{\alpha} \leq \|T_{zw}\|_2 \leq \alpha$ can be found by using the following algorithm. This algorithm is based on parameterizing the controller, K , as a feedback loop of J and Q (see Figure 2.2).

Step 1 Form the following algebraic Riccati equations and solve for X_2 and Y_2 :

$$\begin{aligned} (A_2 - B_{u_2} D_{zu}^T C_z)^T X_2 + X_2 (A_2 - B_{u_2} D_{zu}^T C_z) - X_2 B_{u_2} B_{u_2}^T X_2 \\ + [(I - D_{zu} D_{zu}^T) C_z]^T [(I - D_{zu} D_{zu}^T) C_z] = 0 \end{aligned} \quad (2.12)$$

$$\begin{aligned} (A_2 - B_w D_{yw}^T C_{y_2}) Y_2 + Y_2 (A_2 - B_w D_{yw}^T C_{y_2}) - Y_2 C_{y_2}^T C_{y_2} Y_2 \\ + [B_w (I - D_{yw}^T D_{yw})] [B_w (I - D_{yw}^T D_{yw})]^T = 0 \end{aligned} \quad (2.13)$$

To be valid, the solutions X_2 and Y_2 must each be real, unique, symmetric, and positive semidefinite.

Step 2 Substitute X_2 and Y_2 into the following:

$$K_f = Y_2 C_{y_2}^T + B_w D_{yw}^T \quad (2.14)$$

$$K_c = B_{u_2}^T X_2 + D_{zu}^T C_z \quad (2.15)$$

$$K_{fl} = B_{u_2} \quad (2.16)$$

$$K_{cl} = -C_{y_2} \quad (2.17)$$

which are then substituted into

$$A_J = A_2 - K_f C_{y_2} - B_{u_2} K_c \quad (2.18)$$

Step 3 Now take (2.14) – (2.18) and substitute into:

$$J(s) = \begin{bmatrix} J_{uy} & J_{ur} \\ J_{vy} & J_{vr} \end{bmatrix} = \left[\begin{array}{c|c} A_J & B_J \\ \hline C_J & D_J \end{array} \right] = \left[\begin{array}{c|cc} A_J & K_f & K_{fl} \\ \hline -K_c & 0 & I \\ K_{cl} & I & 0 \end{array} \right] \quad (2.19)$$

Step 4 Choose a Q that is real-rational, stable and strictly proper (this makes $Q \in \mathcal{RH}_2$) that meets the following criterion:

$$\|Q\|_2^2 \leq \alpha^2 - \underline{\alpha}^2 \quad (2.20)$$

Any $Q \in \mathcal{RH}_2$ that satisfies (2.20) is acceptable; it is a freedom parameter.

Step 5 Now, form $K(s)$ from $J(s)$ given in (2.19) and the $Q(s)$ chosen in Step 4.

$K(s)$ is given by the lower linear fractional transformation of $J(s)$ and $Q(s)$ (see Figure 2.2).

This is written as

$$K(s) = J_{uy} + J_{ur}Q(I - J_{vr}Q)^{-1}J_{vy} \quad (2.21)$$

We can see from (2.20) that when the chosen α equals the optimal, $\underline{\alpha}$, $Q := 0$. In this case, (2.21) says $K(s) = J_{uy}$. This is the unique H_2 optimal controller, $K_{2_{opt}}$. Thus, $Q = 0$ yields $K_{2_{opt}}$. If a suboptimal controller is desired (which it will be in mixed H_2/H_∞ optimization), choose $Q \neq 0$.

2.1.2 H_∞ Optimal Control.

2.1.2.1 The H_∞ space. H_∞ is defined as the space of transfer function matrices which are stable (eigenvalues in the open left-half complex plane) and have a bounded infinity norm. \mathcal{RH}_∞ is the subspace of real-rational H_∞ functions. The infinity norm is an induced operator norm and is defined as

$$\gamma = \|T_{ed}\| \quad (2.22)$$

$$:= \|T_{ed}\|_{\infty} \quad (2.23)$$

$$= \sup_{d \neq 0} \frac{\|T_{ed}d\|_2}{\|d\|_2} \quad (2.24)$$

$$= \sup_{\|d\|_2 \leq 1} \|e\|_2 \quad (2.25)$$

$$= \sup_{\omega} \bar{\sigma}[T_{ed}(j\omega)] \quad (2.26)$$

Thus, the infinity norm is the maximum possible energy-to-energy gain of the system. To minimize the energy of an output due to an unknown but deterministic bounded energy input (like a pulse input), we must minimize the infinity-norm of the associated transfer function. An important fact for robustness problems is that since the infinity-norm is an induced operator norm, it has the submultiplicative property [Dai90]; given $F, G \in H_{\infty}$ then

$$\|FG\|_{\infty} \leq \|F\|_{\infty}\|G\|_{\infty} \quad (2.27)$$

An easy way to determine the infinity-norm is to plot the maximum singular values of the transfer function over the appropriate frequency range and determine the maximum on the plot; that is the infinity norm of the system. However, this may not be the most practical method numerically since we don't necessarily know around what frequency range the maximum singular value will attain its maximum.

A more numerically robust approach is based on the Hamiltonian matrix obtained from the state space representation of a proper stable transfer function [Dai90]. Given the transfer function

$$G(s) = \left[\begin{array}{c|c} A & B \\ \hline C & D \end{array} \right] \quad (2.28)$$

we can construct the associated Hamiltonian

$$H = \begin{bmatrix} A + BR^{-1}D^T C & BR^{-1}B^T \\ -C^T(I - \gamma^{-2}DD^T)^{-1}C & -(A + BR^{-1}D^T C)^T \end{bmatrix} \quad (2.29)$$

where $R := \gamma^2 I - D^T D$.

The dual of (2.29) is

$$H = \begin{bmatrix} (A + BD^T R^{-1}C)^T & C^T R^{-1}C \\ -B(I - \gamma^{-2}D^T D)^{-1}B^T & -(A + BD^T R^{-1}C) \end{bmatrix} \quad (2.30)$$

where $R := \gamma^2 I - DD^T$.

Any Hamiltonian matrix has the form

$$\begin{bmatrix} X & Y \\ Z & -X^T \end{bmatrix} \quad (2.31)$$

where $Y = Y^T, Z = Z^T$. Thus, it has the property that the eigenvalues mirror each other across the imaginary axis. That is, if λ is an eigenvalue of H , then $-\lambda$ is also an eigenvalue of H . A theorem in [Dai90] implies that we can use the Hamiltonian and this “mirroring” property to determine the infinity-norm, γ , of the associated system in an iterative way. To do this, we choose a value of γ and calculate the eigenvalues of the Hamiltonian. If any of the eigenvalues are on the imaginary axis, our γ is too small; the next guess should be bigger. If there are no purely imaginary eigenvalues our γ is too big; the next guess should be smaller. We are looking for the value of γ when the eigenvalues first meet on the imaginary axis. By using a bisection method or a golden step search on γ we can quickly converge to $\gamma = \|G\|_\infty$ within any desired accuracy level.

2.1.2.2 H_∞ Optimization. Now consider the H_∞ block diagram in Figure 2.3. This

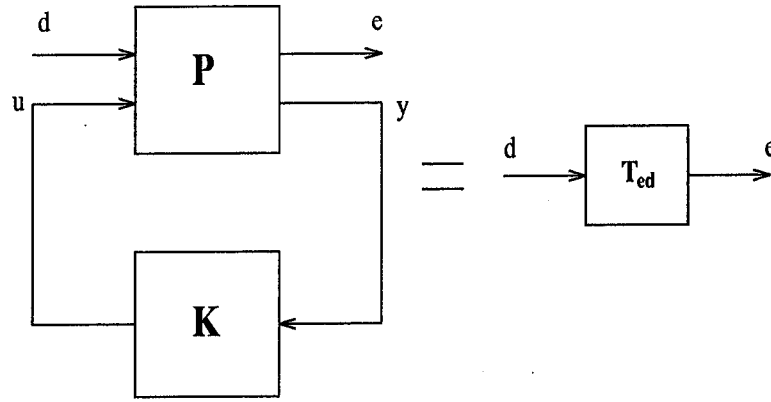


Figure 2.3 Basic Block Diagram for the H_∞ problem

is the same as Figure 2.1, except the exogenous input and output and the closed loop transfer function have been renamed. This is done to keep H_∞ distinct from the H_2 optimization method. The plant, P , includes the design weights. The input, d , is assumed to be unknown but deterministic and have bounded energy. We want to find a stabilizing controller, $K(s)$, which minimizes the energy of the output, e . Since we are trying to minimize the energy of an output to a worst case bounded energy input, we are trying to minimize the infinity-norm of the closed loop transfer function, T_{ed} :

$$\inf_{K_{\text{stabilizing}}} \sup_{\|d\|_2 \leq 1} \|e\|_2 = \inf_{K_{\text{stabilizing}}} \|T_{ed}\|_\infty \equiv \underline{\gamma} \quad (2.32)$$

where the infinity-norm of T_{ed} is

$$\|T_{ed}\|_\infty = \sup_{\omega} \bar{\sigma}[T_{ed}] \quad (2.33)$$

and $\bar{\sigma}$ denotes the maximum singular value. The minimum achievable infinity-norm, as indicated by (2.32), is designated $\underline{\gamma}$. The state space representation of P in Figure 2.3 is given by:

$$\dot{x}_\infty = A_\infty x_\infty + B_d d + B_{u_\infty} u \quad (2.34)$$

$$e = C_e x_\infty + D_{ed} d + D_{eu} u \quad (2.35)$$

$$y = C_{y_\infty} x_\infty + D_{yd} d + D_{yu} u \quad (2.36)$$

where the ∞ subscript indicates the problem setup for H_∞ optimization. As in H_2 there are some underlying assumptions:

- (i) $D_{ed} = 0$
- (ii) $D_{yu} = 0$
- (iii) (A_∞, B_{u_∞}) is stabilizable and (C_{y_∞}, A_∞) is detectable
- (iv) $D_{eu}^T D_{eu} = I$ and $D_{yd} D_{yd}^T = I$
- (v) $\begin{bmatrix} A_\infty - j\omega I & B_{u_\infty} \\ C_e & D_{eu} \end{bmatrix}$ has full column rank for all ω
- (vi) $\begin{bmatrix} A_\infty - j\omega I & B_d \\ C_{y_\infty} & D_{yd} \end{bmatrix}$ has full row rank for all ω

Assumption (i) is *not* a requirement for the H_∞ problem, but does allow the development to be simpler. Assumption (ii) is also not required but makes the problem simpler. Condition (iii) is required for a stabilizing compensator to exist. Condition (iv) is just like condition (iv) in Section 2.1.1.2; it is a simplifying assumption with an underlying necessary condition that the products be full rank to avoid a singular control problem (i.e. we need a direct penalty on all controls and no perfect measurements). Conditions (v) and (vi) are required to ensure the existence of stabilizing solutions to the two AREs in the H_∞ solution. Later, in the mixed H_2/H_∞ problem, conditions (i) and (iv) will be relaxed.

Like H_2 optimal, the H_∞ optimal controller, $K(s)$, is found from equation (2.21) with $J(s)$ defined as in (2.19). Of course, the elements in (2.19) (A_f , K_f , etc) are defined differently. The algorithm for H_∞ optimization is an iterative process.

Step 1 Pick an initial value of γ , and form the following two algebraic Riccati equations:

$$(A_\infty - B_{u_\infty} D_{eu}^T C_e)^T X_\infty + X_\infty (A_\infty - B_{u_\infty} D_{eu}^T C_e) - X_\infty (\gamma^{-2} B_d B_d^T - B_{u_\infty} B_{u_\infty}^T) X_\infty \\ + C_e^T (I - D_{eu} D_{eu}^T)^T (I - D_{eu} D_{eu}^T) C_e = 0 \quad (2.37)$$

$$(A_\infty - B_d D_{yd}^T C_{y_\infty}) Y_\infty + Y_\infty (A_\infty - B_d D_{yd}^T C_{y_\infty})^T + Y_\infty (\gamma^{-2} C_e^T C_e - C_{y_\infty}^T C_{y_\infty}) Y_\infty \\ + B_d (I - D_{yd}^T D_{yd}) (I - D_{yd}^T D_{yd})^T B_d^T = 0 \quad (2.38)$$

Step 2 Solve for X_∞ and Y_∞ . For the parametrization to be valid, the resulting X_∞ and Y_∞ must satisfy the following three conditions:

1. The solutions must be symmetric and positive semidefinite.
2. No eigenvalues of the Hamiltonian matrices associated with (2.37) and (2.38) can be on the imaginary axis.
3. $\rho(X_\infty Y_\infty) < \gamma^2$, where $\rho(M) := \max_i |\lambda_i(M)|$ is the *spectral radius* of M .

Check the three conditions; if any condition fails, increase γ and repeat the process. If all three conditions are met we have a solution, but it is not necessarily the optimal solution. If we are looking for the optimal γ (i.e. $\underline{\gamma}$), we reduce γ and repeat until one of the 3 conditions above just fails. By doing this, we can find the minimum infinity-norm to any desired level of accuracy. Once we have $\underline{\gamma}$ (for optimal) or γ (for sub-optimal) to the accuracy we want, we may continue the algorithm to find the controller(s) which achieves this γ .

Step 3 Take the value of γ , X_∞ , and Y_∞ found in Step 2 and substitute into the following equations:

$$A_J = A_\infty - K_f C_{y_\infty} - B_{u_\infty} K_c + \gamma^{-2} Y_\infty C_e^T (C_e - D_{eu} K_c) \quad (2.39)$$

$$K_f = Y_\infty C_{y_\infty}^T + B_d D_{y_d}^T \quad (2.40)$$

$$K_{fI} = \gamma^{-2} Y_\infty C_e^T D_{eu} + B_{u_\infty} \quad (2.41)$$

$$K_c = B_{u_\infty}^T X_\infty + D_{eu}^T C_e (I - \gamma^{-2} Y_\infty X_\infty)^{-1} \quad (2.42)$$

$$K_{cl} = -(\gamma^{-2} D_{y_d} B_d^T X_\infty + C_{y_\infty})(I - \gamma^{-2} Y_\infty X_\infty)^{-1} \quad (2.43)$$

Step 4 Substitute the answers from Step 3 into equation (2.19) to form the $J(s)$ for the H_∞ problem.

Step 5 Choose *any* Q such that

$$Q \in \mathcal{RH}_\infty \quad (2.44)$$

$$\|Q\|_\infty < \gamma \quad (2.45)$$

Substitute that Q and the elements of J from Step 4 into (2.21) and we have our controller.

Note that the optimal H_∞ controller is not necessarily unique.

2.1.3 Mixed H_2/H_∞ Control.

2.1.3.1 Motivation. Recall that both H_2 and H_∞ optimization minimize the energy of the chosen output(s); however, they each do this for different types of inputs. The input for which H_2 is designed is characterized as white Gaussian noise. Some examples that come to mind for aircraft are sensor noises and wind gusts (which has a definite noise-like quality to it). The type of inputs used in H_∞ are characterized as having bounded energy. An example here would be the error signal produced from a pulse command to a feedback system (see Figure 2.4). This would give us good tracking. By mixing the two, we should be able to get good output characteristics (stability and/or performance) for a system which has both types of inputs.

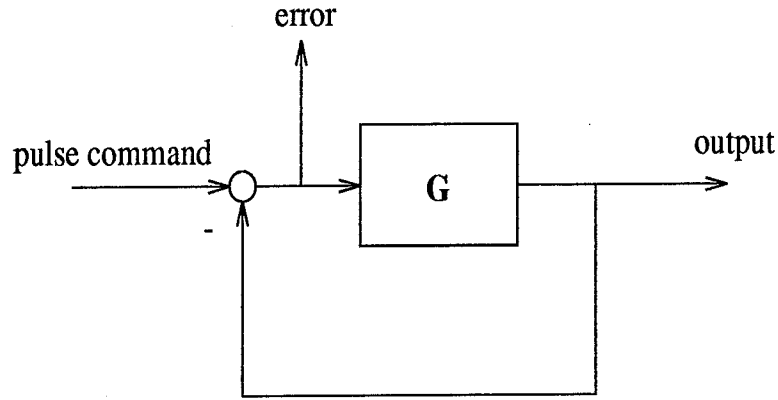


Figure 2.4 Example of an H_∞ problem

We must keep in mind, however, that we are in a sense producing competing goals, in that we will often find ourselves trying to minimize the norm of the sensitivity (say, for good tracking), S , and the norm of the complementary sensitivity (say, for good noise rejection), T . Thus, we can expect to have a trade-off between good H_2 and good H_∞ .

We *could* try to do an optimization scheme where we try to minimize both norms (multi-objective optimization), but that may be too limiting. It would only find one solution and that may be a solution we are not interested in. For example, using the examples above, we may be more interested in getting good tracking than getting rid of most of the noise, so we would, in that case, be willing to let $\|T_{zw}\|_2$ (α) increase a little if we got a lower $\|T_{ed}\|_\infty$ (γ) in return. Therefore, we will not pursue multi-objective optimization here. We will instead follow Ridgely [Rid91] and Walker [Wal94] where they have one objective, minimize α , and append the infinity-norm as a constraint, as

$$\inf_{K_{adm}} \|T_{zw}\|_2, \text{ subject to the constraint } \|T_{ed}\|_\infty \leq \gamma \quad (2.46)$$

Note that in this fashion, we will not be doing H_∞ optimization (Section 2.1.2.2), but rather will only be constraining the infinity-norm (Section 2.1.2.1).

2.1.3.2 State Space Formulation. The development represented here was taken from Walker [Wal94]. The block diagram of the mixed H_2/H_∞ problem is in Figure 2.5. This system

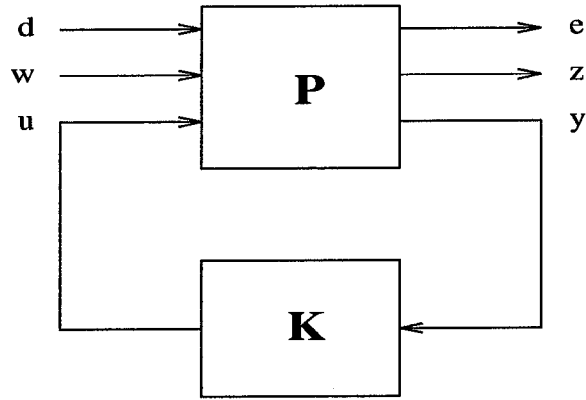


Figure 2.5 Basic Block Diagram for the mixed H_2/H_∞ problem

has exogenous inputs w and d and controlled outputs z and e . The measured output is y and the control is u . These are all defined the same way as in Figures 2.1 and 2.3. P is now the combination of the P 's in those figures¹. The resulting state space representation of P is now

$$\dot{x} = \tilde{A}x + \tilde{B}_d d + \tilde{B}_w w + \tilde{B}_u u \quad (2.47)$$

$$e = \tilde{C}_e x + \tilde{D}_{ed} d + \tilde{D}_{ew} w + \tilde{D}_{eu} u \quad (2.48)$$

$$z = \tilde{C}_z x + \tilde{D}_{zd} d + \tilde{D}_{zw} w + \tilde{D}_{zu} u \quad (2.49)$$

$$y = \tilde{C}_y x + \tilde{D}_{yd} d + \tilde{D}_{yw} w + \tilde{D}_{yu} u \quad (2.50)$$

or, in transfer function form,

$$P = \left[\begin{array}{c|ccc} \tilde{A} & \tilde{B}_d & \tilde{B}_w & \tilde{B}_u \\ \hline \tilde{C}_e & \tilde{D}_{ed} & \tilde{D}_{ew} & \tilde{D}_{eu} \\ \tilde{C}_z & \tilde{D}_{zd} & \tilde{D}_{zw} & \tilde{D}_{zu} \\ \tilde{C}_y & \tilde{D}_{yd} & \tilde{D}_{yw} & \tilde{D}_{yu} \end{array} \right] \quad (2.51)$$

¹this will be made more clear in Chapter III

This may also be represented by the individual H_2 and H_∞ problems, which are

$$\begin{aligned}\dot{x}_2 &= A_2 x_2 + B_w w + B_{u_2} u \\ z &= C_z x_2 + D_{zw} w + D_{zu} u \\ y &= C_{y_2} x_2 + D_{yw} w + D_{yu} u\end{aligned}\tag{2.52}$$

$$\begin{aligned}\dot{x}_\infty &= A_\infty x_\infty + B_d d + B_{u_\infty} u \\ e &= C_e x_\infty + D_{ed} d + D_{eu} u \\ y &= C_{y_\infty} x_\infty + D_{yd} d + D_{yu} u\end{aligned}\tag{2.53}$$

The assumptions used to solve the mixed problem are the same as the assumptions for the H_2 and H_∞ problem except that four assumptions from the H_∞ problem (Section 2.1.2.2) are not included. The assumptions which are not included are:

1. $D_{ed} = 0$
2. $D_{eu}^T D_{eu} = I$ and $D_{yd} D_{yd}^T = I$
3. $\begin{bmatrix} A_\infty - j\omega I & B_{u_\infty} \\ C_e & D_{eu} \end{bmatrix}$ has full column rank for all ω
4. $\begin{bmatrix} A_\infty - j\omega I & B_d \\ C_{y_\infty} & D_{yd} \end{bmatrix}$ has full row rank for all ω

(1) was never necessary, and does not seriously complicate the mixed development. (2) was necessary to ensure a non-singular H_∞ problem. In this development, *no assumption* is made about the ranks of D_{eu} and D_{yd} (we will allow for perfect measurements and/or controls with no penalty). The H_2 part of the problem handles this. (3) and (4) are not necessary, as H_∞ Riccati equations will not

be used in the mixed development. We will be calculating the controller using H_2 optimization, so we *will* have a stabilizing controller.

Therefore, the assumptions for mixed H_2/H_∞ are:

1. $D_{zw} = 0$
2. $D_{yu} = 0$
3. (A_2, B_{u_2}) stabilizable, (C_{y_2}, A_2) detectable
4. $D_{zu}^T D_{zu}$ full rank, $D_{yw} D_{yw}^T$ full rank
5. $\begin{bmatrix} A_2 - j\omega I & B_{u_2} \\ C_z & D_{zu} \end{bmatrix}$ has full column rank for all ω
6. $\begin{bmatrix} A_2 - j\omega I & B_w \\ C_{y_2} & D_{yw} \end{bmatrix}$ has full row rank for all ω

In state space, the controller in Figure 2.5 is given by

$$\begin{aligned}\dot{x}_c &= A_c x_c + B_c y \\ u &= C_c x_c + D_c y\end{aligned}\tag{2.54}$$

Combining (2.52) with (2.54) produces the closed-loop state space equations for T_{zw}

$$\begin{aligned}\dot{x}_2 &= (A + B_{u_2} D_c C_{y_2}) x_2 + B_{u_2} C_c x_c + (B_w + B_{u_2} D_c D_{yw}) w \\ \dot{x}_c &= B_c C_{y_2} x_2 + A_c x_c + B_c D_{yw} w \\ z &= (C_z + D_{zu} D_c C_{y_2}) x_2 + D_{zu} C_c x_c + D_{zu} D_c D_{yw} w\end{aligned}\tag{2.55}$$

Applying assumption (1) to (2.55), we see that $D_{zu} D_c D_{yw}$ must equal zero for the two-norm of T_{zw} to be finite. Applying assumption (4), we find that $D_c = 0$. Thus, the only way this problem will have a solution is for the controller K to be strictly proper.

When we close the loop of the individual H_2 and H_∞ problems with the above controller, we get the following closed-loop state space representations:

$$\dot{x}_2 = \mathcal{A}_2 x_2 + \mathcal{B}_w w \quad (2.56)$$

$$z = \mathcal{C}_z x_2 \quad (2.57)$$

and

$$\dot{x}_\infty = \mathcal{A}_\infty x_\infty + \mathcal{B}_d d \quad (2.58)$$

$$e = \mathcal{C}_e x_\infty + \mathcal{D}_{ed} d \quad (2.59)$$

where

$$x_2 = \begin{bmatrix} x_2 \\ x_c \end{bmatrix} \quad (2.60)$$

$$x_\infty = \begin{bmatrix} x_\infty \\ x_c \end{bmatrix} \quad (2.61)$$

$$\mathcal{A}_2 = \begin{bmatrix} A_2 & B_{u2} C_c \\ B_c C_{y2} & A_c \end{bmatrix} \quad (2.62)$$

$$\mathcal{A}_\infty = \begin{bmatrix} A_\infty & B_{u\infty} C_c \\ B_c C_{y\infty} & A_c \end{bmatrix} \quad (2.63)$$

$$\mathcal{B}_w = \begin{bmatrix} B_w \\ B_c D_{yw} \end{bmatrix} \quad (2.64)$$

$$\mathcal{B}_d = \begin{bmatrix} B_d \\ B_c D_{yd} \end{bmatrix} \quad (2.65)$$

$$\mathcal{C}_z = \begin{bmatrix} C_z & D_{zu} C_c \end{bmatrix} \quad (2.66)$$

$$\mathcal{C}_e = \begin{bmatrix} C_e & D_{eu}C_c \end{bmatrix} \quad (2.67)$$

$$\mathcal{D}_{ed} = D_{ed} \quad (2.68)$$

To simplify the development, the following definitions are made:

$$\begin{aligned} \underline{\gamma} &\equiv \inf_{K_{adm}} \|T_{ed}\|_{\infty} \\ \underline{\alpha} &\equiv \inf_{K_{adm}} \|T_{zw}\|_2 \\ K_{2opt} &\equiv \text{the unique } K(s) \text{ that makes } \|T_{zw}\|_2 = \underline{\alpha} \\ \bar{\gamma} &\equiv \|T_{ed}\|_{\infty} \text{ when } K = K_{2opt} \\ K_{mix} &\equiv \text{a solution to the } H_2/H_{\infty} \text{ problem for some } \gamma \\ \gamma^* &\equiv \|T_{ed}\|_{\infty} \text{ when } K(s) = K_{mix} \\ \alpha^* &\equiv \|T_{zw}\|_2 \text{ when } K(s) = K_{mix} \\ \gamma &\equiv \text{the constraint which } \gamma^* \text{ must stay less than or equal to } (\gamma^* \leq \gamma) \end{aligned}$$

The mixed H_2/H_{∞} problem can now be restated as follows: determine a $K(s)$ such that

1. the underlying H_2 and H_{∞} problems are stable, i.e., \mathcal{A}_2 and \mathcal{A}_{∞} are stable
2. $\gamma^* \leq \gamma$ for some given $\gamma > \underline{\gamma}$
3. $\|T_{zw}\|_2$ is minimized.

To develop this problem, Walker [Wal94] introduced the following theorem:

Theorem 2.1.1 *Let (A_c, B_c, C_c) be given and assume there exists a $Q_{\infty} = Q_{\infty}^T \geq 0$ satisfying*

$$\mathcal{A}_{\infty}Q_{\infty} + Q_{\infty}\mathcal{A}_{\infty}^T + (Q_{\infty}C_e^T + \mathcal{B}_d\mathcal{D}_{ed}^T)R^{-1}(Q_{\infty}C_e^T + \mathcal{B}_d\mathcal{D}_{ed}^T)^T + \mathcal{B}_d\mathcal{B}_d^T = 0 \quad (2.69)$$

where $R = (\gamma^2 I - \mathcal{D}_{ed}\mathcal{D}_{ed}^T) > 0$. Then the following are equivalent:

1. $(\mathcal{A}_{\infty}, \mathcal{B}_d)$ is stabilizable

2. \mathcal{A}_2 is stable.

3. \mathcal{A}_∞ is stable.

Moreover, if the above hold then the following are true:

3. $\|T_{ed}\|_\infty \leq \gamma$

4. the two-norm of the transfer function T_{zw} is given by

$$\|T_{zw}\|_2^2 = \text{tr}[C_z Q_2 C_z^T] = \text{tr}[Q_2 C_z^T C_z]$$

where $Q_2 = Q_2^T \geq 0$ is the solution to the Lyapunov equation

$$\mathcal{A}_2 Q_2 + Q_2 \mathcal{A}_2^T + \mathcal{B}_w \mathcal{B}_w^T = 0$$

5. all real symmetric solutions Q_∞ of Equation (2.69) are positive semidefinite

6. there exists a unique minimal solution Q_∞ to Equation (2.69) in the class of real symmetric solutions

7. Q_∞ is the minimal solution of Equation (2.69) if and only if

$$\text{Re}[\lambda_i(\mathcal{A}_\infty + \mathcal{B}_d \mathcal{D}_{ed}^T R^{-1} \mathcal{C}_e + Q_\infty \mathcal{C}_e^T R^{-1} \mathcal{C}_e)] \leq 0 \quad \text{for all } i \quad (2.70)$$

8. $\|T_{ed}\|_\infty < (\leq) \gamma$ iff $\text{Re}[\lambda_i(\mathcal{A}_\infty + \mathcal{B}_d \mathcal{D}_{ed}^T R^{-1} \mathcal{C}_e + Q_\infty \mathcal{C}_e^T R^{-1} \mathcal{C}_e)] < (\leq) 0$ where Q_∞ is the minimal solution to Equation (2.69).

The main result from this theorem is that the constraint $\|T_{ed}\|_\infty \leq \gamma$ ($\gamma^* \leq \gamma$) is equivalent to the constraint found in (2.70). The only way (2.70) can be satisfied is for Q_∞ to solve (2.69). So we have replaced an inequality constraint with an equality constraint. Note that (2.69) is the Riccati

equation associated with the H_∞ Hamiltonian (2.30). Walker backs that up with his Theorem 2.5.11 [Wal94:pages 2-23 thru 2-25].

Using this theorem, the mixed problem can be restated as: Find the $K(s)$ which minimizes the objective function

$$J(A_c, B_c, C_c) = \text{tr}[Q_2 C_z^T C_z] \quad (2.71)$$

where Q_2 is the real, symmetric, positive semidefinite solution to

$$\mathcal{A}_2 Q_2 + Q_2 \mathcal{A}_2^T + \mathcal{B}_w \mathcal{B}_w^T = 0 \quad (2.72)$$

and satisfying the constraint

$$\mathcal{A}_\infty Q_\infty + Q_\infty \mathcal{A}_\infty^T + (Q_\infty \mathcal{C}_e^T + \mathcal{B}_d \mathcal{D}_{ed}^T) R^{-1} (Q_\infty \mathcal{C}_e^T + \mathcal{B}_d \mathcal{D}_{ed}^T)^T + \mathcal{B}_d \mathcal{B}_d^T = 0 \quad (2.73)$$

where Q_∞ is the real, symmetric, positive semidefinite solution.

This is a minimization problem with two equality constraints and is very amenable to the Lagrange multiplier method. In brief, the Lagrange multiplier method takes the function you wish to minimize (the objective), adds on the constraints to it, and multiplies those constraints by Lagrange multipliers. The resulting equation is called the Lagrangian. This does not change the equation since the constraints equal 0 (so we are adding nothing to the equation).

The Lagrangian corresponding to this problem is

$$\begin{aligned} \mathcal{L} = & \text{tr}[Q_2 C_z^T C_z] + \text{tr}\{[\mathcal{A}_2 Q_2 + Q_2 \mathcal{A}_2^T + \mathcal{B}_w \mathcal{B}_w^T] \mathcal{X}\} \\ & + \text{tr}\{[\mathcal{A}_\infty Q_\infty + Q_\infty \mathcal{A}_\infty^T + (Q_\infty \mathcal{C}_e^T + \mathcal{B}_d \mathcal{D}_{ed}^T) R^{-1} (Q_\infty \mathcal{C}_e^T + \mathcal{B}_d \mathcal{D}_{ed}^T)^T \\ & + \mathcal{B}_d \mathcal{B}_d^T] \mathcal{Y}\} \end{aligned} \quad (2.74)$$

where \mathcal{X} and \mathcal{Y} are symmetric Lagrange multiplier matrices.

When we take the derivative of the Lagrangian and set it equal to zero, we obtain the following equations (partial derivatives of the Lagrangian with respect to each independent variable):

$$\frac{\partial \mathcal{L}}{\partial A_c} = 2[X_{12}^T Q_{12} + X_2 Q_2 + Y_{12}^T Q_{ab} + Y_2 Q_b] = 0 \quad (2.75)$$

$$\begin{aligned} \frac{\partial \mathcal{L}}{\partial B_c} = & 2[X_{12}^T Q_1 C_{y_2}^T + X_2 Q_{12}^T C_{y_2}^T + X_{12}^T V_{12} + X_2 B_c V_2 + Y_{12}^T Q_a C_{y_\infty}^T \\ & + Y_2 Q_{ab}^T C_{y_\infty}^T + Y_{12}^T V_{ab} + Y_2 B_c V_b + (Y_{12}^T Q_a + Y_2 Q_{ab}^T) C_e^T M \\ & + (Y_{12}^T Q_{ab} + Y_2 Q_b) C_c^T D_{eu}^T M] = 0 \end{aligned} \quad (2.76)$$

$$\begin{aligned} \frac{\partial \mathcal{L}}{\partial C_c} = & 2[B_{u_2}^T X_1 Q_{12} + B_{u_2}^T X_{12} Q_2 + R_{12}^T Q_{12} + R_2 C_c Q_2 + B_{u_\infty}^T Y_1 Q_{ab} \\ & + B_{u_\infty}^T Y_{12} Q_b + R_{ab}^T Q_a Y_1 Q_{ab} + R_{ab}^T Q_a Y_{12} Q_b + R_{ab}^T Q_{ab} Y_{12} Q_{ab} \\ & + R_{ab}^T Q_{ab} Y_2 Q_b + R_b C_c Q_{ab}^T Y_1 Q_{ab} + R_b C_c Q_b Y_{12}^T Q_{ab} \\ & + R_b C_c Q_{ab}^T Y_{12} Q_b + R_b C_c Q_b Y_2 Q_b \\ & + P_1(Y_1 Q_{ab} + Y_{12} Q_b) + P_2(Y_{12}^T Q_{ab} + Y_2 Q_b)] = 0 \end{aligned} \quad (2.77)$$

$$\frac{\partial \mathcal{L}}{\partial \mathcal{X}} = \mathcal{A}_2 Q_2 + Q_2 \mathcal{A}_2^T + \mathcal{B}_w \mathcal{B}_w^T = 0 \quad (2.78)$$

$$\frac{\partial \mathcal{L}}{\partial Q_2} = \mathcal{A}_2^T \mathcal{X} + \mathcal{X} \mathcal{A}_2 + \mathcal{C}_z^T \mathcal{C}_z = 0 \quad (2.79)$$

$$\begin{aligned} \frac{\partial \mathcal{L}}{\partial \mathcal{Y}} = & \mathcal{A}_\infty Q_\infty + Q_\infty \mathcal{A}_\infty^T + (Q_\infty \mathcal{C}_e^T + \mathcal{B}_d \mathcal{D}_{ed}^T) R^{-1} (Q_\infty \mathcal{C}_e^T + \mathcal{B}_d \mathcal{D}_{ed}^T)^T \\ & + \mathcal{B}_d \mathcal{B}_d^T = 0 \end{aligned} \quad (2.80)$$

$$\begin{aligned} \frac{\partial \mathcal{L}}{\partial Q_\infty} = & (\mathcal{A}_\infty + \mathcal{B}_d \mathcal{D}_{ed}^T R^{-1} \mathcal{C}_e + Q_\infty \mathcal{C}_e^T R^{-1} \mathcal{C}_e)^T \mathcal{Y} \\ & + \mathcal{Y} (\mathcal{A}_\infty + \mathcal{B}_d \mathcal{D}_{ed}^T R^{-1} \mathcal{C}_e + Q_\infty \mathcal{C}_e^T R^{-1} \mathcal{C}_e) = 0 \end{aligned} \quad (2.81)$$

where

$$M = R^{-1} D_{ed} D_{y_d}^T \quad (2.82)$$

$$P_1 = D_{eu}^T R^{-1} D_{ed} \mathcal{B}_d^T \quad (2.83)$$

$$P_2 = D_{eu}^T M \mathcal{B}_c^T \quad (2.84)$$

$$Q_2 = \begin{bmatrix} Q_1 & Q_{12} \\ Q_{12}^T & Q_2 \end{bmatrix} \quad (2.85)$$

$$\mathcal{X} = \begin{bmatrix} X_1 & X_{12} \\ X_{12}^T & X_2 \end{bmatrix} \quad (2.86)$$

$$Q_\infty = \begin{bmatrix} Q_a & Q_{ab} \\ Q_{ab}^T & Q_b \end{bmatrix} \quad (2.87)$$

$$\mathcal{Y} = \begin{bmatrix} Y_1 & Y_{12} \\ Y_{12}^T & Y_2 \end{bmatrix} \quad (2.88)$$

$$\begin{aligned} \mathcal{B}_w \mathcal{B}_w^T &= \begin{bmatrix} B_w \\ B_c D_{yw} \end{bmatrix} \begin{bmatrix} B_w^T & D_{yw}^T B_c^T \end{bmatrix} \\ &= \begin{bmatrix} V_1 & V_{12} B_c^T \\ B_c V_{12}^T & B_c V_2 B_c^T \end{bmatrix} \end{aligned} \quad (2.89)$$

$$\begin{aligned} \mathcal{B}_d (\mathcal{D}_{ed}^T R^{-1} \mathcal{D}_{ed} + I) \mathcal{B}_d^T &= \begin{bmatrix} B_d \\ B_c D_{yd} \end{bmatrix} (\mathcal{D}_{ed}^T R^{-1} \mathcal{D}_{ed} + I) \begin{bmatrix} B_d^T & D_{yd}^T B_c^T \end{bmatrix} \\ &= \begin{bmatrix} V_a & V_{ab} B_c^T \\ B_c V_{ab}^T & B_c V_b B_c^T \end{bmatrix} \end{aligned} \quad (2.90)$$

$$\begin{aligned} \mathcal{C}_z^T \mathcal{C}_z &= \begin{bmatrix} C_z^T \\ C_c^T D_{zu}^T \end{bmatrix} \begin{bmatrix} C_z & D_{zu} C_c \end{bmatrix} \\ &= \begin{bmatrix} R_1 & R_{12} C_c \\ C_c^T R_{12}^T & C_c^T R_2 C_c \end{bmatrix} \end{aligned} \quad (2.91)$$

$$\begin{aligned} \mathcal{C}_e^T R^{-1} \mathcal{C}_e &= \begin{bmatrix} C_e^T \\ C_c^T D_{eu}^T \end{bmatrix} R^{-1} \begin{bmatrix} C_e & D_{eu} C_c \end{bmatrix} \\ &= \begin{bmatrix} R_a & R_{ab} C_c \\ C_c^T R_{ab}^T & C_c^T R_b C_c \end{bmatrix} \end{aligned} \quad (2.92)$$

These equations have yet to be solved analytically, so a numerical approach will be necessary.

Note that (2.81) has the form

$$A_y^T \mathcal{Y} + \mathcal{Y} A_y = 0 \quad (2.93)$$

where $A_y = (\mathcal{A}_\infty + \mathcal{B}_d \mathcal{D}_{ed}^T R^{-1} \mathcal{C}_e + Q_\infty \mathcal{C}_e^T R^{-1} \mathcal{C}_e)$.

There are two theorems from [SZ70] regarding this form which are relevant at this point:

Theorem 2.1.2 *If A_y is stable, then $\mathcal{Y} = 0$ is the only solution to*

$$A_y^T \mathcal{Y} + \mathcal{Y} A_y = 0 \quad (2.94)$$

This theorem tells us that if A_y is stable then $\mathcal{Y} = 0$ is the only solution to (2.81). Theorem 2.1.1 #8 tells us that if A_y is not neutrally stable, Q_∞ is not the minimal solution to (2.69). Moreover, since $\mathcal{Y} = 0$, the Lagrangian (2.74) reduces to

$$\mathcal{L} = \text{tr}[Q_2 \mathcal{C}_z^T \mathcal{C}_z] + \text{tr}\{[\mathcal{A}_2 Q_2 + Q_2 \mathcal{A}_2^T + \mathcal{B}_w \mathcal{B}_w^T] \mathcal{X}\} \quad (2.95)$$

This is the Lagrangian associated with the H_2 problem (the Lyapunov equation in the constraint must be solved to evaluate the objective which is the two-norm, see Section 2.1.1.1).

The other theorem applicable to (2.81) is:

Theorem 2.1.3 *Let A_y be neutrally stable. Then*

$$A_y^T \mathcal{Y} + \mathcal{Y} A_y = 0 \quad (2.96)$$

has infinitely many $\mathcal{Y} \geq 0$ solutions of possibly varying ranks.

This theorem says if A_y is neutrally stable, \mathcal{Y} can be nonzero. From Theorem 2.1.1 #8, Q_∞ is the minimal solution. The following theorem from [Wal94] will show how we can relate this to the original $\gamma^* \leq \gamma$ constraint.

Theorem 2.1.4 *Assume \mathcal{A}_∞ is stable and $R = (\gamma^2 I - D_{ed} D_{ed}^T) > 0$. If there exists a $Q_\infty \geq 0$ satisfying*

$$\mathcal{A}_\infty Q_\infty + Q_\infty \mathcal{A}_\infty^T + (Q_\infty \mathcal{C}_e^T + \mathcal{B}_d \mathcal{D}_{ed}^T) R^{-1} (Q_\infty \mathcal{C}_e^T + \mathcal{B}_d \mathcal{D}_{ed}^T)^T + \mathcal{B}_d \mathcal{B}_d^T = 0 \quad (2.97)$$

then the following are equivalent:

1. $\|T_{ed}\|_\infty = \gamma$
2. $(\mathcal{A}_\infty + \mathcal{B}_d \mathcal{D}_{ed}^T R^{-1} \mathcal{C}_e + Q_\infty \mathcal{C}_e^T R^{-1} \mathcal{C}_e)$ is neutrally stable

Furthermore, in this case Q_∞ is unique.

Thus, (2.81) tells us one of two things. Either:

1. $\mathcal{Y} = 0$ in which case we have the unconstrained H_2 problem ($\gamma^* = \gamma$)

or,

2. $A_y = (\mathcal{A}_\infty + \mathcal{B}_d \mathcal{D}_{ed}^T R^{-1} \mathcal{C}_e + Q_\infty \mathcal{C}_e^T R^{-1} \mathcal{C}_e)$ is neutrally stable. In this case, we are on the boundary of the original $\gamma^* \leq \gamma$ constraint and Q_∞ is the neutrally stabilizing solution to the H_∞ Riccati equation (2.81).

At this point, we follow Walker [Wal94] and fix the order of the controller to the order of the underlying H_2 problem, n_2 , or greater. We can now ask ourselves the question, what are the possible regions in which we may place the **constraint**, γ ($\|T_{ed}\|_\infty \leq \gamma$ i.e. $\gamma^* \leq \gamma$) and what is the solution (γ^*) in that region? We will look at three possible regions (see Figure 2.6).

I $\gamma < \underline{\gamma}$ There is *no* controller which can reduce the infinity-norm below $\underline{\gamma}$ (the optimal H_∞ problem). Therefore, in the mixed H_2/H_∞ problem, there is no solution for $\gamma < \underline{\gamma}$.

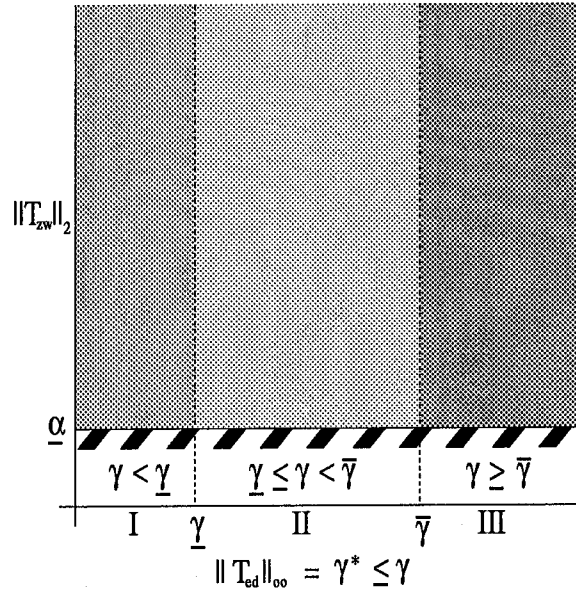


Figure 2.6 Possible regions for γ

III $\gamma \geq \bar{\gamma}$ Since the order of the controller can be equal to n_2 , $K_{2_{opt}}$ is admissible. Using the $K_{2_{opt}}$ controller, $\gamma^* = \bar{\gamma}$. Thus, for the mixed H_2/H_∞ problem with $\gamma \geq \bar{\gamma}$ the optimal controller is the H_2 optimal controller ($K_{mix} = K_{2_{opt}} \Rightarrow \gamma^* = \bar{\gamma}$). There is no possible decrease in α achievable by choosing $\gamma > \bar{\gamma}$. In fact, since α is the global minimum and the K which achieves it is unique, any forced increase in γ above $\bar{\gamma}$ will increase α .

II $\underline{\gamma} \leq \gamma < \bar{\gamma}$ Since the optimal H_∞ controller usually has a non-zero D_c term, the two-norm of the H_2 problem with the optimal H_∞ controller would be infinite. That leaves us with the only interesting region being $\underline{\gamma} < \gamma < \bar{\gamma}$. In this region, $\mathcal{Y} \neq 0$ (or we would have $\gamma^* = \bar{\gamma}$ which is a contradiction). Thus, $\mathcal{Y} \neq 0$ which we have already shown means $\|T_{ed}\|_\infty = \gamma$ ($\gamma^* = \gamma$).

These facts are summarized in the following theorem from Walker [Wal94].

Theorem 2.1.5 Assume $n_c \geq n_2$. Then the following hold:

- (i) If $\gamma < \underline{\gamma}$, no solution to the mixed H_2/H_∞ problem exists
- (ii) If $\underline{\gamma} < \gamma \leq \bar{\gamma}$, K_{mix} is such that $\gamma^* = \gamma$
- (iii) If $\gamma \geq \bar{\gamma}$, $K_{2_{opt}}$ is the solution to the mixed H_2/H_∞ problem.

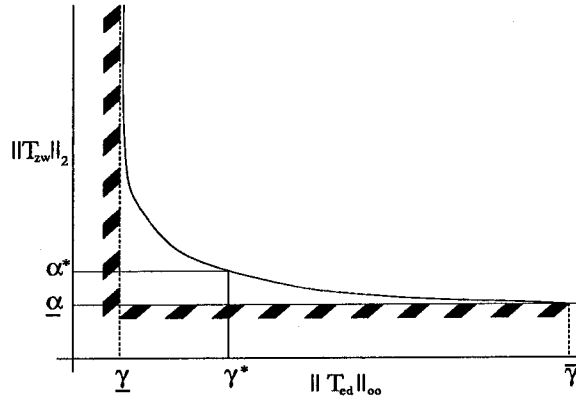


Figure 2.7 Typical mixed H_2/H_∞ γ vs. α curve

For a controller with order greater than or equal to the order of the H_2 problem, the solution to the mixed H_2/H_∞ problem with $\underline{\gamma} < \gamma \leq \bar{\gamma}$ lies on the boundary of the H_∞ constraint, $\gamma^* = \gamma$. Thus, in this region, α^* is a monotonically decreasing function of γ as shown in Figure 2.7. Unfortunately, since the solution to (2.80) must be the neutrally stabilizing solution, (2.81) becomes very difficult to handle.

2.1.3.3 Practical (Numerical) approach. As stated earlier, a numerical approach is needed to synthesize a mixed H_2/H_∞ controller. The method used in this thesis is based on Sequential Quadratic Programming (SQP). The normal approach to this problem is to compute the H_2 optimal controller (since it's easy to compute) which gives us a starting point on the curve. Then we step along the α versus γ curve by incrementally reducing γ from $\bar{\gamma}$ to near $\underline{\gamma}$. At each γ , SQP will determine the controller which minimizes α subject to the constraint $\gamma^* \leq \gamma$. When it minimizes α as much as it can (we don't know if it's a local minimum or global minimum) it puts that point on the curve and the controller is saved. More information on the program used can be found in [Smi94].

2.1.4 μ Analysis and Synthesis. Consider the problem represented in Figure 2.8. In this figure, d_p is the exogenous input, e_p is the controlled output, G is the core plant, ACT is the actuator and K is the controller. The system has uncertainties in the actuator and in the

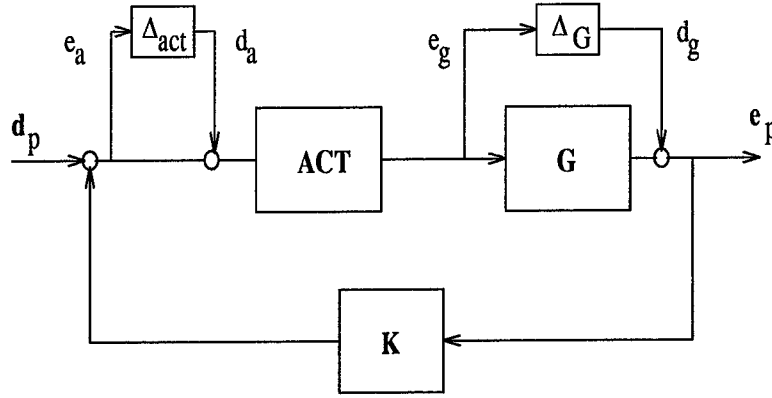


Figure 2.8 System with uncertainty

core plant itself. These uncertainties can be due to unmodelled dynamics or uncertain parameters (among other things). The actuator, as represented in Figure 2.8, is represented as having an input multiplicative uncertainty, Δ_{act} . The uncertainty in the plant, Δ_G , is represented as an additive uncertainty. We can see from the figure that there is a structure to the uncertainty (there is one kind of uncertainty for the actuator and another for the plant and the uncertainties occur at different places). The complex structured singular value, μ , allows us to use this structure to come up with a less conservative design for robustness than the standard singular value.

Figure 2.8 can be put into P-K form as in Figure 2.9. Here we see that the uncertainties are combined in a matrix format with a block diagonal structure. The input to the matrix in the Δ block is a vector made up of the two inputs to the individual uncertainty blocks in Figure 2.8. The output of the matrix in the Δ block is a vector made up of the two outputs of the uncertainty blocks in Figure 2.8. Let $\Delta \in \mathbf{\Delta}$, where $\mathbf{\Delta}$ is a set of block diagonal matrices with a given structure. There are two types of blocks for any $\Delta \in \mathbf{\Delta}$. They must either be *repeated scalar* blocks (a block which is formed by multiplying a scalar, δ , times an identity matrix of order r_i , I_{r_i}) or *full* blocks (something in every element of the block). In mathematical terms

$$\mathbf{\Delta} := \{ \text{diag}[\delta_1 I_{r_1}, \dots, \delta_S I_{r_S}, \Delta_1, \dots, \Delta_F] \mid \delta_i \in \mathcal{C}, \Delta_j \in \mathcal{C}^{m_j \times m_j} \} \quad (2.98)$$

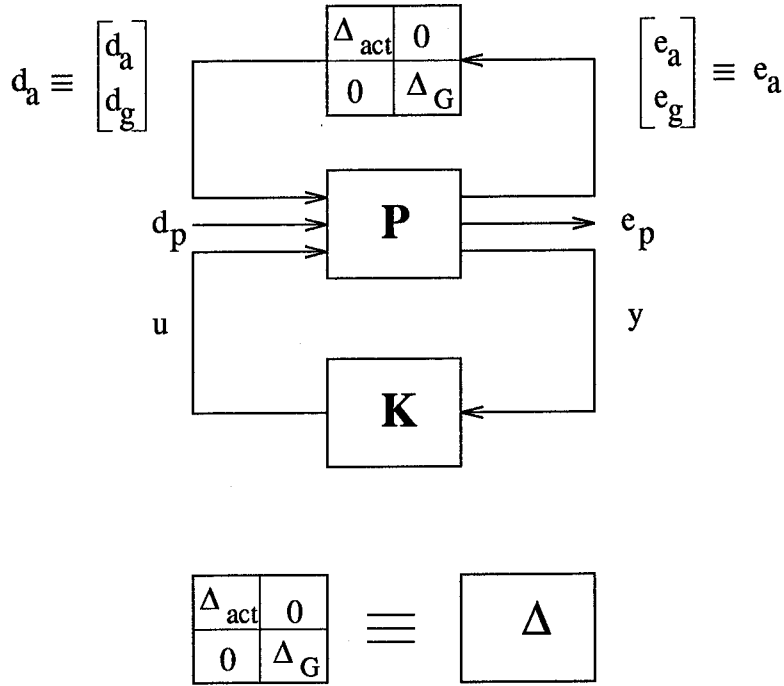


Figure 2.9 P-K version of the system with uncertainty

where $\delta_i I_{r_i}$ is the i th scalar block of order r_i and Δ_j is the j th full block of order m_j . For simplicity of development, it will be assumed that Δ is square, but the theory applies as well for non-square perturbations. The dimension n of $\Delta \in \mathbf{\Delta}$ is given by

$$n = \sum_{i=1}^S r_i + \sum_{j=1}^F m_j \quad (2.99)$$

We will eventually want to place a limit on the maximum infinity-norm that Δ can have. By doing this, we have defined a norm bounded subset of Δ .

$$\mathbf{B}_{\Delta} := \{\Delta \in \mathbf{\Delta} \mid \bar{\sigma}(\Delta) \leq \gamma^{-1}\} \quad (2.100)$$

The structured singular value of a matrix $M \in C^{n \times n}$ is defined as

$$\mu_{\Delta}(M) := \frac{1}{\min \{\bar{\sigma}(\Delta) \mid \Delta \in \mathbf{\Delta}, \det(I - M\Delta) = 0\}} \quad (2.101)$$

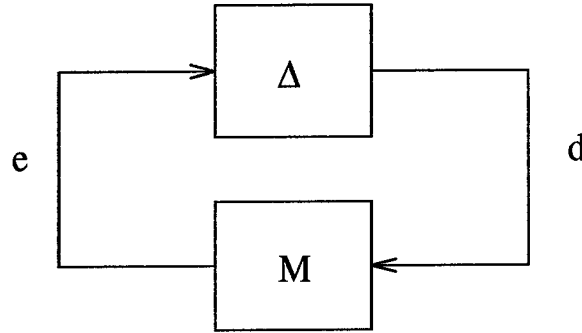


Figure 2.10 M- Δ version of a matrix with uncertainty

unless there is no $\Delta \in \Delta$ which makes $I - M\Delta$ singular, in which case $\mu_{\Delta}(M) := 0$.

[B⁺93] gives a good interpretation of μ . For the rest of this discussion on the interpretation of μ we will not be talking about dynamical systems, but simply constant matrices. Consider the system in Figure 2.10. This loop represents the following equations:

$$e = Md \tag{2.102}$$

$$d = \Delta e$$

which is the same as

$$\begin{bmatrix} I & -M \\ -\Delta & I \end{bmatrix} \begin{bmatrix} e \\ d \end{bmatrix} = \begin{bmatrix} 0 \\ 0 \end{bmatrix} \tag{2.103}$$

If $I - M\Delta$ is nonsingular, the only solutions to the loop equations are $e = d = 0$. However, if $I - M\Delta$ is singular, then there are an infinite number of solutions to (2.103), and the values of e and d can be arbitrarily large. We will call this system “unstable”. In the same way, we will call the system “stable” when the only solution to (2.103) is $e = 0, d = 0$. In this context, we see that $\mu_{\Delta}(M)$ gives us a measure of the smallest Δ which causes the system in Figure 2.10 to go “unstable”.

At this point, we don't know how to calculate μ itself (except in certain special cases which are not very useful practically). However, we can define upper and lower bounds of μ due to the following property (see [B⁺93] for a proof).

$$\rho(M) \leq \mu_{\Delta}(M) \leq \bar{\sigma}(M) \quad (2.104)$$

Unfortunately, the upper bound has been found to be too conservative. One method of reducing this conservativeness is by introducing a transformation on M that does not affect the value of $\mu_{\Delta}(M)$ but does affect $\bar{\sigma}(M)$. This requires another definition. We will define a set of scaling transfer functions \mathbf{D} which has the same block structure as Δ . This set is defined as

$$\begin{aligned} \mathbf{D} &:= \{ [D_1, \dots, D_S, d_1 I_{m_1}, \dots, d_{F-1} I_{m_{F-1}}, I_{m_F}] \mid \\ &D_i \in \mathbb{C}^{r_i \times r_i}, D_i = D_i^* > 0, d_j \in \mathbb{R}, d_j > 0 \} \end{aligned} \quad (2.105)$$

Now, the less conservative upper bound on $\mu_{\Delta}(M)$ is given by the following:

Theorem 2.1.6 *Assume $M \in \mathbb{C}^{n \times n}$, Δ is defined by (2.98), and \mathbf{D} is defined by (2.105). Then*

$$\mu_{\Delta}(M) \leq \inf_{D \in \mathbf{D}} \bar{\sigma}(DM D^{-1}) \quad (2.106)$$

Proof: See [B⁺93], Theorem 2.3.3. ■

We have now reduced the upper bound on μ to computing the maximum singular value of a matrix and a search on D .

Let the matrix M have two uncertainties which are represented by Δ_s and Δ_p (see Figure 2.11). We can partition M and Δ as follows

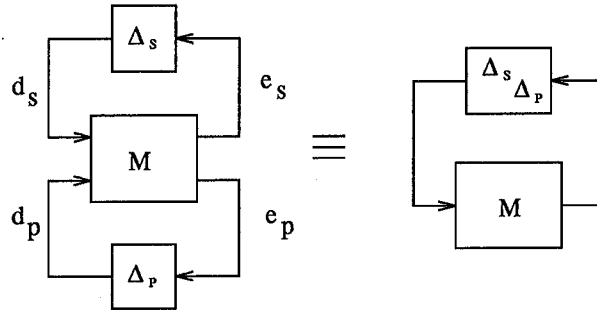


Figure 2.11 M- Δ version of a matrix with two uncertainties

$$M = \begin{bmatrix} M_{11} & M_{12} \\ M_{21} & M_{22} \end{bmatrix} \quad (2.107)$$

$$\Delta \in \Delta = \left\{ \left[\begin{array}{cc} \Delta_s & 0 \\ 0 & \Delta_p \end{array} \right] \mid \Delta_s \in \Delta_s, \Delta_p \in \Delta_p \right\} \quad (2.108)$$

We can now state a very important theorem from [PD93].

Theorem 2.1.7 (Main Loop Theorem) *The following are equivalent:*

1. $\mu_{\Delta}(M) < \gamma$
2. (a) $\mu_{\Delta_s}(M_{11}) < \gamma$, and
 (b) $\max_{\Delta_s \in \mathbf{B}\Delta_s} \mu_{\Delta_p}[F_u(M, \Delta_s)] < \gamma$

Proof: See [PD93], Corollary 4.7. ■

We can see where 2(a) comes from by looking at the following definition, which is used in 2(b)

$$F_u(M, \Delta_s) = M_{22} + M_{21}\Delta_s(I - M_{11}\Delta_s)^{-1}M_{12} \quad (2.109)$$

Item 2(a) is simply the requirement that the system be **well posed** (i.e. the inverse of $(I - M_{11}\Delta_s)$ exists).

We can see how well posed-ness is related to μ by noting 3 facts from the definition of μ .

1. μ is inversely proportional to $\bar{\sigma}(\Delta)$.
2. For $\mu \neq 0$, $(I - M\Delta)$ must be singular for some $\Delta \in \Delta$.
3. μ tells us the size of the smallest Δ which makes the system unstable.

If $\mu_{\Delta_s} < \gamma$, then $\bar{\sigma}(\Delta_s) > \gamma^{-1}$. This means that as long as $\Delta_2 \in \mathcal{B}_{\Delta_2}$, no Δ_s will destabilize the system.

2.1.4.1 Frequency Domain μ . In terms of dynamical systems, let $M(s)$ be a stable MIMO transfer function with n_d inputs and n_e outputs. Let Δ be a block structure, as in (2.98). Let \mathcal{M}_S denote the entire set of real-rational, proper, stable, transfer matrices. Associated with any block structure Δ , let $\mathcal{M}(\Delta)$ represent the set of all block diagonal, stable rational transfer functions, with block structure like Δ .

$$\mathcal{M}(\Delta) := \left\{ \Delta(\cdot) \in \mathcal{M}_S : \Delta(s) \in \mathcal{RH}_\infty \mid \Delta(s_0) \in \Delta \text{ for all } s_0 \in \overline{C}^+ \right\} \quad (2.110)$$

where \overline{C}^+ is the closed right-half complex plane.

μ of a dynamic transfer matrix $M(s)$ with the structured perturbations $\Delta(s) \in \mathcal{M}(\Delta)$ is defined by

$$\|M(s)\|_\Delta := \sup_{\omega \in \mathbb{R}} \mu_\Delta [M(j\omega)] \quad (2.111)$$

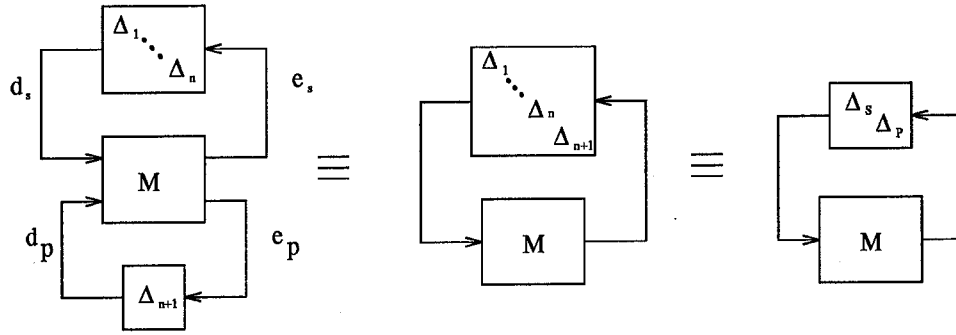


Figure 2.12 M- Δ version of the system for robust stability and robust performance

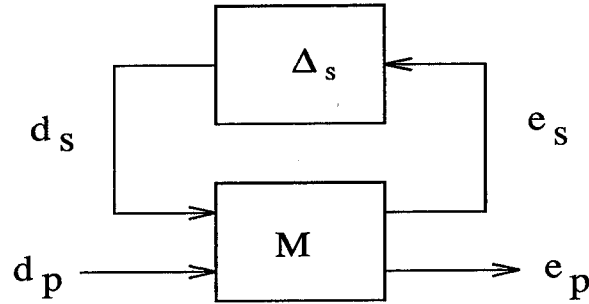


Figure 2.13 LFT system with uncertainty and exogenous inputs and outputs

Note that even though we use the norm symbol for μ , it is not a true norm since it doesn't satisfy the triangle inequality.

Now consider the dynamical system in Figure 2.12. Assume that Δ_1 through Δ_n are the model uncertainties which have been arranged into the standard block-diagonal form. The vectors e_s and d_s are made up of signals such as e_a and d_a in Figure 2.9. The vectors e_p and d_p are the vectors associated with the performance part of the problem. Now define an augmented block structure

$$\Delta := \left\{ \left[\begin{array}{cc} \Delta_S & 0 \\ 0 & \Delta_P \end{array} \right] \middle| \Delta_S \in \mathcal{M}(\Delta_S), \Delta_P \in \mathcal{M}(\Delta_P) \right\} \quad (2.112)$$

The perturbed transfer function from d_p to e_p is given by $F_u(M, \Delta_S)$ (see Figure 2.13).

The transfer function equations for Figure 2.12 are

$$\begin{bmatrix} e_s \\ e_p \end{bmatrix} = [M] \begin{bmatrix} d_s \\ d_p \end{bmatrix} = \begin{bmatrix} M_{11} & M_{12} \\ M_{21} & M_{22} \end{bmatrix} \begin{bmatrix} d_s \\ d_p \end{bmatrix} \quad (2.113)$$

Now the following theorems from [B⁺93] relate robust stability and robust performance to dynamic systems.

Theorem 2.1.8 (Robust Stability) *Let $\gamma > 0$. The loop in Figure 2.12 is well-posed and internally stable for all $\Delta_S \in \mathcal{M}(\Delta_s)$ with $\|\Delta_S\|_\infty < \gamma$ iff*

$$\|M_{11}\|_{\Delta_s} := \sup_{\omega \in \mathbb{R}} \mu_{\Delta_s} [M_{11}] \leq \frac{1}{\gamma} \quad (2.114)$$

Proof: See [B⁺93], Theorem 2.6. ■

Theorem 2.1.9 (Robust Performance) *Let $\gamma > 0$. The loop in Figure 2.12 is well-posed and internally stable, and $\|F_u(M, \Delta_S)\|_\infty \leq \frac{1}{\gamma}$ for all $\Delta_S \in \mathcal{M}(\Delta_s)$ with $\|\Delta_S\|_\infty < \gamma$ iff*

$$\|M\|_{\Delta} := \sup_{\omega \in \mathbb{R}} \mu_{\Delta} [M] \leq \frac{1}{\gamma} \quad (2.115)$$

Proof: This is Theorem 2.7 in [B⁺93]. ■

2.1.4.2 Frequency Domain μ synthesis. Recall from (2.106) that we can find an overbound to μ using the infinity-norm (in fact, for 3 or fewer full blocks in Δ , the overbound is an equality). To keep from being tedious, we will refer to the overbound of μ as μ unless the term *real μ* is used. Thus, we could attempt to use H_∞ optimization on μ (the overbound). If we make

$$M = F_l(P, K) \quad (2.116)$$

Figure 2.9 becomes Figure 2.13. Our optimization problem then becomes

$$\inf_{D \in \mathbf{D}} \inf_{K \text{ stabilizing}} \|DM D^{-1}\|_{\infty} \quad (2.117)$$

Finding a controller which gets arbitrarily close to this infimum is μ synthesis. Unfortunately, it is not known how to solve this minimization problem directly. Rather, we can approximate it by using an iterative process known as *D-K iteration*. The process is:

Step 1 Choose a set of frequencies to represent the system. Choose the scaling matrix D , defined in (2.105), which minimizes $\bar{\sigma}(DM D^{-1})$ at each of those frequencies. This is done through μ analysis software, which will give the D matrices and give the value of μ for the system. The D matrices may be dynamic or static. If dynamic, their states are added to P . This will, after H_{∞} optimization, increase the order of the controller, so choose static D 's or as low order as possible. Obviously the choice of the set of frequencies is important and must have a sufficient range and density to adequately represent the system. Usually, for the first iteration, just start with $D = I$.

Step 2 Once you have the D -scales (frequency dependent scaling matrices), fit the D -scales in magnitude with stable, minimum phase (giving stable inverse) rational functions. The result will be stable, diagonal transfer function matrices $D(s)$ that have stable inverses. It is this "best fit" which is absorbed into P . Again, it is best to get as low of an order of fit as possible.

Step 3 Once an appropriate D is chosen, use H_{∞} optimization to compute the controller $K(s)$ which minimizes $\|DM D^{-1}\|_{\infty}$.

Step 4 If μ is less than whatever value is predetermined or if you can't reduce μ any further, stop. If not, go to Step 1.

In general, each Δ in $\mathbf{\Delta}$ will have its own D matrix. MATLAB's μ Toolbox will not find a D matrix for the last block. The reason is explained in [B⁺93].

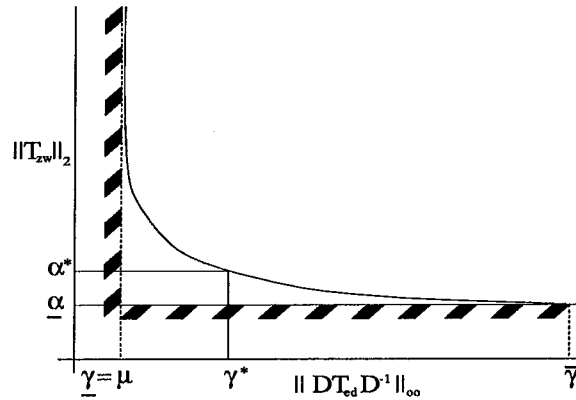


Figure 2.14 Mixed H_2/μ curve

2.1.5 Mixed H_2/μ Control. H_2/μ is just H_2/H_∞ with a twist. The theoretical framework for H_2/μ was laid out in Section 2.1.3. This section will just discuss the practical differences. H_2 is done as before, but now the H_∞ part of the problem is scaled by the D matrices mentioned in Section 2.1.4.

First, μ synthesis is done on the portion of the problem that deals with the uncertainties and any energy-to-energy part of the problem. Normally, we would only be interested in the resulting controller. However, now we are interested in the D scales. These D scales will be absorbed into the open loop P of the H_∞ problem, and *that* will be our new H_∞ problem. It will be from that P that we will do the H_∞ calculations. Other than that, there is no difference from H_2/H_∞ . For notational purposes, refer to Figure 2.14.

2.2 Control Preliminaries

2.2.1 Dynamic Inversion. Dynamic inversion is described in [LS88] and a short summary is in [ABSB92]. This summary is paraphrased here.

Dynamic inversion, as will be used in this thesis, will allow us to develop a control law which will make a given system have approximately the same dynamics as a desired system. The nonlinear aircraft dynamics can take the form

$$\dot{x} = f(x, u) \quad (2.118)$$

$$y = Cx \quad (2.119)$$

where x is an $(n \times 1)$ state vector, u is an $(m \times 1)$ input vector and C is a $(p \times n)$ constant matrix.

To use inverse dynamics as described in [LS88], our equations must be in the following form

$$\dot{x} = A(x) + B(x)u \quad (2.120)$$

$$y = C(x) \quad (2.121)$$

where $A(x)$ is an $(n \times 1)$ vector and $B(x)$ is an $(n \times m)$ matrix. To transform (2.118) and (2.119) into (2.120) and (2.121), we can augment the system dynamics with derivatives of appropriate control inputs. To get the inverse dynamics of (2.120) and (2.121) we differentiate each of the elements of y until a term containing a u appears. Since only m outputs can be controlled independently by m inputs, we will assume that $p = m$. We can now represent our equations as

$$y^{[d]} = \begin{bmatrix} y_1^{[d_1]} \\ y_2^{[d_2]} \\ \vdots \\ y_p^{[d_p]} \end{bmatrix} = h(x) + g(x)u \quad (2.122)$$

where $y_i^{d_i}$ is the d_i th derivative of the output y_i . We will use ν to represent the output of the desired dynamics. By setting $\nu = y^{[d]}$, we can develop the inverse dynamics control law.

$$u = g(x)^{-1}(\nu - h(x)) \quad (2.123)$$

2.2.2 Control Selector. The flight control system in this thesis will have as a result of the pilot commanded inputs what will be called generalized commands. These will be the commands from the controller, K and will be rotational rate commands for the corresponding actuators (for example, pitch rate corresponds to the elevators — the pilot doesn't care what his actuators are commanded to do, as long as they give him the desired pitch rate). A control selector will be used in this thesis to transform generalized rotational rate commands, δ^* , into actuator position commands, δ . However, we want the contribution of δ^* to the system to be the same as the corresponding δ . In other words, we want

$$B\delta = B^*\delta^* \quad (2.124)$$

There are cases where different actuators combine to produce a desired effect. For instance, an aircraft with asymmetric horizontal tail and asymmetric flaps (as the VISTA F-16 has) could use both control surfaces to achieve a desired roll rate. Put another way, both control surfaces combine to form, in effect, an aileron. The VISTA F-16 is just such an aircraft [ABSB92]. This thesis will focus on the lateral/directional part of the VISTA F-16. The control surfaces used are asymmetric horizontal tail, asymmetric flaps, and rudder. This is represented as

$$\delta_{TFR} = \begin{bmatrix} \delta_{DT} \\ \delta_{DF} \\ \delta_R \end{bmatrix} \quad (2.125)$$

However, we can capture the effects described above by combining asymmetric horizontal tail and asymmetric flaps into a single effective control which we will call aileron (δ_A).

$$\delta_{TFR} = N \begin{bmatrix} \delta_A \\ \delta_R \end{bmatrix} = N \delta_{AR} \quad (2.126)$$

Now, substituting (2.126) into (2.124) and solving for δ_{AR} gives

$$\delta_{AR} = (BN)^{\#} B^* \delta_{AR}^* \quad (2.127)$$

The operator $(\cdot)^{\#}$ represents the left pseudo-inverse of (\cdot) . Since our real actuators are δ_{TFR} , we need to substitute (2.127) into (2.126)

$$\delta_{TFR} = T \delta_{AR}^* \quad (2.128)$$

where

$$T = N(BN)^{\#} B^* \quad (2.129)$$

which is the equation which relates our generalized controls, δ_{AR}^* (hereafter known as δ^*) to our actual controls δ_{TFR} (hereafter known as δ). Note that B is function of flight condition. Thus, the control selector (T) is a function of flight condition (Mach number, altitude, and angle of attack) as well.

III. F-16 Design Example

The example used in this thesis will be a manual flight control system for the lateral/directional axis of the VISTA F-16 test vehicle. The basic problem was taken from [ABSB92]. The first section of this chapter will give a brief overview of their design. In Section 3.2 we will delve into the details (define equations of motion, actuator, develop K_{eq} , etc.), and introduce noise into the system. The result will be the basic design model. This design model will not be complete. To complete it we will have to select the inputs we will concern ourselves with, then select the outputs we wish to minimize and weight them if necessary. This is done in Chapters 4 and 5. In Section 3.3 we will highlight the differences between the design model and the evaluation model we will use. The evaluation model will not be used to simulate the system with uncertain parameters. The assumption is made that the designed system will be given sufficient robustness to handle parameter variations. To evaluate the robustness, a robust analysis model will be developed in Section 3.4.

3.1 Overview

The basic design was taken from [ABSB92]. They design a 2-degree-of-freedom, manual flight control system for the lateral/directional axis of the VISTA F-16. The block diagram of this basic design is found in Figure 3.1. A key element of their design is the use of an "inner equalization loop" containing the controller K_{eq} . The purpose of this loop is to reduce the amount of gain scheduling required by making "the input/output behavior of the closed loop system uniform for all operating conditions by using a nonlinear static feedback matrix $[K_{eq}]$ " [ABSB92:page 44]. In other words, they try to make the outer loop see the same desired dynamics from the inner loop no matter what the flight condition. This is done through K_{eq} , which is formed using dynamic inversion [ABSB92:pages 28-29,53-55]. It is dependent on flight condition and can be found using table-look-up methods.

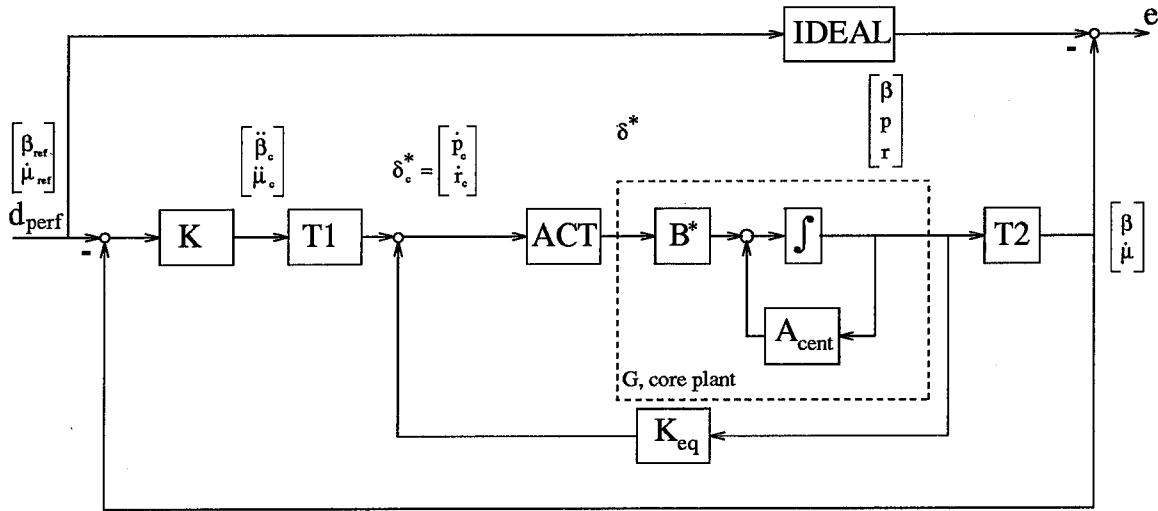


Figure 3.1 Basic Design Model of the VISTA F-16

The inputs to the system are the pilot generated commands (or references) β_{ref} (sideslip angle about the stability axis) and $\dot{\mu}_{ref}$ (roll rate about the stability axis). The commands are differenced with the corresponding outputs of the system and fed into the controller, K . The outputs of the controller are $\ddot{\beta}_c$ (yaw acceleration command about the stability axis) and $\ddot{\mu}_c$ (roll acceleration command about the stability axis). These are then input into a transformation matrix $T1$ which transforms from the stability axis to the body axis.

The output of $T1$ enters the inner loop and, when combined with the output of K_{eq} , is converted to the generalized commands \dot{p}_c (roll acceleration command) and \dot{r}_c (yaw acceleration command) both in the body axis. The outputs of the inner loop are the states of the core plant (in the body axis) β (sideslip angle), p (roll rate) and r (yaw rate). These are fed into $T2$ which transforms from the body axis to the stability axis.

3.2 Details

3.2.1 Lateral/Directional Equations of Motion. The equations of motion for the linear model are represented in state space as:

$$\begin{bmatrix} \dot{\beta} \\ \dot{p} \\ \dot{r} \end{bmatrix} = \begin{bmatrix} Y_{\beta} & \sin \alpha & -\cos \alpha \\ L_{\beta} & L_p & L_r \\ N_{\beta} & N_p & N_r \end{bmatrix} \begin{bmatrix} \beta \\ p \\ r \end{bmatrix} + \begin{bmatrix} Y_{\delta DT} & Y_{\delta DF} & Y_{\delta R} \\ L_{\delta DT} & L_{\delta DF} & L_{\delta R} \\ N_{\delta DT} & N_{\delta DF} & N_{\delta R} \end{bmatrix} \begin{bmatrix} \delta_{DT} \\ \delta_{DF} \\ \delta_R \end{bmatrix} \quad (3.1)$$

The parameters in this equation are a function of flight condition (Mach number, altitude and angle of attack). Only one flight condition will be used in this thesis. That flight condition is the *central* flight condition. *Central* just means that the flight condition was at some dynamic pressure between the minimum and maximum values for the design envelope. The flight condition chosen as central corresponds to $V = 622.43 \text{ ft/sec}$, $\alpha = 4.3^\circ$ at an altitude of 20,000 ft. The A and B matrices associated with this condition are found in Appendix A. Engineering judgement was used in choosing the *central* flight condition.

The "states" which we are ultimately interested in controlling are β and $\dot{\mu}$. These will be compared to the reference signal from the pilot and entered into the outer loop controller, K . β is one of the states of the core plant. The stability axis roll rate, $\dot{\mu}$, can be found from

$$\dot{\mu} = p \cos \alpha + r \sin \alpha \quad (3.2)$$

Another output which we may be interested in is n_y , the lateral acceleration in g's. This can be determined from:

$$n_y = \frac{V}{g}(\dot{\beta} + r) \quad (3.3)$$

$$n_y = \frac{V}{g} \begin{bmatrix} Y_\beta & \sin \alpha & (1 - \cos \alpha) \end{bmatrix} \begin{bmatrix} \beta \\ p \\ r \end{bmatrix} \quad (3.4)$$

3.2.2 Control Selector. Recall from Section 2.2.2 that T (the control selector) transforms the generalized rotational rate commands, δ^* , into the actual actuator position commands, δ . Our generalized commands are actually rate commands (p and r), so our generalized rate commands are rotational acceleration commands \dot{p}_c and \dot{r}_c . The control effectiveness matrix for δ is:

$$B = \begin{bmatrix} Y_{\delta DT} & Y_{\delta DF} & Y_{\delta R} \\ L_{\delta DT} & L_{\delta DF} & L_{\delta R} \\ N_{\delta DT} & N_{\delta DF} & N_{\delta R} \end{bmatrix} \quad (3.5)$$

The control effectiveness matrix for δ^* is:

$$B^* = \begin{bmatrix} 0 & 0 \\ 1 & 0 \\ 0 & 1 \end{bmatrix} \quad (3.6)$$

The generalized rate commands, δ^* , are the body axis roll acceleration command, \dot{p}_c , and body axis yaw acceleration command, \dot{r}_c . By substituting the B from (3.1) into (2.124), we see that

$$B\delta = \begin{bmatrix} Y_{\delta DT} & Y_{\delta DF} & Y_{\delta R} \\ L_{\delta DT} & L_{\delta DF} & L_{\delta R} \\ N_{\delta DT} & N_{\delta DF} & N_{\delta R} \end{bmatrix} \begin{bmatrix} \delta_{DT} \\ \delta_{DF} \\ \delta_R \end{bmatrix} = \begin{bmatrix} 0 & 0 \\ 1 & 0 \\ 0 & 1 \end{bmatrix} \begin{bmatrix} \dot{p}_c \\ \dot{r}_c \end{bmatrix} = B^*\delta^* \quad (3.7)$$

Recall from (2.129) that the control selector is :

$$T = N(BN)^{\#} B^*$$

It was found that by choosing the N in (2.129) to be the identity matrix, unreasonable control deflections would occur [ABSB92]. This problem can be prevented by combining the asymmetric flaps and asymmetric horizontal tail into a single effective control as described in Section 2.2.2. This effective control was the “aileron”. Thus, N fixes the proportion between asymmetric horizontal tail and asymmetric flap commands for the effective aileron. Since the horizontal tail’s primary purpose is pitch control, a ratio of 1/4 was used [ABSB92].

N was chosen to be

$$N = \begin{bmatrix} 0.25 & 0.0 \\ 1.0 & 0.0 \\ 0.0 & 1.0 \end{bmatrix} \quad (3.8)$$

This choice was an engineering judgement decision.

3.2.3 Inner Loop Design. In this section we will use the information found in Sections 2.2.1 and 2.2.2 to form the inner loop controller, K_{eq} .

With the control selector implemented and neglecting actuator dynamics, the equations of motion are:

$$\begin{bmatrix} \dot{\beta} \\ \dot{p} \\ \dot{r} \end{bmatrix} = \begin{bmatrix} Y_{\beta} & \sin \alpha & -\cos \alpha \\ L_{\beta} & L_p & L_r \\ N_{\beta} & N_p & N_r \end{bmatrix} \begin{bmatrix} \beta \\ p \\ r \end{bmatrix} + \begin{bmatrix} 0 & 0 \\ 1 & 0 \\ 0 & 1 \end{bmatrix} \begin{bmatrix} \dot{p}_c \\ \dot{r}_c \end{bmatrix} \quad (3.9)$$

Note that our inner loop is full state feedback, so our outputs are:

$$Y = \begin{bmatrix} 1 & 0 & 0 \\ 0 & 1 & 0 \\ 0 & 0 & 1 \end{bmatrix} \begin{bmatrix} \beta \\ p \\ r \end{bmatrix} \quad (3.10)$$

Now we want to use inverse dynamics to form K_{eq} . We can see that by taking the derivative of (3.10) once, we get (3.9) back and we have both of the controls appearing in the output equations.

$$\begin{bmatrix} \dot{\beta} \\ \dot{p} \\ \dot{r} \end{bmatrix} = \overbrace{\begin{bmatrix} Y_{\beta} & \sin \alpha & -\cos \alpha \\ L_{\beta} & L_p & L_r \\ N_{\beta} & N_p & N_r \end{bmatrix}}^{h(x)} \begin{bmatrix} \beta \\ p \\ r \end{bmatrix} + \overbrace{\begin{bmatrix} 0 & 0 \\ 1 & 0 \\ 0 & 1 \end{bmatrix}}^{g(x)} \begin{bmatrix} \dot{p}_c \\ \dot{r}_c \end{bmatrix} \quad (3.11)$$

We now have the form in (2.122),

$$y^{[d]} = h(x) + g(x)u$$

However, we have more outputs than inputs which violates the assumption in Section 2.2.1. We can see why this is so important by naively continuing on. By taking the left-inverse of $g(x)$ which is, in our case, the left-inverse of B^* , we can form our version of (2.123).

We then have

$$\begin{bmatrix} \dot{\beta}_c \\ \dot{p}_c \\ \dot{r}_c \end{bmatrix} = \begin{bmatrix} 0 & 1 & 0 \\ 0 & 0 & 1 \end{bmatrix} \left(\nu - \begin{bmatrix} Y_{\beta} & \sin \alpha & -\cos \alpha \\ L_{\beta} & L_p & L_r \\ N_{\beta} & N_p & N_r \end{bmatrix} \begin{bmatrix} \beta \\ p \\ r \end{bmatrix} \right) \quad (3.12)$$

We immediately see that we have an incongruity in dimensions. The left side is (3×1) but the product on the right side is (2×1) .

The 2 outputs, p and r represent the dominant fast dynamics of the open loop system [ABSB92]. By limiting ourselves to p and r , we represent the system well and meet the assumption that the number of outputs equal the number of inputs.

(3.10) then becomes

$$Y = \begin{bmatrix} p \\ r \end{bmatrix} = \begin{bmatrix} 0 & 1 & 0 \\ 0 & 0 & 1 \end{bmatrix} \begin{bmatrix} \beta \\ p \\ r \end{bmatrix} \quad (3.13)$$

After we differentiate once, we get

$$\begin{bmatrix} \dot{p} \\ \dot{r} \end{bmatrix} = \begin{bmatrix} L_\beta & L_p & L_r \\ N_\beta & N_p & N_r \end{bmatrix} \begin{bmatrix} \beta \\ p \\ r \end{bmatrix} + \begin{bmatrix} 1 & 0 \\ 0 & 1 \end{bmatrix} \begin{bmatrix} \dot{p}_c \\ \dot{r}_c \end{bmatrix} \quad (3.14)$$

which is the correct form found in (2.122).

This makes our real inverse dynamics control law

$$\begin{bmatrix} \dot{p}_c \\ \dot{r}_c \end{bmatrix} = \begin{bmatrix} 0 & 1 & 0 \\ 0 & 0 & 1 \end{bmatrix} \left(\nu - \begin{bmatrix} L_\beta & L_p & L_r \\ N_\beta & N_p & N_r \end{bmatrix} \begin{bmatrix} \beta \\ p \\ r \end{bmatrix} \right) \quad (3.15)$$

Note that the $\dot{\beta}$ dynamics are not represented in (3.14). This will cause the inner loop equalization to be less than perfect.

Remember that ν is the matrix which represents the desired linear dynamics. This is obviously an important step in the control synthesis for the inner equalization loop. A linear quadratic regulator design was performed at the *central* flight condition described in Section 3.2.1. The desired dynamics for the dynamic inversion calculations are the regulated dynamics at this flight condition.

$$A_{nom} = (A_{central} - B^* K_{LQ}) \quad (3.16)$$

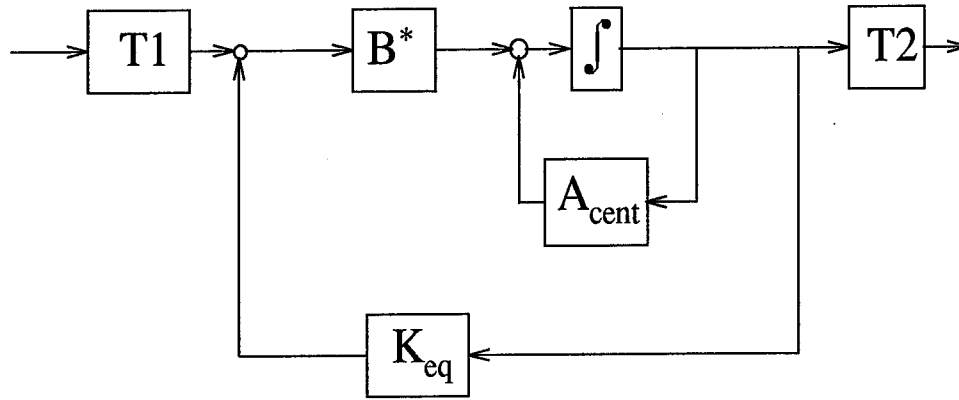


Figure 3.2 Design Block Diagram of the Inner Loop

$$\nu = \begin{bmatrix} A_{nom_{21}} & A_{nom_{22}} & A_{nom_{23}} \\ A_{nom_{31}} & A_{nom_{32}} & A_{nom_{33}} \end{bmatrix} \begin{bmatrix} \beta \\ p \\ r \end{bmatrix} \quad (3.17)$$

The compensator for the inner equalization loop can be represented as a linear state feedback compensator of the form.

$$\begin{bmatrix} \dot{p} \\ \dot{r} \end{bmatrix} = K_{eq} \begin{bmatrix} \beta \\ p \\ r \end{bmatrix} \quad (3.18)$$

where

$$K_{eq} = \begin{bmatrix} A_{nom_{21}} - L_{\beta} & A_{nom_{22}} - L_p & A_{nom_{23}} - L_r \\ A_{nom_{31}} - N_{\beta} & A_{nom_{32}} - N_p & A_{nom_{33}} - N_r \end{bmatrix} \quad (3.19)$$

The aerodynamic parameters in (3.19) are stored in a database for future table lookup.

Note that the description of the design of K_{eq} above corresponds to the block diagram of the inner loop found in Figure 3.2. The most notable feature of this block diagram is that it has no actuator dynamics. On top of that, it uses the generalized version of B . This will be one source of error between the design model and the evaluation model.

3.2.4 Actuator. In the design of the outer loop controller, K , we will include a model of the actuator. The actuator model used in the design model is a linear system which is based on the generalized commands. We are simulating a "generalized actuator". Just as a real actuator takes control deflection commands and produces actual control deflections, this "generalized actuator" will take the rotational acceleration commands and produce rotational accelerations. This is represented in transfer function matrix form as

$$\delta^*(s) = \frac{(19.7)(65.0)^2}{(s + 19.7)(s^2 + 2(0.71)(65.0)s + (65.0)^2)} I_{2 \times 2} \delta_{com}^*(s) \quad (3.20)$$

This is the actuator which has been used in previous work [ABSB92]. However, to simplify things and reduce the order even further, we will use an even more simplified model.

$$\delta^*(s) = \frac{19.7}{(s + 19.7)} \delta_{com}^*(s) \quad (3.21)$$

This corresponds to the state space representation found in Appendix A.

3.2.5 T1 and T2. As already described, T1 and T2 are the transformation matrices between the stability axis and the body axis. These are a function of angle of attack, α , and are defined as

$$T1 = \begin{bmatrix} \sin \alpha & \cos \alpha \\ -\cos \alpha & \sin \alpha \end{bmatrix} \quad (3.22)$$

$$T2 = \begin{bmatrix} 1 & 0 & 0 \\ 0 & \cos \alpha & \sin \alpha \end{bmatrix} \quad (3.23)$$

Since $\alpha = 4.3^\circ$ at our central flight condition,

$$T1 = \begin{bmatrix} 7.4979e-02 & 9.9719e-01 \\ -9.9719e-01 & 7.4979e-02 \end{bmatrix}$$

$$T2 = \begin{bmatrix} 1.0000e+00 & 0 & 0 \\ 0 & 9.9719e-01 & 7.4979e-02 \end{bmatrix}$$

Note that by regulating in the stability axis, the control will have a dependence on angle of attack that will eliminate some of the need for gain scheduling with α .

3.2.6 The Ideal Model. The ideal model of the desired aircraft response to pilot inputs will drive the flying qualities aspect of the design. The ideal model is made from the ideal low order equivalent system transfer function parameters. We will include the flying qualities in the design process by forcing the complementary sensitivity transfer function to take the frequency response shape (the loop shape) of this ideal model.

The *ideal* loop is just to give us a reference so we can see how well we tracked the *ideal* model. It is not on the actual aircraft, although it could be. To effectively use such a model following system in that manner would be an adaptive control type procedure which is out of the scope of this thesis. The *ideal model* for this design has the form

$$\frac{\beta}{\beta_c} = \frac{\omega_D^2}{s^2 + 2\zeta_D\omega_D^2 s + \omega_D^2} \quad (3.24)$$

$$\frac{\dot{\mu}}{\dot{\mu}_c} = \frac{1/T_R}{(s + 1/T_R)} \quad (3.25)$$

where ω_D is the desired Dutch roll frequency, ζ_D is the desired Dutch roll damping, and T_R is the desired roll mode time constant. Note that in the ideal model, we are not allowing for coupling between sideslip and roll rate. Not only does the ideal model provide the desired flying qualities, but it will force the design to attempt to decouple the responses.

For this thesis, the ideal model parameters are $\omega_D = 3.0$ rad/s, $\zeta_D = 0.71$, and $T_R = 0.33$ seconds. The state space representation of the ideal model using the above parameters can be found in Appendix A.

3.2.7 Noises. We will attempt to design for robustness, noise and disturbance rejection. The sensor noises and the wind gust (disturbance) will be modeled as white, Gaussian noise inputs which are taken through coloring filters to more realistically represent the class of noises.

3.2.7.1 Wind. The wind gust “noise” isn’t actually a white noise (uniform energy across all frequencies) , but more of a colored noise (more energy in one set of frequencies than in others). Most of its energy is at low frequencies, so the wind gust is passed through a low-pass filter to be represented more accurately. The filter chosen here was taken from [Bai92]. The filter is represented in the frequency domain as:

$$W_g = \frac{0.0187k_g}{(s + 6.7)} \quad (3.26)$$

The wind gust enters the system as a perturbation in β . This is effectively accomplished by multiplying the filtered wind times the first column of the A matrix of the plant and adding this to the states. The first column of A will be denoted by Γ .

3.2.7.2 Sensors. There are three sensors in the system which measure the states of the core plant. Sensor noise is a high frequency type noise. To model the sensor noise, a white Gaussian noise is taken through a high pass filter. This is done for each of the three sensors. The transfer function is:

$$W_s = \frac{0.08(s + 0.01)}{(s + 10)} K_s \quad (3.27)$$

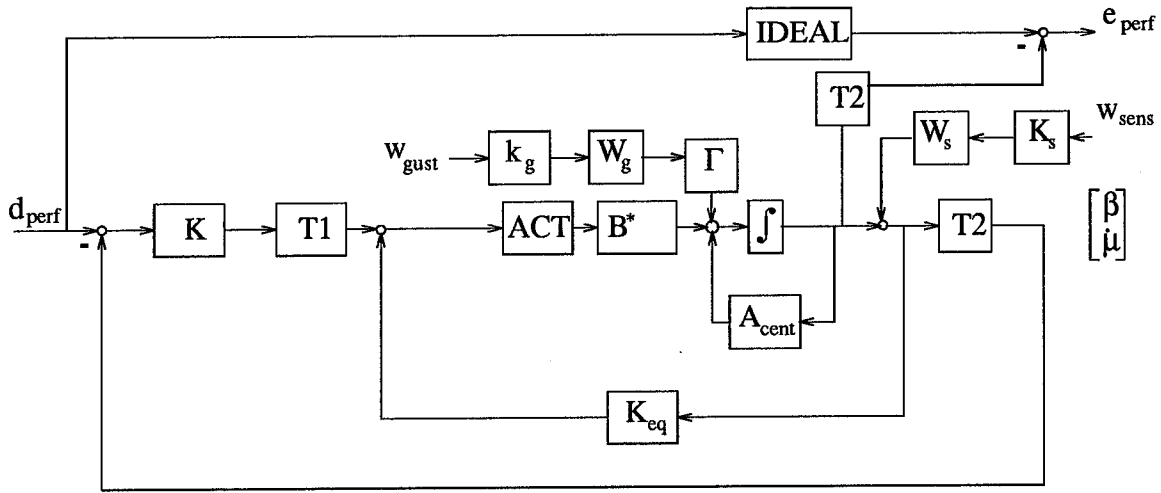


Figure 3.3 Design Block Diagram of the VISTA F-16 with Noise

where

$$K_s = \begin{bmatrix} k_{s_b} & 0 & 0 \\ 0 & k_{s_p} & 0 \\ 0 & 0 & k_{s_r} \end{bmatrix} \quad (3.28)$$

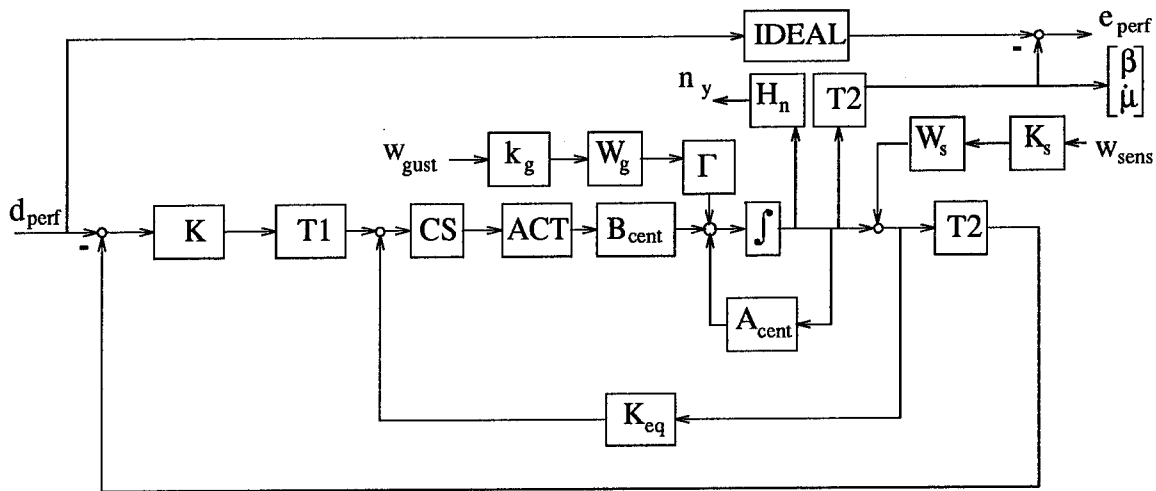
k_b , k_p , and k_r are the gains for the β , p , and r sensor noise respectively.

The noise gains k_g and K_s are the “design knobs” used in designing an H_2 controller. They will also be used to develop a simulation model of the noise, which will be discussed later.

Figure 3.3 shows the design model with noise. Note that except for e_{perf} , this figure has none of the outputs or weightings associated with an actual design problem. The main purpose here is to highlight the difference between the design and evaluation models. Later, when we design an outer loop controller, we will choose what outputs we wish to minimize and their associated weightings.

3.3 Evaluation Model

The evaluation model for this example is shown in Figure 3.4. One of the main differences here when compared to the design model are the actuators. The actuators in the aircraft are not the generalized actuators used in the design. They are the actuators for the differential tail, the



differential flaps and the rudder. The model for the actuators is now

The control selector will be used to convert from δ_c^* to δ_{TFR_c} and will be required prior to the actuator. Of course, the evaluation model will not recognize that we designed K_{eq} for a perfect actuator (ACT = I). Therefore, there are enough differences between the design and the evaluation model that the controller we design (K) will have to be fairly robust to handle the differences between the two models.

To choose K_s , the open loop system was simulated with $k_g = 1$ using various K_s 's. The noisy responses were compared with the noiseless responses to get a good ratio. Again, the goal was to get responses which weren't too outrageous but were big enough to see improvements in the

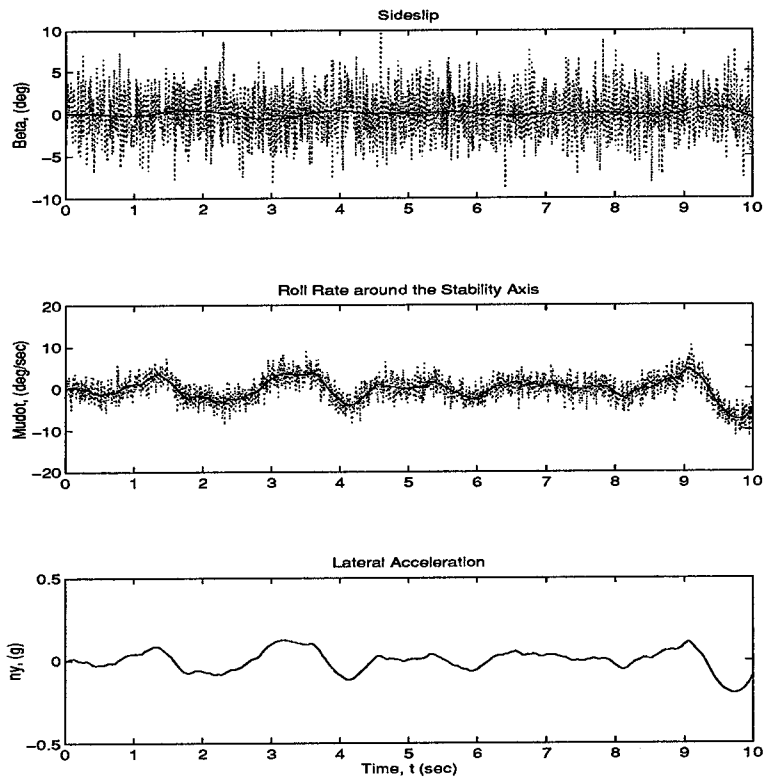


Figure 3.5 Wind Gust (solid) compared to Sensor Noise (dashed)

subsequent designs (hopefully). The values finally chosen were :

$$k_g = 1 \quad K_s = \begin{bmatrix} 0.04 & 0 & 0 \\ 0 & 0.03 & 0 \\ 0 & 0 & 0.01 \end{bmatrix}$$

See Figure 3.5 to get an idea of the size of the sensor noise compared to the wind gust. To get a feel for the response of the system to the wind gust and noise, see Figure 3.6. We can see that the noise produces a fairly strong response especially in $\dot{\mu}$ ($\approx 9^\circ/sec$) and n_y ($0.25 g$'s). β is not too bad at $\approx 1^\circ$. This noise is strong enough that we should be able to see a difference in the design.

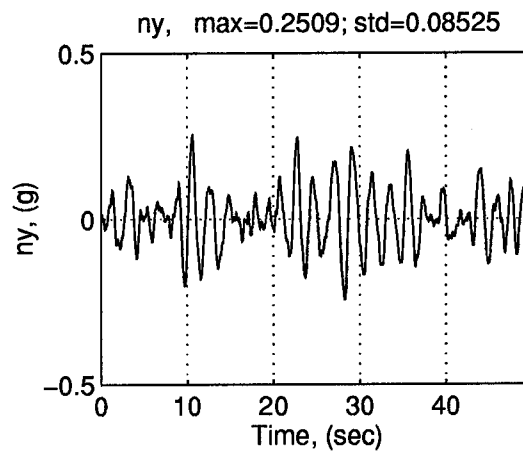
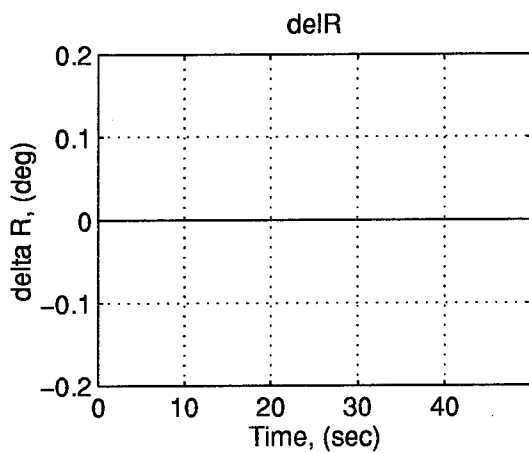
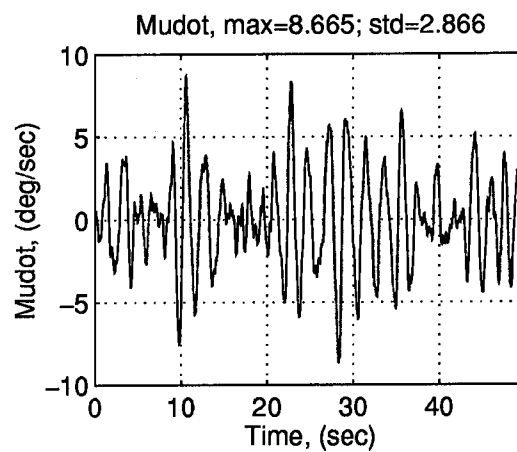
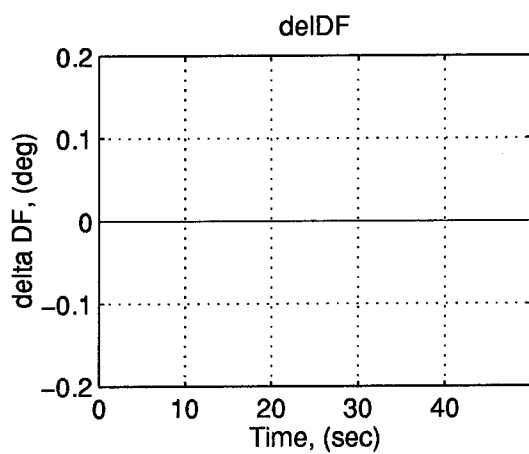
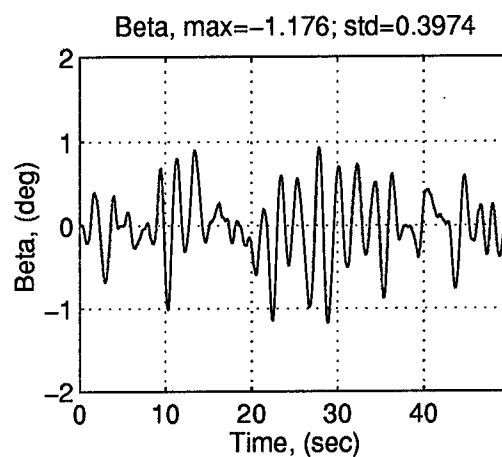
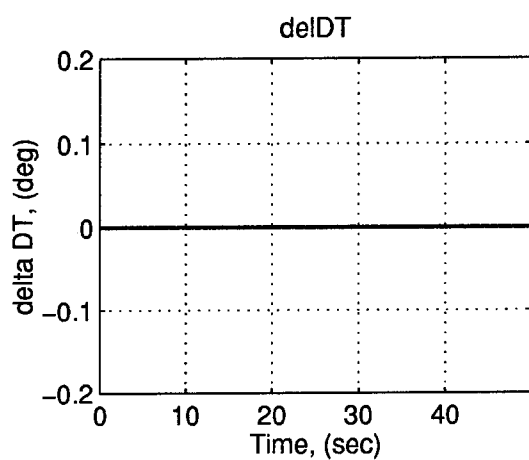


Figure 3.6 Open Outer Loop Response to Wind Gust and Sensor Noise, angles in degrees

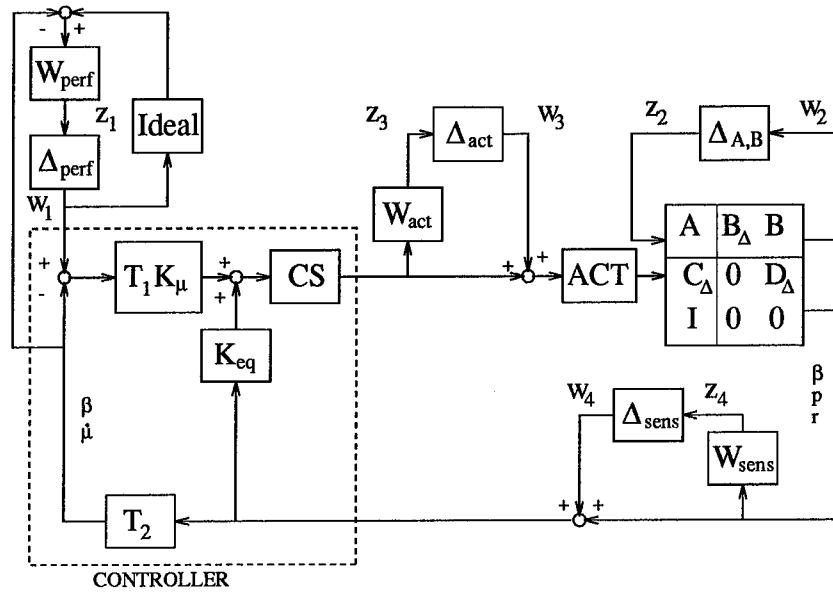


Figure 3.7 Robust Analysis Model for the VISTA F-16

3.4 Robust Analysis Model

To analyze the robustness of our controllers, a robust analysis model developed in [ABSB92] was used; see Figure 3.7. This model will analyze the ability of the controller, K , to handle the structured uncertainty in the plant, $(\Delta_{A,B})$, unstructured uncertainty in the actuator (Δ_{act}) and the sensors (Δ_{sens}) , and the performance (Δ_{perf}) . Following [ABSB92], robust stability analysis is performed on the $\Delta_{A,B}$, Δ_{act} , and Δ_{sens} blocks separately due to the lack of highly accurate models for the different uncertainties. Robust performance analysis is performed on all four blocks together (the four blocks are combined into one large block).

3.4.1 Structured Uncertainty. The plant uncertainty, represented as structured uncertainty, is driven by perturbations in aerodynamic parameters. As in [ABSB92], seven stability derivatives and seven control derivatives are identified for robustness analysis. The perturbed state equations can be written as:

$$\dot{x} = (A + \Delta A)x + (B + \Delta B)u \quad (3.30)$$

where

$$\Delta A = \begin{bmatrix} \Delta Y_\beta & 0 & 0 \\ \Delta L_\beta & \Delta L_p & \Delta L_r \\ \Delta N_\beta & \Delta N_p & \Delta N_r \end{bmatrix} \quad (3.31)$$

$$\Delta B = \begin{bmatrix} \Delta Y_\beta & 0 & 0 \\ \Delta L_\beta & \Delta L_p & \Delta L_r \\ \Delta N_\beta & \Delta N_p & \Delta N_r \end{bmatrix} \quad (3.32)$$

Now, incorporating the $\Delta_{A,B}$ block, we can rewrite the system equations as:

$$\dot{x} = Ax + Bu + B_\Delta \Delta_{A,B} z_2 \quad (3.33)$$

$$z_2 = C_\Delta x + D_\Delta u \quad (3.34)$$

When $\bar{\sigma}(\Delta_{A,B}) \leq 1$, we can represent the maximum uncertainty in the system matrices as:

$$\Delta A = B_\Delta C_\Delta \quad (3.35)$$

$$\Delta B = B_\Delta D_\Delta \quad (3.36)$$

where

$$B_\Delta = \begin{bmatrix} 1 & 0 & 0 & 0 & 0 & 0 & 0 & 0 & 0 & 0 & 0 & 1 & 0 & 0 \\ 0 & 1 & 0 & 1 & 0 & 1 & 0 & 1 & 0 & 1 & 0 & 0 & 1 & 0 \\ 0 & 0 & 1 & 0 & 1 & 0 & 1 & 0 & 1 & 0 & 1 & 0 & 0 & 1 \end{bmatrix} \quad (3.37)$$

$$C_{\Delta} = \begin{bmatrix} \Delta Y_{\beta} & 0 & 0 \\ \Delta L_{\beta} & 0 & 0 \\ \Delta N_{\beta} & 0 & 0 \\ 0 & \Delta L_p & 0 \\ 0 & \Delta N_p & 0 \\ 0 & 0 & \Delta L_r \\ 0 & 0 & \Delta N_r \\ 0_{7 \times 3} \end{bmatrix} \quad (3.38)$$

$$D_{\Delta} = \begin{bmatrix} 0_{7 \times 3} \\ \Delta L_{\delta DT} & 0 & 0 \\ \Delta N_{\delta DT} & 0 & 0 \\ 0 & \Delta L_{\delta DF} & 0 \\ 0 & \Delta N_{\delta DF} & 0 \\ 0 & 0 & \Delta Y_{\delta R} \\ 0 & 0 & \Delta L_{\delta R} \\ 0 & 0 & \Delta N_{\delta R} \end{bmatrix} \quad (3.39)$$

The level of uncertainty for the parameters at each flight condition is represented as a percentage of its nominal value. These values are found in Table 3.1 [ABSB92:page 77].

Table 3.1 Structured Uncertainty Levels

stability derivatives	control derivatives
$\Delta Y_{\beta} = 0.15 Y_{\beta}$	$\Delta Y_{\delta R} = 0.15 Y_{\delta R}$
$\Delta L_{\beta} = 0.10 L_{\beta}$	$\Delta L_{\delta DT} = 0.15 L_{\delta DT}$
$\Delta L_p = 0.30 L_p$	$\Delta L_{\delta DF} = 0.10 L_{\delta DF}$
$\Delta L_r = 0.20 L_r$	$\Delta L_{\delta R} = 0.40 L_{\delta R}$
$\Delta N_{\beta} = 0.30 N_{\beta}$	$\Delta N_{\delta DT} = 0.15 N_{\delta DT}$
$\Delta N_p = 0.50 N_p$	$\Delta N_{\delta DF} = 0.20 N_{\delta DF}$
$\Delta N_r = 0.15 N_r$	$\Delta N_{\delta R} = 0.15 N_{\delta R}$

3.4.2 Unstructured Uncertainty. The uncertainties in the actuator and the sensors are represented as unstructured uncertainties. Since we wish to analyze the “real” system, we will use the “real” actuators. The actuator uncertainties represent unmodeled dynamics as well as saturation effects. As per [ABSB92], the uncertainty is assumed to be 30% for each actuator. By putting the value of 0.30 ahead of Δ_{act} , we are ensuring that for any $(\Delta_{act}|\overline{\sigma}(\Delta_{act}) \leq 1)$, if $\mu \leq 1$ we will be able to handle the 30% uncertainty. So

$$W_{act} = \begin{bmatrix} 0.3 & 0 & 0 \\ 0 & 0.3 & 0 \\ 0 & 0 & 0.3 \end{bmatrix} \quad (3.40)$$

The uncertainties in the sensor are caused by the quality of the sensors. The body axis rotational rates can be measured very precisely and reliably by gyros. The sideslip angle, however, is usually estimated or reconstructed using complementary filtering [ABSB92] and is not as accurate or reliable. The analysis for the sensors are accomplished for the following levels of maximum uncertainty: 10% in body axis rotational rates and 40% in sideslip measurements.

$$W_{sens} = \begin{bmatrix} 0.4 & 0 & 0 \\ 0 & 0.1 & 0 \\ 0 & 0 & 0.1 \end{bmatrix} \quad (3.41)$$

3.4.3 Robust Performance. There are three differences in the analysis of robust performance when compared to the robust stability analysis.

1. The level of structured uncertainty is reduced from the uncertainty used for the robust stability analysis. The levels of uncertainty used in robust stability analysis were the worst case tests of closed loop stability. In general, we will lose robust performance long before we lose robust stability as the size of Δ is increased. It is, therefore, unreasonable to expect robust

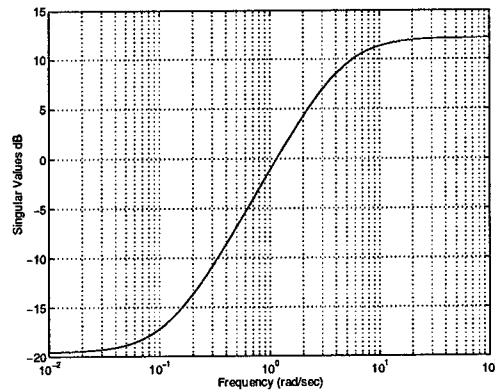


Figure 3.8 Singular Value plot of W_{perf}^{-1}

performance to the same worst case set used in robust stability. For this reason, the robust performance analysis is accomplished using uncertainty levels which are 25% those shown in Table 3.1.

2. The performance weight, W_{perf} , used here is not the same as that used in robust stability. That design weight was mainly chosen to give good nominal performance. Here, we are concerned with how much error there is between the *ideal model* and the evaluation model. We want a weight which will bound the allowable error between the two models. The weight chosen here was designed to ensure that the steady state error to commands is less than 10% and is an estimation of the weight used in [ABSB92].

$$W_{perf} = \frac{0.2471(s + 4.5389)}{(s + .1176)} I_{2 \times 2} \quad (3.42)$$

The SV plot of the inverse of (3.42) shows a graphical representation of the error allowed between the two models and is found in Figure 3.8.

3. The robust performance analysis will be performed using all four blocks simultaneously.

Now we are ready to start the design process.

IV. μ Design

4.1 Outer Loop Design

We will attempt to design the outer loop compensator, K , to provide flying qualities, robustness, and sensor noise and wind gust disturbance rejection. We will first design a μ controller which will meet the flying qualities and robustness objectives, and then examine its noise and disturbance rejection capability. Next, we will attempt to design an H_2 controller which will do better in sensor noise and wind gust disturbance rejection than the μ controller. We will then “combine” the two controllers using mixed H_2/μ to get the best of both worlds in the next chapter.

4.2 μ design

The design model for μ -synthesis is shown in Figure 4.1. In this design, we are modeling an input-multiplicative actuator uncertainty and an additive plant uncertainty. The flying qualities will be characterized as being good if the actual output of the system is close to an *ideal model* of the desired aircraft response to pilot inputs. This will be our performance requirement.

4.2.1 The Ideal Model and the Performance Weighting. The *ideal model* for this design has the form

$$\frac{\beta}{\beta_c} = \frac{\omega_D^2}{s^2 + 2\zeta_D\omega_D^2 s + \omega_D^2} \quad (4.1)$$

$$\frac{\dot{\mu}}{\dot{\mu}_c} = \frac{1/T_R}{(s + 1/T_R)} \quad (4.2)$$

where ω_D is the desired Dutch roll frequency, ζ_D is the desired Dutch roll damping, and T_R is the desired roll mode time constant.

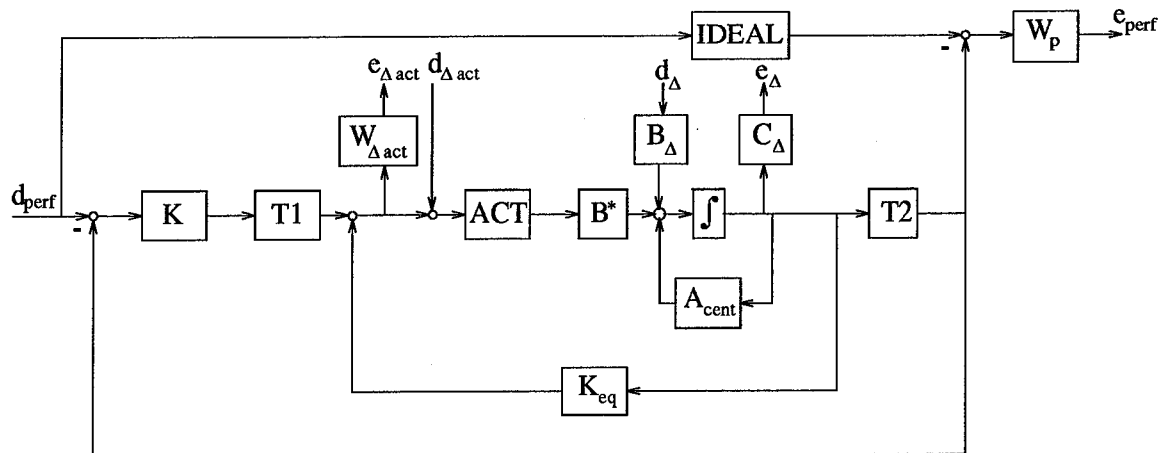


Figure 4.1 Design Model for μ -synthesis

The performance weight, W_P , is designed to provide a frequency weighting on the “performance error”. We want this error to be small, but we are mainly concerned with frequencies which are between 1 and 10 rad/s. These are the frequencies which “dominate the transient response of the closed loop system to pilot commands. If the performance error is not reduced adequately in this frequency region, higher order dynamics will show up in the transient response, destroying flying qualities.” [ABSB92]

For this thesis, the ideal model parameters are $\omega_D = 3.0$ rad/s, $\zeta_D = 0.71$, and $T_R = 0.33$ seconds. The performance weight chosen was

$$W_P = \frac{(s + 30)}{(s + 0.03)} I_{2 \times 2} \quad (4.3)$$

To incorporate robust performance, the Δ block associated with the performance will be represented as a full block.

4.2.2 Actuator. The description of the actuator is found in Chapter III. The input multiplicative uncertainty model is represented mathematically as $(I + \Delta)ACT$ where Δ represents the uncertainty in the actuator. We will assume that we have fairly accurate models of the actuator at low frequencies, but that our model becomes less accurate at higher frequencies. There is no

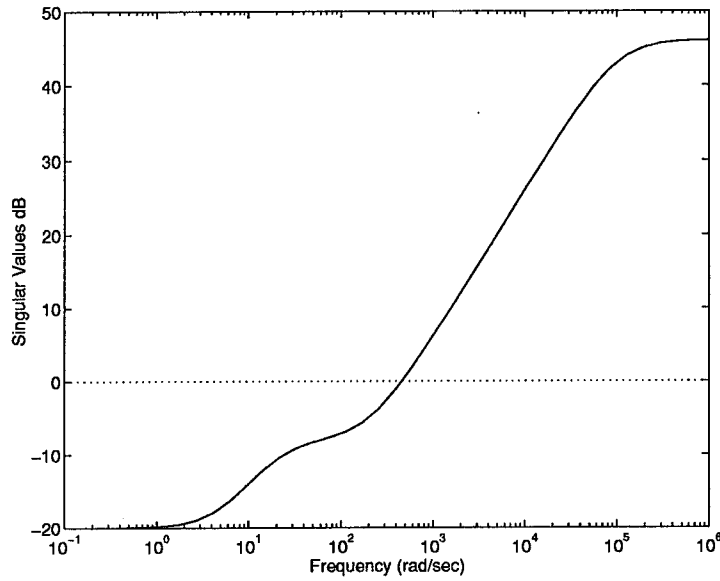


Figure 4.2 Singular Value plot of $W_{\Delta ACT}$

frequency information in Δ . That information is incorporated through the weighting associated with Δ .

The weighting chosen for the actuator in the μ design is

$$W_{\Delta ACT} = \frac{200(s+5)(s+200)}{(s+20)(s+10,000)} \quad (4.4)$$

the singular value plot of which can be found in Figure 4.2. This weighting is designed to indicate an uncertainty of 10% at low frequencies and an uncertainty of 100% at approximately 400 rad/sec. As can be seen in Figure 4.2, the uncertainty continues to grow until the frequency is approximately 10,000 rad/sec, where it is flattened out to avoid an improper transfer function.

The uncertainty in the actuator is not very well known. It could have magnitude and phase variations and the control surfaces could interact with each other. Therefore, the Δ block used for the actuator is of the unstructured kind (a full block).

4.2.3 Parameter Uncertainty Weighting. The uncertainties in the plant come from equalization errors and uncertainty in aerodynamic stability derivatives. Robustness to parameter variations is incorporated into the μ -synthesis design model through the weights B_Δ and C_Δ . Section 3.4.1 presented a detailed description of this method using variations in 14 parameters.

Unfortunately, the order of the controller produced by μ synthesis is proportional to the number of outputs and inputs to each Δ block and the order of the fit used for the D matrix for each of those blocks. In our case we will have 3 blocks; one for the actuator, one for the plant, and one for performance. MATLAB's *μ -Synthesis Toolbox* will always set the last block equal to the identity matrix and therefore has no D -scale associated with it [B⁺93]. That leaves us with two Δ 's we have to worry about. We will let n_a and m_a equal the number of inputs and outputs respectively for the actuator block. We will let n_{cp} and m_{cp} equal the number of inputs and outputs respectively for the core plant block. The order of the weighted plant (P) is n_p and the orders of the D scale fit for each block are n_{da} and n_{dcp} . The order of the controller n_c will be

$$n_c = n_p + n_{da}(n_a + m_a) + n_{dcp}(n_{cp} + m_{cp}) \quad (4.5)$$

Note that the above assumes all blocks are full blocks. If any part of the blocks are repeated scalar blocks, they will have their own D scale and will contribute in the same way.

Now, if we were to use the 14 input, 14 output Δ block from Section 3.4.1, and if we chose a 2nd order fit of the D scaling for that block, we would add 56 states to our controller from that block alone. This is not acceptable. To try to reduce the order, we will attempt to make the system robust to the inner loop equalization error and do extensive analysis of the actual uncertainty using the Robust Analysis model.

We saw in Section 3.2.3 that the inner loop design does not perfectly equalize the plant. In this case, the error in equalization will be due to Y_β , $\sin \alpha$, and $\cos \alpha$ not existing in the inner loop

controller. By treating these parameters as uncertainties in the μ design, we will make the overall control system more robust to the errors in the equalization [ABSB92:pg. 63].

Our uncertainty block will allow for the fact that there can exist interaction between the parameters when it comes to uncertainty. This means we will use a full block to represent the uncertainty. The weighting matrices are scaled such that the maximum uncertainty (when $\bar{\sigma}(\Delta) = 1$) in the A matrix is represented as :

$$\Delta A = B_{\Delta} C_{\Delta} \quad (4.6)$$

The parameter uncertainty weights used in this design are:

$$B_{\Delta} = \begin{bmatrix} 0.1 & 0.1 \\ 0 & 0 \\ 0 & 0 \end{bmatrix} \quad (4.7)$$

$$C_{\Delta} = \begin{bmatrix} 0.05 & 0 & 0 \\ 0 & 0.26 & 0 \end{bmatrix} \quad (4.8)$$

4.2.4 State space formulation. The state space formulation is as follows:

ACTUATOR: (assume strictly proper)

$$\dot{x}_{act} = A_{act}x_{act} + B_{act}u_{act} \quad (4.9)$$

$$y_{act} = C_{act}x_{act} \quad (4.10)$$

G: (assume strictly proper)

$$\dot{x}_c = A_c x_c + B_{\Delta} d_{\Delta} + B^* u_c \quad (4.11)$$

$$y_c = C_c x_c \quad (4.12)$$

$W_{\Delta_{act}}$:

$$\dot{x}_{\Delta_{act}} = A_{\Delta_{act}}x_{\Delta_{act}} + B_{\Delta_{act}}u_{\Delta_{act}} \quad (4.13)$$

$$e_{\Delta_{act}} = C_{\Delta_{act}}x_{\Delta_{act}} + D_{\Delta_{act}}u_{\Delta_{act}} \quad (4.14)$$

W_p :

$$\dot{x}_{wp} = A_{wp}x_{wp} + B_{wp}u_{wp} \quad (4.15)$$

$$e_{perf} = C_{wp}x_{wp} + D_{wp}u_{wp} \quad (4.16)$$

IDEAL: (strictly proper)

$$\dot{x}_{idl} = A_{idl}x_{idl} + B_{idl}u_{idl} \quad (4.17)$$

$$y_{idl} = C_{idl}x_{idl} \quad (4.18)$$

The state vector and disturbance vector are:

$$x_2 = \begin{bmatrix} x_c & x_{act} & x_{idl} & x_{wp} & x_{\Delta_{act}} \end{bmatrix}^T \quad (4.19)$$

$$d = \begin{bmatrix} d_{\Delta_{act}} & d_{\Delta} & d_{perf} \end{bmatrix}^T \quad (4.20)$$

This makes the state space representation of P :

$$A_\mu = \begin{bmatrix} A_c & B^* C_{act} & 0 & 0 & 0 \\ B_{act} K_{eq} & A_{act} & 0 & 0 & 0 \\ 0 & 0 & A_{idl} & 0 & 0 \\ -B_{act} T_2 & 0 & B_{wp} C_{idl} & A_{wp} & 0 \\ B_{\Delta act} K_{eq} & 0 & 0 & 0 & A_{\Delta act} \end{bmatrix} \quad (4.21)$$

$$B_d = \begin{bmatrix} 0 & B_\Delta & 0 \\ B_{act} & 0 & 0 \\ 0 & 0 & B_{idl} \\ 0 & 0 & B_{wp} D_{idl} \\ 0 & 0 & 0 \end{bmatrix} \quad (4.22)$$

$$B_{u_\mu} = \begin{bmatrix} 0 \\ B_{act} T_1 \\ 0 \\ 0 \\ B_{\Delta act} T_1 \end{bmatrix} \quad (4.23)$$

$$C_e = \begin{bmatrix} D_{\Delta act} K_{eq} & 0 & 0 & 0 & C_{\Delta act} \\ C_\Delta & 0 & 0 & 0 & 0 \\ -D_{wp} T_2 & 0 & D_{wp} C_{idl} & C_{wp} & 0 \end{bmatrix} \quad (4.24)$$

$$C_{y_\mu} = \begin{bmatrix} -T_2 & 0 & 0 & 0 & 0 \end{bmatrix} \quad (4.25)$$

$$D_{ed} = \begin{bmatrix} 0 & 0 & 0 \\ 0 & 0 & 0 \\ 0 & 0 & D_{wp}D_{idl} \end{bmatrix} \quad (4.26)$$

$$D_{eu} = \begin{bmatrix} D_{\Delta act}T_1 \\ 0 \\ 0 \end{bmatrix} \quad (4.27)$$

$$D_{yd} = \begin{bmatrix} 0 & 0 & I \end{bmatrix} \quad (4.28)$$

$$D_{yu} = [0] \quad (4.29)$$

4.2.5 Results. The μ -Toolbox was used and gave the controller found in Appendix B. It is a 26th order, strictly proper controller. The singular value plots of the controller can be found in Figure 4.3.

The controller was entered into the Evaluation Model for simulation.

4.2.5.1 Tracking Capability. The tracking capability (ability to follow the ideal model) can be seen in Figure 4.4. The ideal response is represented by the dashed line, the actual response is shown as a solid line.

Since in this case we are dealing only with angles and angular rates, we can assign whatever angular units we wish to the plots and nothing would change. We will assume the inputs to be in degrees.

As seen in Figure 4.4, a step in β produces a maximum deviation from the ideal β response of 0.05 deg. The response of $\dot{\mu}$ for a β step stays very close to zero (within 0.1 degrees). A step in

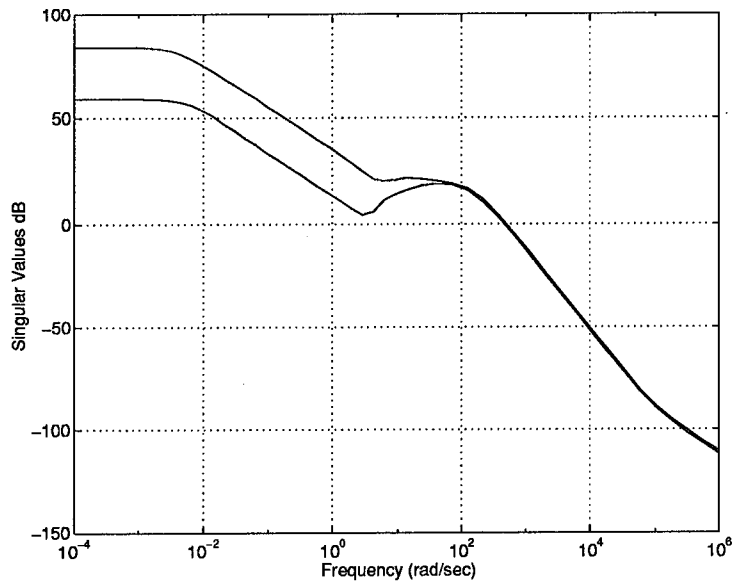


Figure 4.3 Singular Value plot for the optimal μ controller

$\dot{\mu}$ has a tougher time tracking the ideal model but still has an acceptable maximum error of 0.19 degrees/sec. The β response to the $\dot{\mu}$ step is almost negligible. We can see that μ synthesis did a very good job of tracking and decoupling the responses.

The noisy tracking response can be found in Figure 4.5. It can be seen that, besides the expected noisiness, there is no significant change from the noiseless response.

4.2.5.2 Robustness. Recall from Section 3.4 that, except for Δ_{perf} , we are going to analyze each uncertainty separately for robust stability. This means we will perform μ analysis on the $\Delta_{A,B}$, Δ_{act} , and Δ_{sens} blocks in Figure 3.7 one at a time, treating each as if it were the only block in the system. We will also treat these blocks as a block diagonal of the appropriate number of Δ s, where each Δ is a 1×1 full block. This will allow us to simulate an uncertainty for *each* sensor, actuator and parameter. Note that we are designing for a “tougher” uncertainty than that which is used in the evaluation. We are *designing* for uncertainties which interact with each other. We are *evaluating* uncertainties which do not. Besides the fact that we are always justified to design conservatively, we are also justified in that we are including more uncertainties

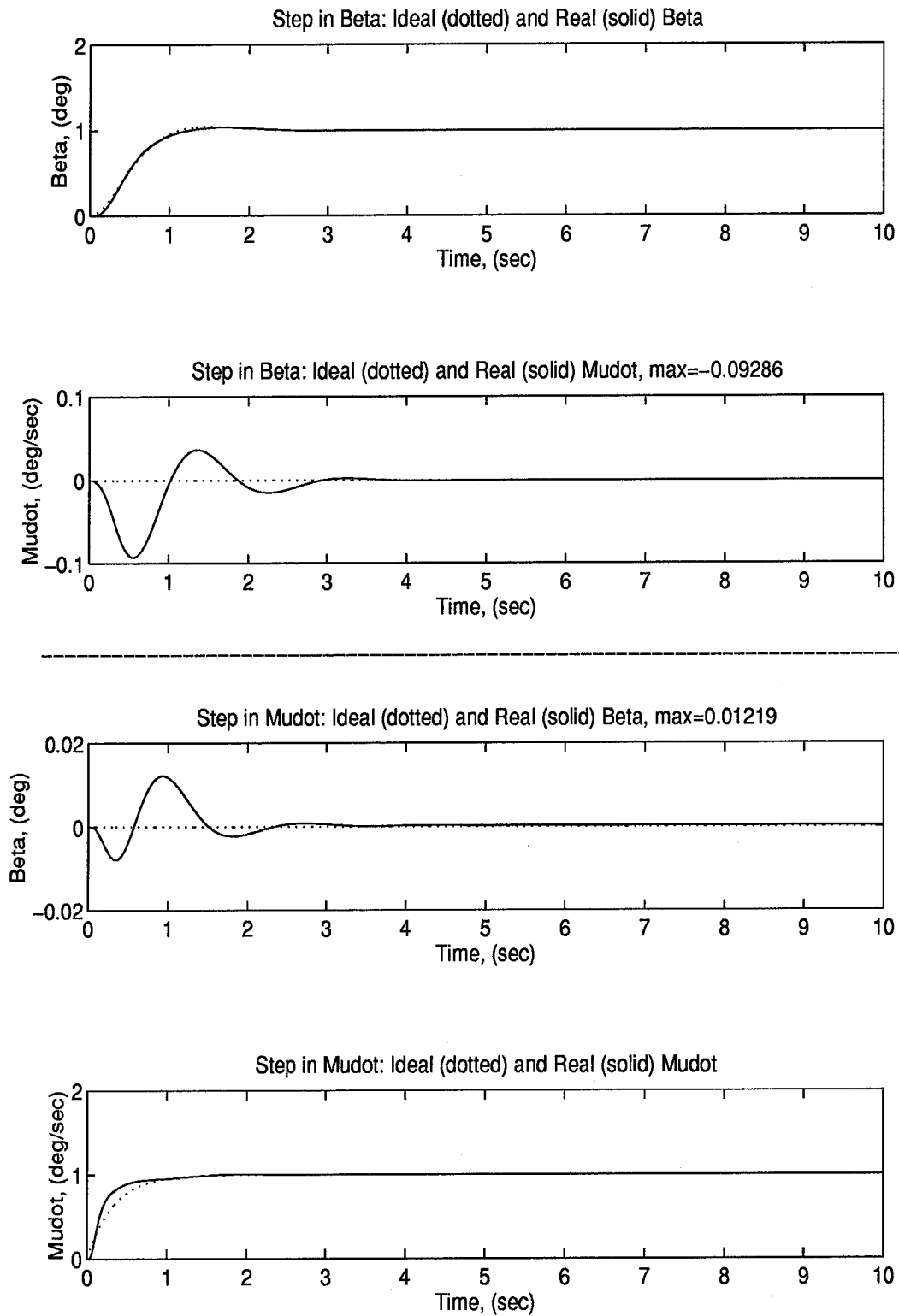


Figure 4.4 Noiseless Tracking Capability of the μ controller (solid line) compared to the ideal response (dashed) for a step in β and a step in $\dot{\mu}$

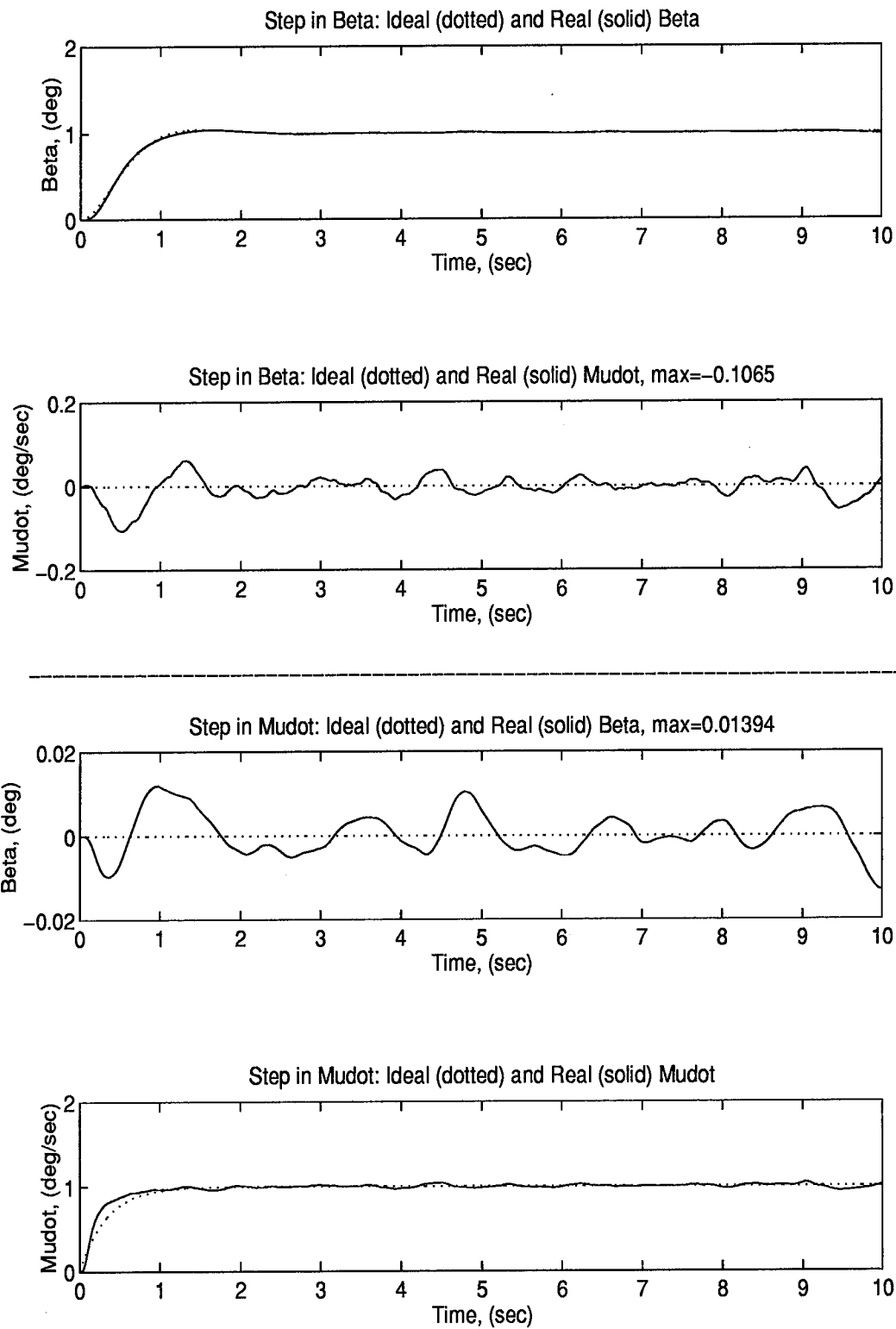


Figure 4.5 Noisy Tracking Capability of the μ controller (solid line) compared to the ideal response (dashed) for a step in β and a step in $\dot{\mu}$

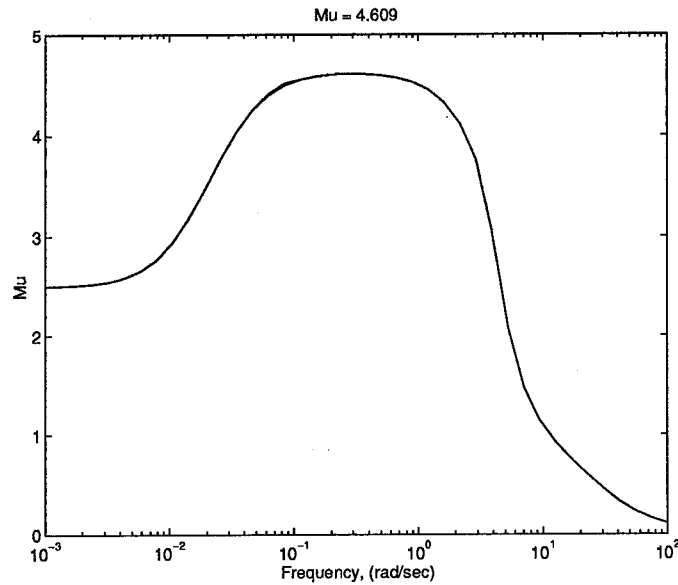


Figure 4.6 μ bounds for the μ controller

in the evaluation than was used in the design (for controller order purposes), such as the sensors and more uncertain parameters in the plant.

The μ plot for the design (three full blocks forming one big block) is found in Figure 4.6. The robust analysis plots are calculated using the robust analysis model and are found in Figure 4.7. We can see that even though $\mu = 4.609$, we still satisfy the conditions set in the robust analysis. This is just saying that the weighting we gave μ in the design sets us up for a much tougher problem than what we actually need in our robust analysis model. Or put another way, the weightings we used in the design are much more conservative than the weightings we used in the analysis (which is our best guess of the model of the uncertainty).

The system responses to wind gusts and sensor noise only (no command) are shown in Figure 4.8. When compared to the open loop response in Figure 3.6, we see that μ did fairly well even in noise and disturbance rejection. For a complete and accurate comparison later, we will look at two things when talking about the state response to noise: the standard deviation, which is a more mathematical measure; and the maximum value, which is more intuitive. Table 4.1 summarizes the reduction in noise compared to the open loop (Figure 3.6) using both measures.

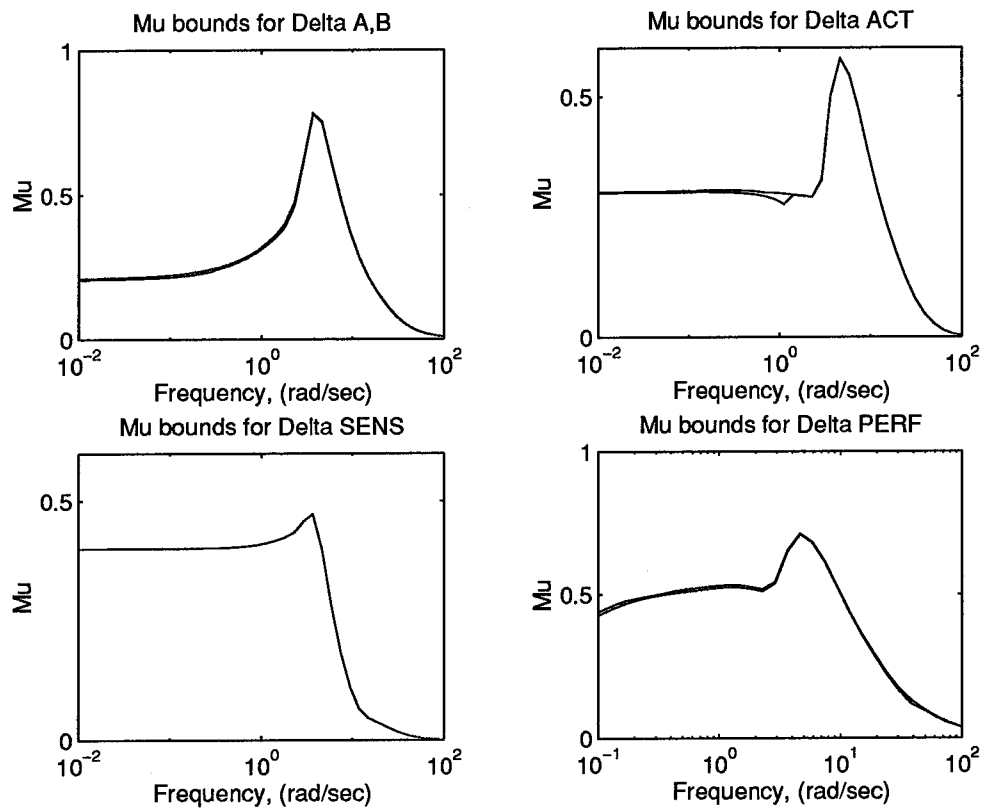


Figure 4.7 Robust Analysis of the μ controller

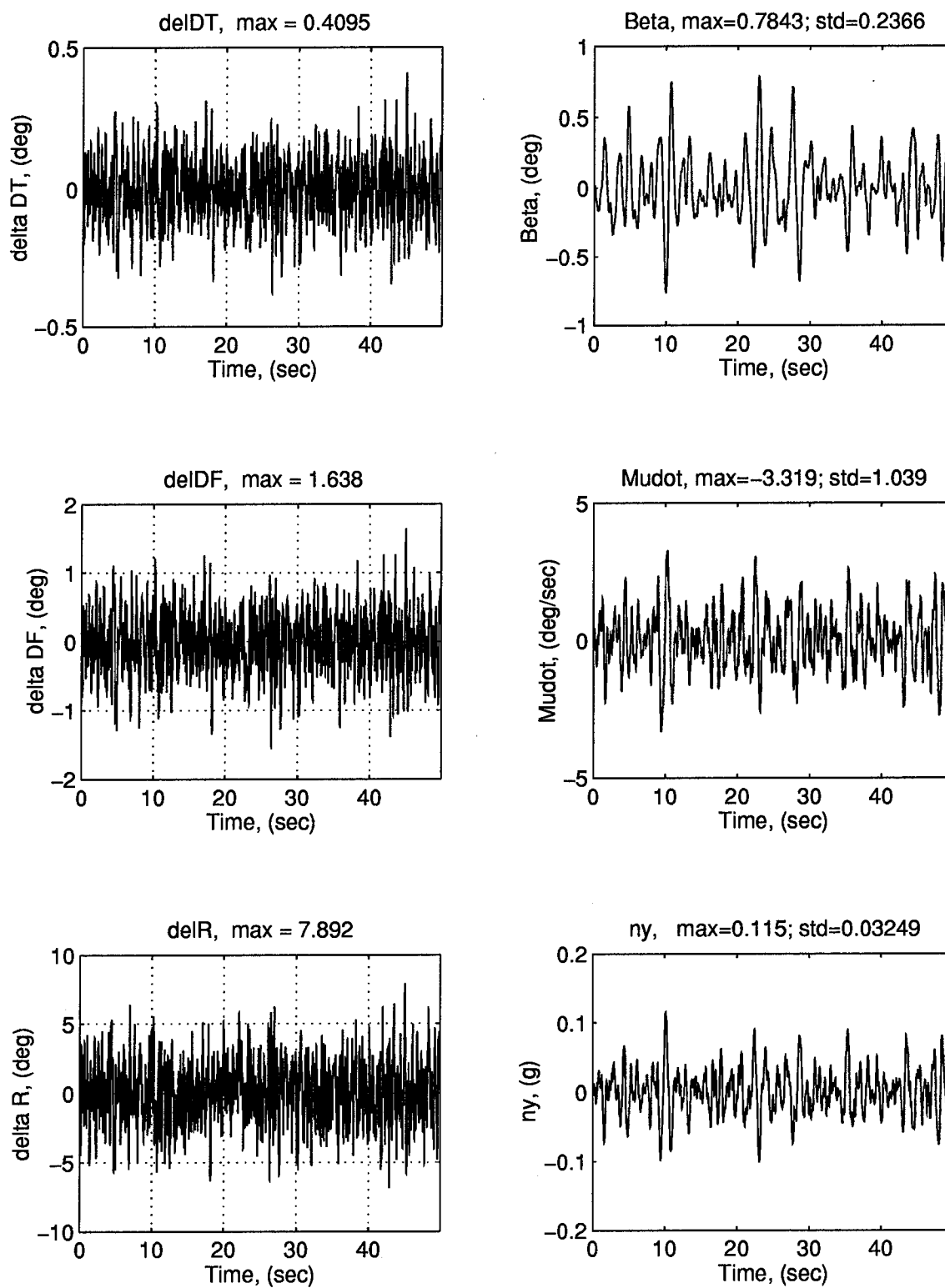


Figure 4.8 System's Response to Wind Gust and Sensor noise, μ Controller

Table 4.1 Reduction in Open Loop Noise and Wind Effects using μ Controller

state	maximum value	standard deviation
β	-33%	-40%
$\dot{\mu}$	-62%	-64%
n_y	-54%	-62%

Note that (ignoring the rates, which would be washed out) the control deflections are reasonable with the possible exception of the rudder. It is moving $\pm 8^\circ$ for just noise!

For comparison purposes, Figure 4.9 shows the response of the system given sensor noise only. This is to get an idea of the size of the high frequency content of the noise, which is lost in the much larger wind gust effects.

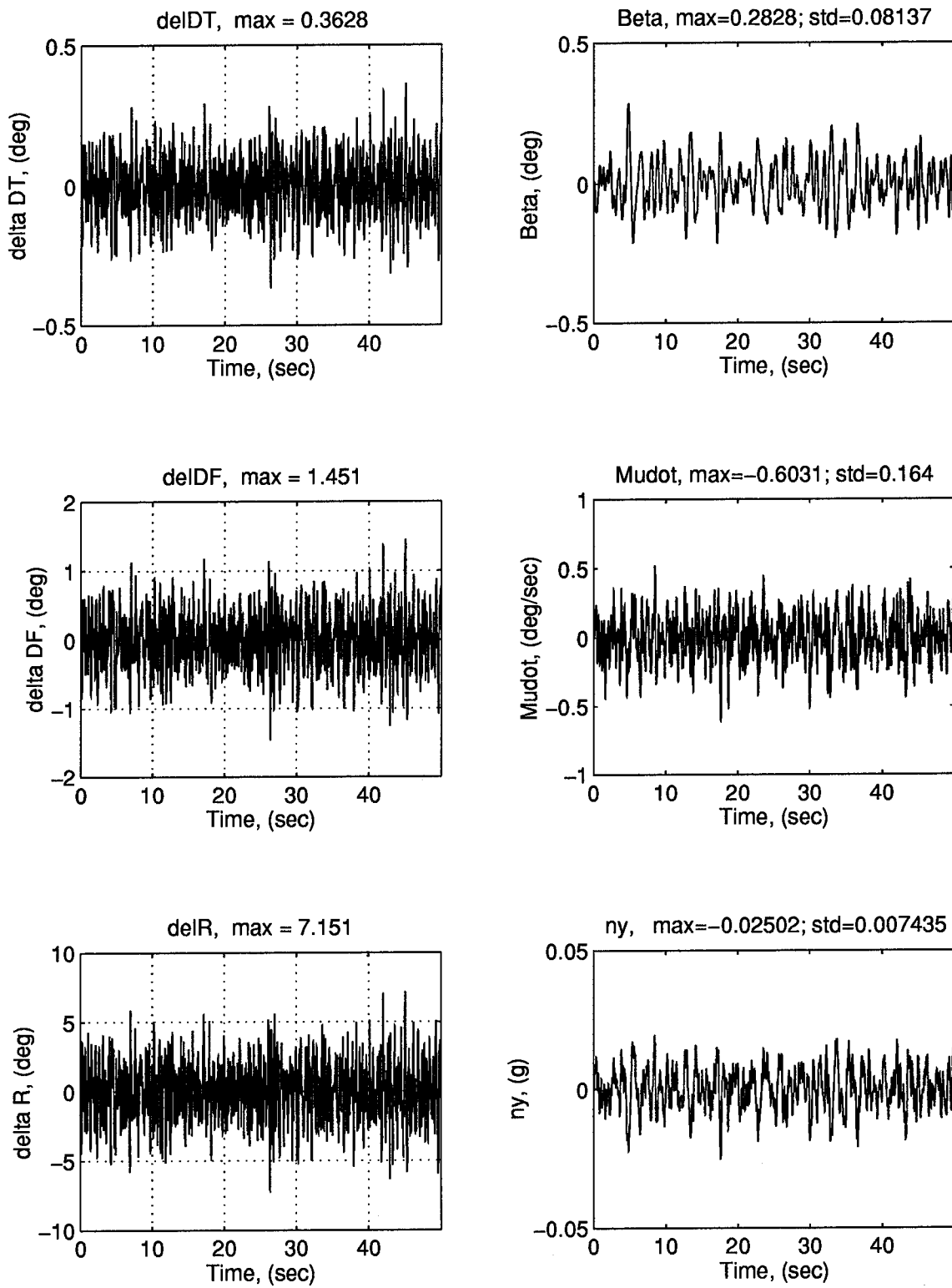


Figure 4.9 System's Response to Sensor Noise only, μ Controller

V. H_2 and Mixed H_2/μ Design A

We can see from the preceding figures that the μ controller does a good job on the robustness and the tracking problems. In fact, it is good enough in those areas that we could sacrifice some of those features in trade for something else. While the μ controller also does reasonably well on noise and disturbance rejection, there is room for improvement. Our objective now is to design an H_2 controller which will show even more improvement on noise and disturbance rejection. Then, an appropriate mix of H_2/μ should provide better noise rejection than μ alone without losing much of μ 's robustness or tracking capability.

5.1 H_2 Design

The design model for the H_2 problem is found in Figure 5.1. Note that in this design, we have the wind gust entering the system directly into the states (specifically, into β). We have the sensor noises entering into the inner loop since we must be able to measure the outputs of the plant to bring those values into K_{eq} . We would normally put the penalty on control usage, $z_{control}$, right after ACT. In this way we would be penalizing actual control usage. However, since our actuator is strictly proper, this penalty would produce a zero D_{zu} term which would violate H_2/H_∞ assumption (4) in Section 2.1.3.2. Moving the penalty to just before ACT would take care of that assumption, but would violate $D_{zw} = 0$ (assumption 1) since w_{noise} enters the inner loop. This, in turn, could be taken care of by moving w_{noise} outside of the inner loop, but that makes the problem unrealistic (we would have perfect measurements entering K_{eq} but not K). It was decided to move $z_{control}$ to just after the controller, K . In the same way, z_{states} must be prior to w_{noise} instead of after it. That way, all assumptions involving z will be met.

The weightings ρ_u , K_s , k_g , K_{states} are all design chosen variables to "tune" the H_2 problem to produce the desired controller. The weights W_g and W_s are coloring filters to model the wind gust and sensor noise as colored noise. W_g is a low pass filter to model the wind gust as having

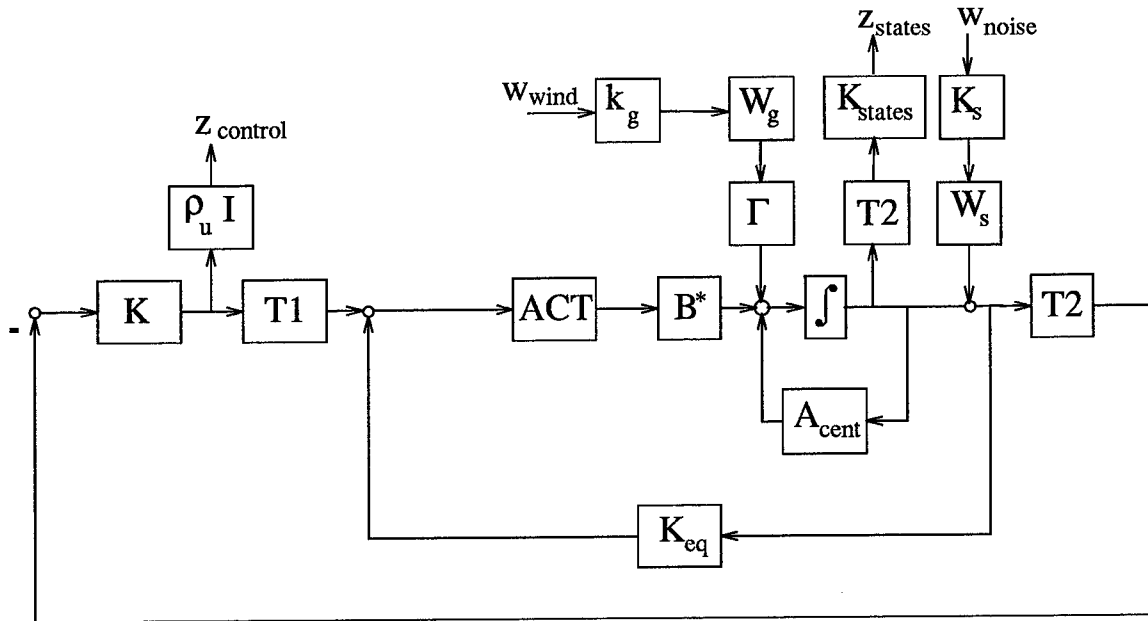


Figure 5.1 Design Model for H_2 -synthesis

most of its energy at lower frequencies. The filter chosen is the same filter used in the evaluation model. The filter for the sensor noise W_s is also the same high pass filter used in the evaluation model.

5.1.1 State Space. The state space equations for the actuator and core plant are found in Section 4.2.4. The only other dynamical elements in Figure 5.1 are W_g and W_s .

W_g :

$$\dot{x}_g = A_g x_g + B_g u_g \quad (5.1)$$

$$y_g = C_g x_g + D_g u_g \quad (5.2)$$

W_s :

$$\dot{x}_s = A_s x_s + B_s u_s \quad (5.3)$$

$$y_s = C_s x_s + D_s u_s \quad (5.4)$$

where

$$u_s = K_s w_{noise} \quad (5.5)$$

and

$$K_s = \begin{bmatrix} k_{s_b} & 0 & 0 \\ 0 & k_{s_p} & 0 \\ 0 & 0 & k_{s_r} \end{bmatrix} \quad (5.6)$$

The state vector and disturbance vector are:

$$x_2 = \begin{bmatrix} x_c & x_{act} & x_g & x_s \end{bmatrix}^T \quad (5.7)$$

$$w = \begin{bmatrix} w_{gust} & w_{noise} \end{bmatrix}^T \quad (5.8)$$

This makes the state space representation of P :

$$A_2 = \begin{bmatrix} A_c & B^* C_{act} & \Gamma C_g & 0 \\ B_{act} K_{eq} & A_{act} & 0 & B_{act} K_{eq} C_s \\ 0 & 0 & A_g & 0 \\ 0 & 0 & 0 & A_s \end{bmatrix} \quad (5.9)$$

$$B_w = \begin{bmatrix} \Gamma D_g k_g & 0 \\ 0 & B_{act} K_{eq} D_s K_s \\ B_g k_g & 0 \\ 0 & B_s K_s \end{bmatrix} \quad (5.10)$$

$$B_{u_2} = \begin{bmatrix} 0 \\ B_{act}T_1 \\ 0 \\ 0 \end{bmatrix} \quad (5.11)$$

$$C_z = \begin{bmatrix} K_{states}T_2 & 0 & 0 & 0 \\ 0 & 0 & 0 & 0 \end{bmatrix} \quad (5.12)$$

$$C_{y_2} = \begin{bmatrix} -T_2 & 0 & 0 & -T_2C_s \end{bmatrix} \quad (5.13)$$

$$D_{zw} = \begin{bmatrix} 0 & 0 \\ 0 & 0 \end{bmatrix} \quad (5.14)$$

$$D_{zu} = \begin{bmatrix} 0 \\ \rho_u I \end{bmatrix} \quad (5.15)$$

$$D_{yw} = \begin{bmatrix} 0 & -T_2D_sK_s \end{bmatrix} \quad (5.16)$$

$$D_{yu} = [0] \quad (5.17)$$

H_2 optimization design is a very "hit and miss" type of process. Everything depends on finding the correct design variables to get an acceptable answer. Methods to "find" the correct values of these variables are few and far between. If we do not "happen" to choose the correct values, we will not get an acceptable controller. In our case, we must find the correct design weights

for the H_2 system which will produce a controller that does better than the μ controller on noise and disturbance rejection. This proved to be one of the hardest tasks of this thesis. Even when successful, the changes were minor; however, we are looking at the concept of mixed H_2/μ and interesting things were found. In this problem, it was possible to beat the μ controller in *either* the noise *or* the control usage, but it seemed impossible to beat μ in both. Months were spent trying to vary the individual weightings and look for trends. The only thing noticed here was that the two-norm itself means little when changing the weights. When we change a weight, we are changing the problem and we cannot compare the new two-norm with the old two-norm in the weighted H_2 system.

Traditionally, the method used is to try to shape the open loop singular value (SV) plot to get the desired loop shape. This was tried with no success. What we are really interested in is the closed loop response of the system. That is where our attention will now focus.

The method which seemed to have the most success in finding the weights which would produce a controller that beats μ involved studying the frequency content of the signal coming out of the system. If we want to observe the response of the system due to the sensor noise, we need an outer loop controller. The identity matrix was chosen for ease of use.

The system's response to wind gust and noise for $K = I$ is found in Figure 5.2. Even though the input to the system is a white noise (uniform power at all frequencies), the output will not be white. In addition to going through the coloring filters which make the input more realistic, the system itself is a filter and will favor certain frequencies above others. Our objective here, then, is to determine the frequencies which the system "favors". To do that, we need to examine the power spectrum of the output signal (a plot of power vs. frequency). MATLAB has a discrete Fourier transform function "FFT" which can be used to estimate the power spectrum of a signal. The result of FFT for each of the "states" is found in Figure 5.3.

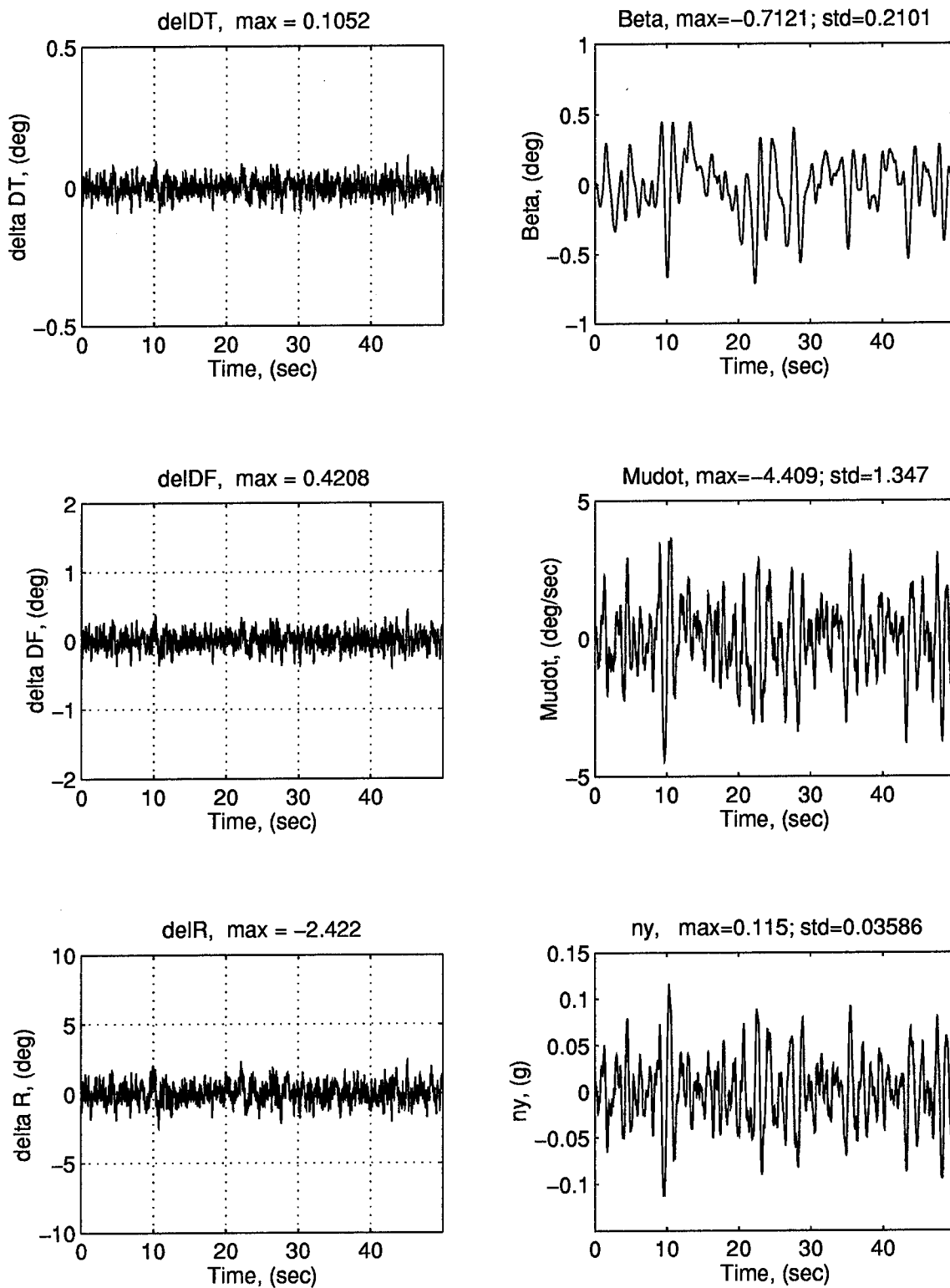


Figure 5.2 System's Response to Wind Gust and Sensor Noise, $K = I$

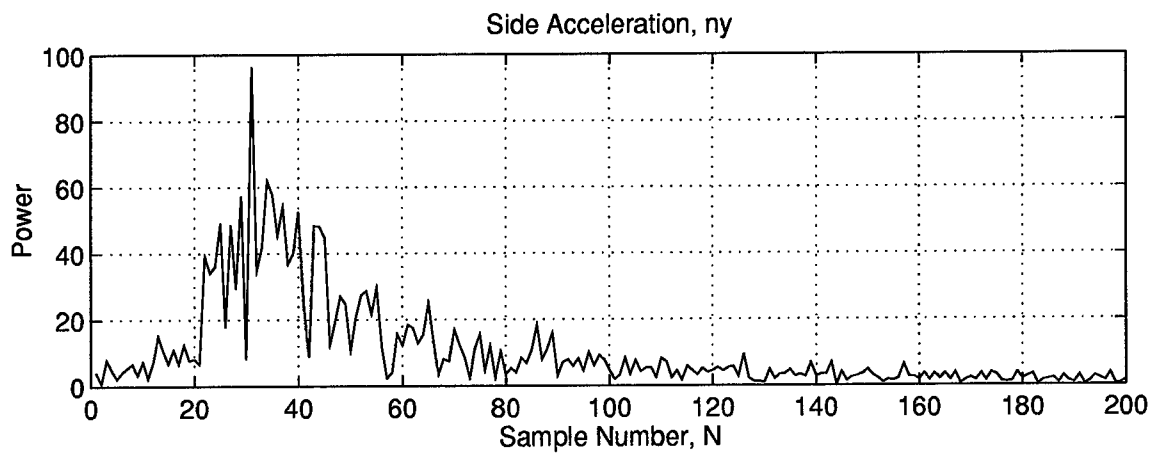
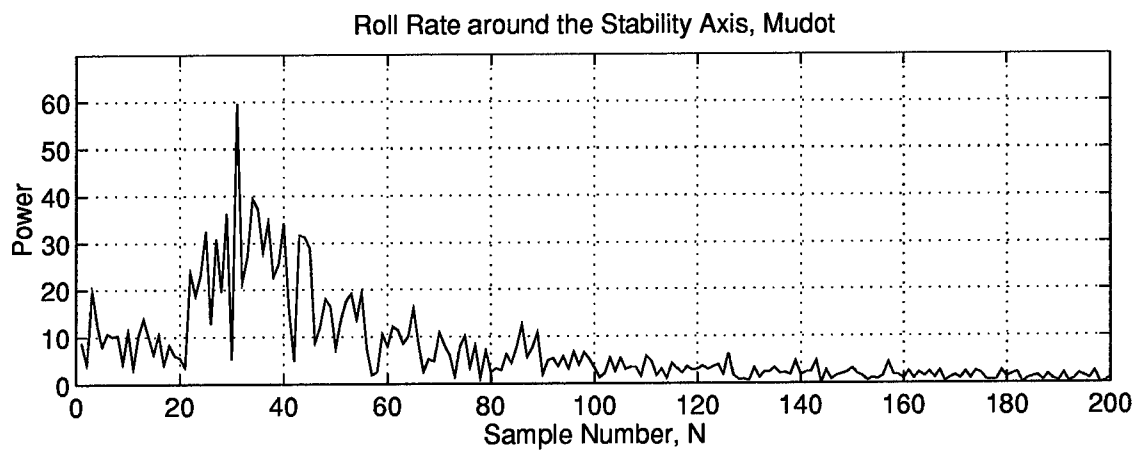
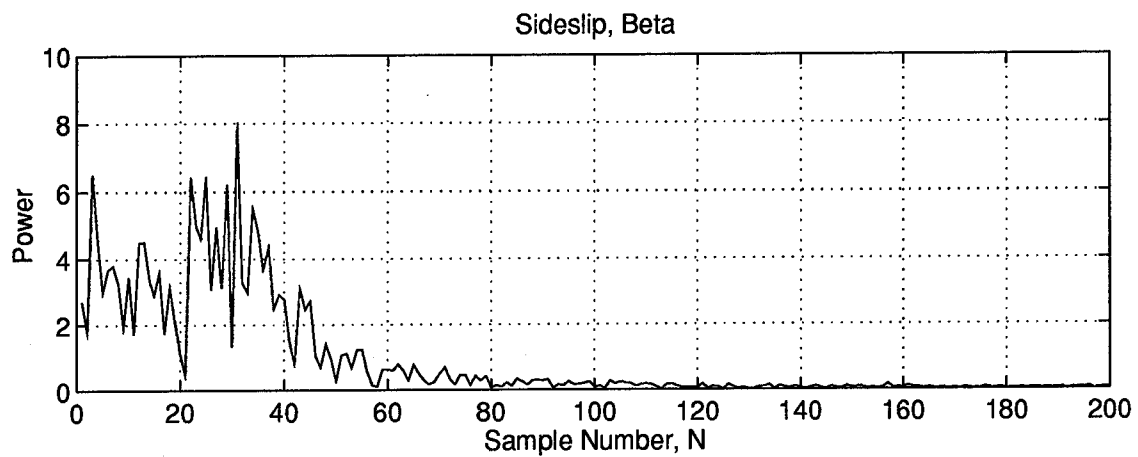


Figure 5.3 FFT of the state responses to noise

To estimate the power spectrum of a signal from a plot such as Figure 5.3, we can apply the following equation to determine the frequency for a given index or sample number [OS89].

$$Actual\ freq = 2\pi(index)\left(\frac{1}{TN}\right) \quad (5.18)$$

where T is the sample time used in the simulation and N is the total number of samples. We can see from Figure 5.3 that all three responses have most of their energy around $index = 30$. In our case, $T = 0.005$ and $N = 10000$. Hence, most of our energy is around 3.8 rad/sec.

On a purely theoretical basis, if our simulation accurately simulated white noise, this should be sufficient since white noise has a flat power spectrum and the system would filter all noise in the same manner. However, our samples are probably not accurate representations of white noise. Thus, any analysis which only includes one sample of noise is incomplete. We need to do a series of samples at various random number generator seeds. Several seeds were used and the peaks of the power of all samples had frequencies around 3.8 (± 0.9) rad/sec. Thus, it was felt that 3.8 rad/sec was an appropriate representation of the frequency that had the most power.

Now we have a more quantitative way to help us in determining the design weights needed for our H_2 design. We now know that we want the gain of the *closed-loop* response to be low around 3.8 rad/sec since this is where most of our noise is coming from. This can be seen directly in an SV plot of Z_{states}/W_s or Z_{states}/W_g . We can vary a weight and measure the gain at the frequency of interest using the SV plot. As we change the weight we can see the corresponding change in gain. An example of the type of plots which will be produced is seen in Figure 5.4. We can see from these plots that there is a hump around 3.8 rad/sec. It is this hump which must be lowered if we want a less noisy response.

We can now make a program which will systematically vary each of the weights and record the maximum gain of the closed loop Z_{states}/W_g and Z_{states}/W_s SV plots at the frequency(ies) of interest and make a plot which will show the data graphically. An example of such a plot is

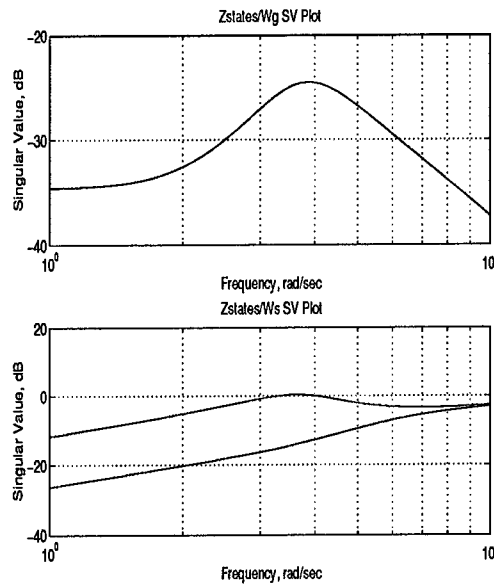


Figure 5.4 Closed loop SV plots for Z_{states} vs. wind gust and sensor noise, $K = I$

in Figure 5.5. In this way, gains can be found which produce the lowest singular value at the frequency(ies) of interest. Using this method produced the most favorable response of any other method tried up to this point. The weights which produced the best responses are found in Table 5.1.

Table 5.1 Design Weights for the 1st controller

Design Weight		value
	ρ	0.001
K_{states}	k_b	1
	k_m	1
K_s	k_{sb}	1
	k_{sp}	1
	k_{sr}	1
	k_g	1

The plots of the response to wind and noise are in Figures 5.6. The closed loop SV plots are in Figure 5.7. Note how the humps in Figure 5.7 have decreased. This corresponds with Figure 5.6.

Unfortunately, this controller, when evaluated on the *evaluation* model, is unstable. This is possibly a problem. H_2 guarantees us a stabilizing controller and this controller does indeed

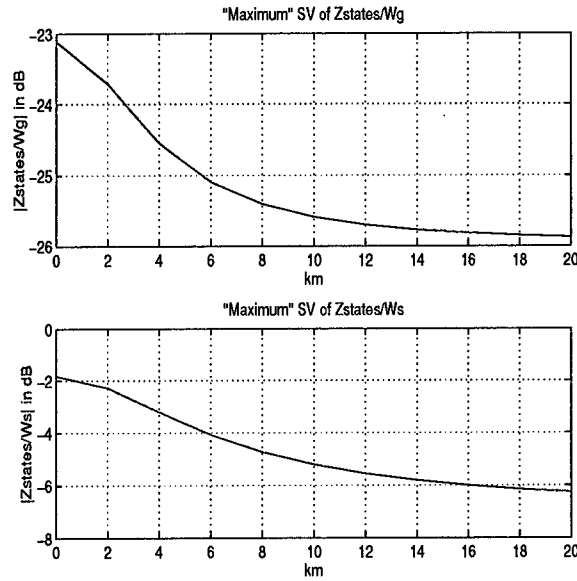


Figure 5.5 Effect of varying one design weight, k_m , on closed loop gain of Z_{states} for wind gust and noise input at $\omega \approx 3.8$ rad/sec

stabilize the design model. But the controller isn't robust enough to handle the differences between the design model and the evaluation model. The major difference between the two models is that in our design model, we are using generalized controls instead of the actual controls. This is too large a Δ for this H_2 controller to handle. Recall that H_2 optimization wasn't designed to handle uncertainty, but μ synthesis was (note that μ had no problem with this Δ). This is consistent with what we know already about H_2 and μ . While a mixed controller might be acceptable, it was felt that this controller was not preferable as an "anchor" to the mixed H_2/μ problem (i.e., as the right end of the curve).

At this point there were two alternatives: either go back and make the design have the same actuators as the evaluation model, or choose larger controller weights to see if the resulting controller will be acceptable noise-wise and not drive the evaluation model unstable. The latter approach was used. The design chosen had the weights shown in Table 5.2. This controller will be denoted H_2 Controller A. The results of this controller are discussed in the next section.

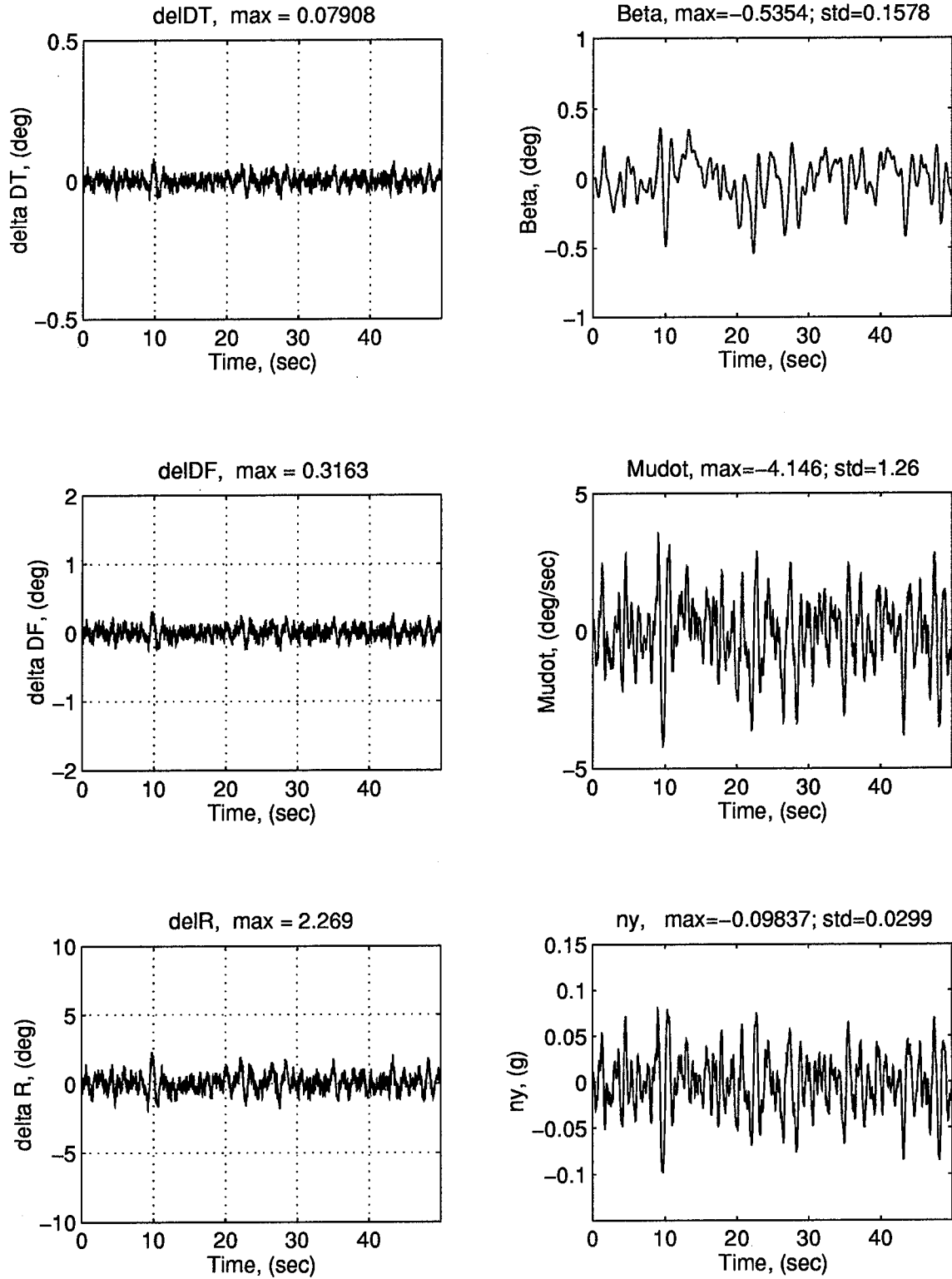


Figure 5.6 System's Response to Wind Gust and Sensor Noise, 1st controller

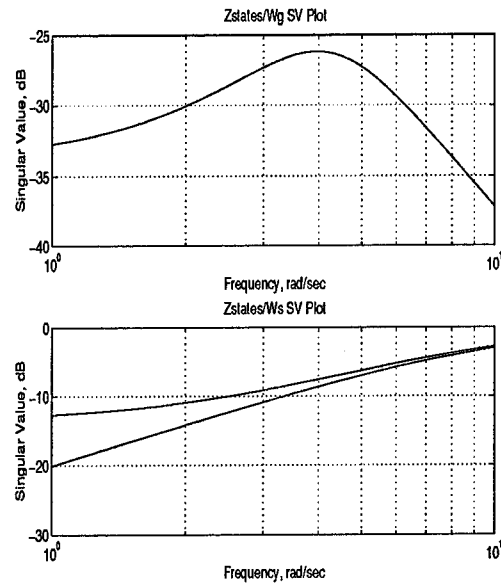


Figure 5.7 Closed loop SV plots for Z_{states} vs. wind gust and sensor noise for the 1st controller

Table 5.2 Design Weights for H_2 Controller A

Design Weight		value
	ρ	0.7
K_{states}	k_b	1
	k_m	1
K_s	k_{s_b}	0.1
	k_{s_p}	0.1
	k_{s_r}	0.1
	k_g	10

5.1.2 Results. Recall that our objective in the H_2 portion is to do better than μ in noise and disturbance rejection. We don't necessarily care about its tracking capability or robustness, although these will be interesting to look at and compare with the μ controller and the final mixed H_2/μ controller. For right now, though, we will only concern ourselves with the noise and disturbance.

The response and closed loop SV plot of H_2 Controller A are found in Figures 5.8 thru 5.9. The response marginally improved over the μ controller for two of the "states" (β and n_y), while $\dot{\mu}$ got worse. Also note that the "hump" in Z_{states}/W_s in Figure 5.9 has appeared again. A more quantitative look is in Table 5.3, which summarizes the change in maximum noise value and the

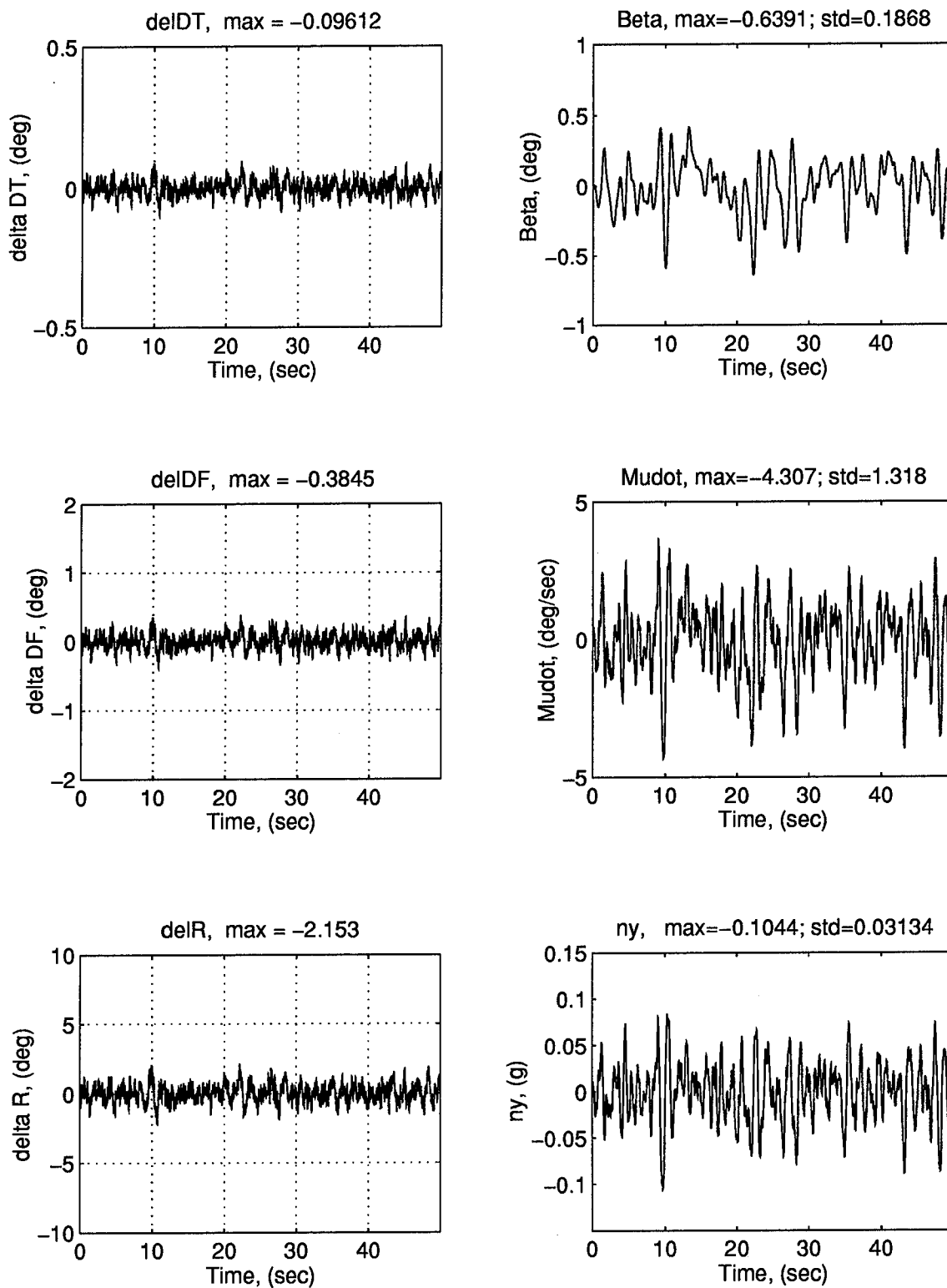


Figure 5.8 System's Response to Wind Gust and Sensor Noise, H_2 Controller A

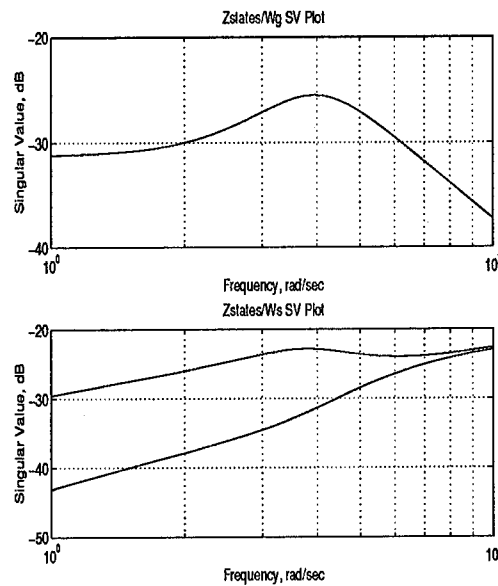


Figure 5.9 Closed loop SV plots for Z_{states} vs. wind gust and sensor noise for H_2 Controller A

standard deviation when compared to the μ controller. We will also include the maximum value of the control deflections to get an idea of the control power used.

Table 5.3 Change in μ Controller Noise and Wind Effects using H_2 Controller A

state	maximum value	standard deviation	control surface	maximum control deflection
β	-19%	-21%	δ_{DT}	-77%
$\dot{\mu}$	+30%	+27%	δ_{DF}	-77%
n_y	-9%	-4%	δ_R	-73%

We see that with one exception, the noise response is better and we have gained an enormous reduction in control usage. Therefore, we expect that the mixed controllers should show an overall improvement in noise and wind response.

5.2 Mixed H_2/μ using H_2 Controller A

5.2.1 More Definitions. Before we continue and discuss mixed H_2/μ for Design A, we will add another definition to the list in Section 2.1.3.2 and make a notational comment.

We will define $\bar{\alpha}$ as the two-norm of the μ part of the system with the $K_{2_{opt}}$ controller in place. Recall from Section 2.1.3.2 that normally $\bar{\alpha}$ would be infinite since the H_∞ controller usually has a nonzero D_c term. That is not the case for us (see the μ controller in Appendix B). Hence, we will have a finite $\bar{\alpha}$ and the definition has meaning.

Recall from Section 2.1.5 that mixed H_2/μ is mixed H_2/H_∞ with the H_∞ problem scaled by the D scales. Calculating the infinity-norm of this scaled H_∞ problem is calculating the overbound of μ . To keep the distinction straight, when we refer to the mixed H_2/μ problem and talk of the infinity-norms, we will continue to use the γ 's defined in Section 2.1.3.2. This will remind us that we are calculating the overbound to μ and not μ itself. We will also occasionally refer to the H_2 open loop system and the μ open loop system (H_∞ open loop multiplied by the D scales). These will be designated P_2 and P_μ , respectively; the corresponding closed loop systems will be designated T_{zw} and $DT_{ed}D^{-1}$, respectively.

5.2.2 The Mix. At this point we know the general shape of the curve (Section 2.1.5), one end point (associated with the H_2 optimal solution, the "anchor"), and a point where the curve may not be able to reach (the point associated with the μ controller). Remember, all two-norm calculations are done with T_{zw} and all infinity-norm calculations are done with $DT_{ed}D^{-1}$. Therefore, using the μ controller and using the H_2 optimal controller found above, our end points yield:

$$\begin{array}{llll} \mu : & \bar{\alpha} = 6.567 & \underline{\gamma} = 4.709 & 26^{th} \text{ order} \\ H_2 : & \underline{\alpha} = 0.6532 & \bar{\gamma} = 2.923e + 4 & 9^{th} \text{ order} \end{array}$$

These can serve as a check on our optimization routine.

The H_2/H_∞ optimization program was run on MATLAB for a 9^{th} order controller. The resulting γ vs. α curve is found in Figure 5.10. The location on the curve of each controller

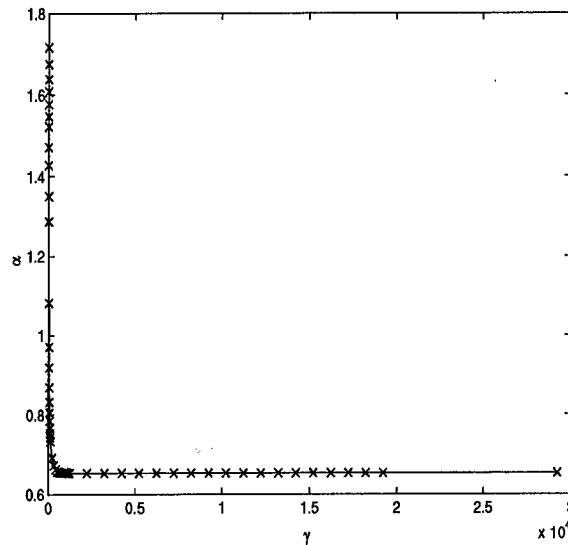


Figure 5.10 γ vs. α curve using Design A

calculated is shown by an 'x'. A controller from this set of controllers must now be chosen. Usually, a point near the "knee" of the curve is chosen to get a "lowest α for the lowest γ " type point. The "knee" in Figure 5.10 is shown in more detail in Figure 5.11. As long as we stay in the vicinity of γ , we should keep most of our tracking and robustness characteristics. The lower α should give us the better noise performance when compared to μ .

The chosen controller has a $\gamma = 7.992$ and $\alpha = 1.716$. This controller will be denoted as Mixed Controller A. The plots of the noise and disturbance response are in Figure 5.12.

We can see immediately that the control usage decreases dramatically but the response is worse for all three "states". We might have expected that $\dot{\mu}$ would increase since it was higher in the H_2 optimal response compared to the μ controller. However, the two-norm is lower for the mixed controller than in the μ controller; at least one of the state responses should improve. It is the states that concern us the most. Table 5.4 summarizes the changes when compared to μ .

5.2.2.1 Possible Problem — Order. One possible explanation for the discrepancy is the fact that the mixed curve is 9th order (order of the H_2 optimal system) and a minimal

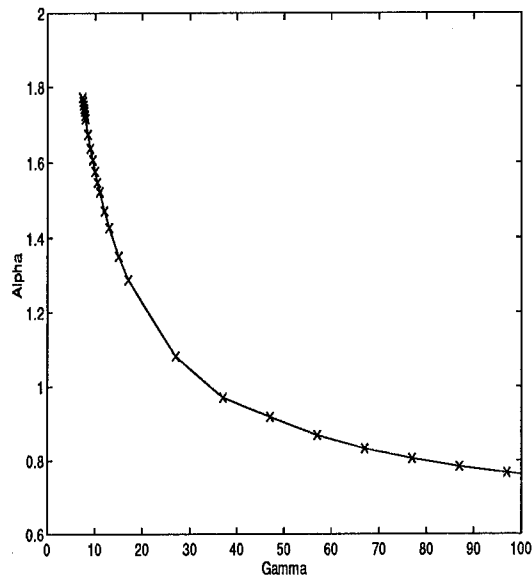


Figure 5.11 "Knee" of the γ vs. α curve using Design A

Table 5.4 Change in μ Controller Noise and Wind Effects using Mixed Design A

state	maximum value	standard deviation	control surface	maximum control deflection
β	+10%	+12%	δ_{DT}	-65%
$\dot{\mu}$	+73%	+66%	δ_{DF}	-65%
n_y	+50%	+51%	δ_R	-65%

realization of the μ controller is 23rd order. To examine this possibility, a 23rd order controller was formed from H_2 Controller A by adding 14 pole/zero cancellations. If order is indeed the explanation, then with the 23rd order controller as our starting point, our mixed controllers (which will also be 23rd order) should have responses which are better than μ (possibly β and n_y better, $\dot{\mu}$ worse). This was not the case. All state responses were worse.

5.2.2.2 Possible Problem — Robustness . It is known that μ is designed for robustness and H_2 is not. We have already seen how one H_2 design was stable for the design model but not for the evaluation model. Perhaps H_2 Controller A was also not robust, not in a stability sense (the controller did stabilize the evaluation model), but in a performance-to-noise sense. Maybe at some point on the curve, the μ side starts to take over and the noise performance gets better, while

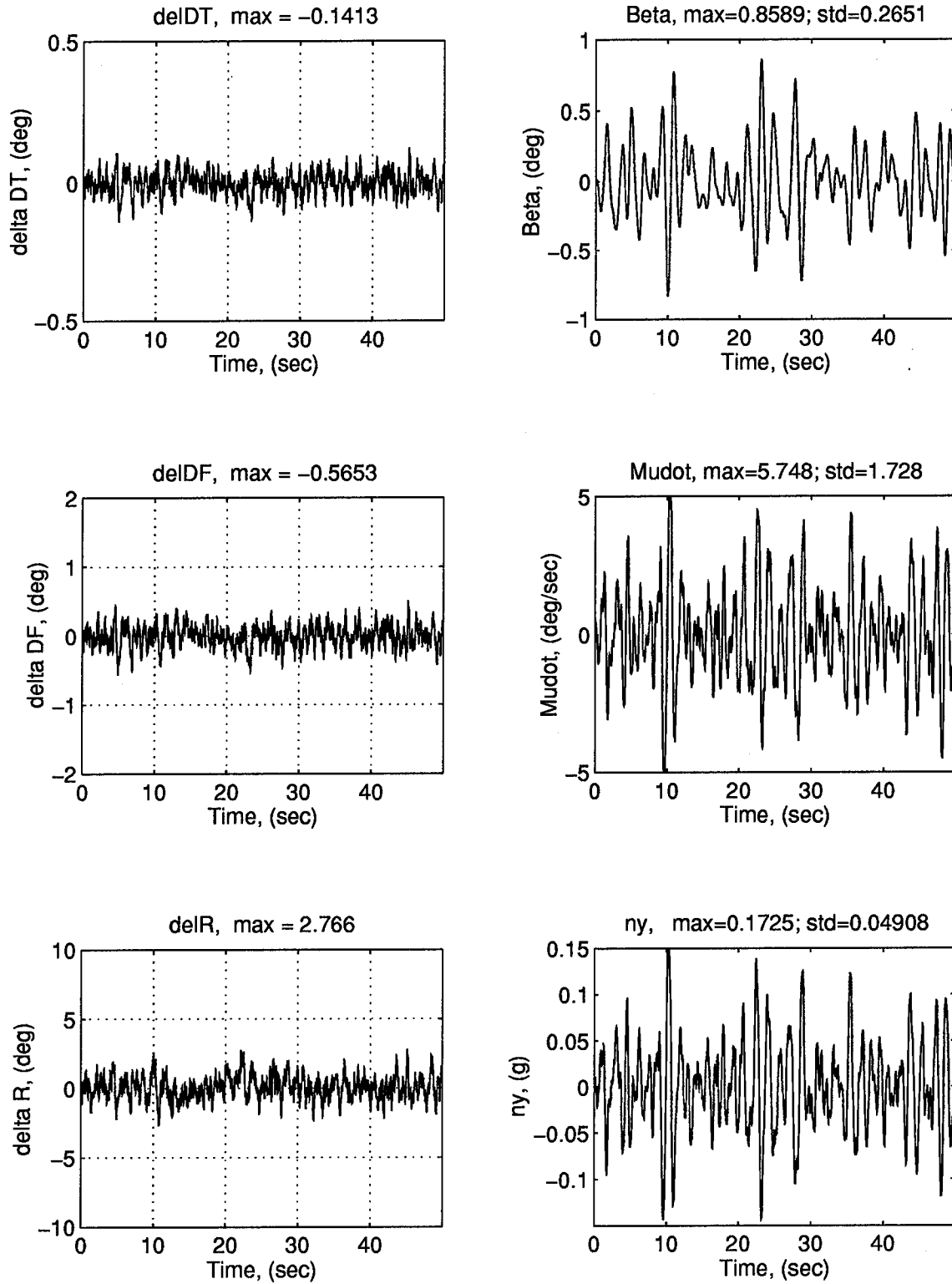


Figure 5.12 System's Response to Wind Gust and Sensor Noise, Mixed Controller A

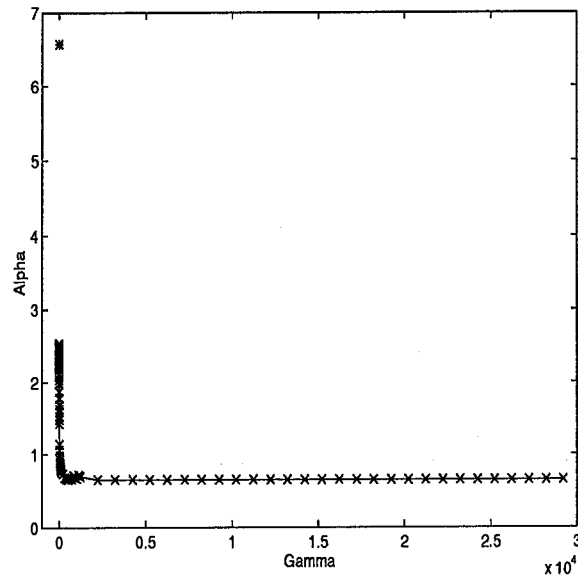


Figure 5.13 γ vs. α for 23rd order based on Mixed Design A, μ controller shown by *

lower on the curve the performance gets worse. If that was the case, then it may be that the area μ extends its robustness to wasn't reached by our curve. We can see in Figure 5.13 that there is a large gap between the point where our 23rd order curve ends and the point associated with the μ controller.

In this case, the problem is, again, the difference between our design model and our evaluation model. We are saying that our two-norm, which is calculated using the design model, does not accurately reflect the "truth" which we see in our evaluation model. Therefore, to test this theory, we can use the evaluation model to calculate our two-norm. We will form the open loop system (P) from the evaluation model, close the system with the controller and calculate *that* two-norm. This will give us the "true" two-norm. We will do this for the 9th order controller that we used (Mixed Controller A) and for the μ controller. Appendix C gives the state space representation of the open loop evaluation model and the resulting matrices. The resulting two-norms are:

$$\alpha_{\mu} = 0.27$$

$$\alpha_A = 0.12$$

The two-norm for Mixed Controller A is less than half that of the μ controller, and should have less noise than μ . Since this two-norm was calculated from the evaluation model and we are simulating using the evaluation model, we know that we have an accurate measure of the two-norm. This is in direct contrast to what we've seen in the time responses. There is only one choice left to us. The overall two-norm isn't an accurate measure of the noise. This will be examined in the next chapter.

VI. H_2 Revisited

6.1 Another Look at the Two-norm

So far we've been taking the two-norm of the whole system as our objective and using the two-norm as an indication of the "noisiness" in our system. However, we have seen that it isn't a reliable indicator. Even though the two-norm for Mixed Controller A is less than the two-norm of the μ controller, the time responses are much noisier. How can this be?

The answer lies in a basic property of the two-norm. We can split up an H_2 system into components (when we are calculating the two-norm). In the case of the system in Figure 6.1, we can consider the system as two systems that are the same except for the choice of outputs. One system (designated T_{st}) will have only $Z_{states} = [\beta, \mu]^T$ and the other system (designated T_{ctr}) will have only $Z_{control} = [\delta_A, \delta_R]^T$ (the generalized controls). The two-norms are related by

$$\|T_{zw}\|_2^2 = \|T_{st}\|_2^2 + \|T_{ctr}\|_2^2 \quad (6.1)$$

Two proofs are available. One uses the Lyapunov equations which are used to calculate the two-norm (2.4 through 2.6), the other uses the definition of the two-norm (2.1). We will use the

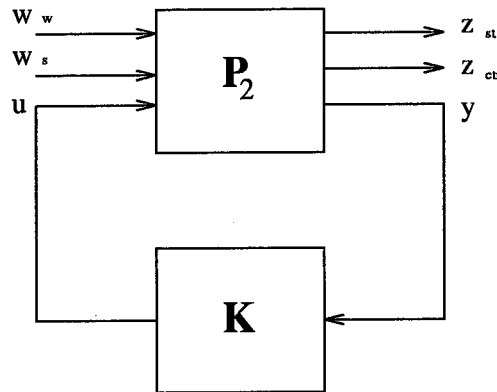


Figure 6.1 P-K version of the H_2 part of the H_2/H_∞ problem

latter. Let

$$Z = \begin{bmatrix} Z_{st} \\ Z_{ctr} \end{bmatrix} \quad (6.2)$$

where Z_{st} is the output concerning the states and Z_{ctr} the output that weights control usage. For now, leave the exogenous input as one vector, w . Then

$$T_{zw} = \begin{bmatrix} Z_{st}/w \\ Z_{ctr}/w \end{bmatrix} := \begin{bmatrix} T_{st} \\ T_{ctr} \end{bmatrix} \quad (6.3)$$

Now, by the definition of the two-norm,

$$\alpha_{tot} := \|T_{zw}\|_2^2 \quad (6.4)$$

$$:= \frac{1}{2\pi} \int_{-\infty}^{+\infty} \text{tr} [T_{zw}^* T_{zw}] d\omega \quad (6.5)$$

$$= \frac{1}{2\pi} \int_{-\infty}^{+\infty} \text{tr} \begin{bmatrix} T_{st}^* & T_{ctr}^* \end{bmatrix} \begin{bmatrix} T_{st} \\ T_{ctr} \end{bmatrix} d\omega \quad (6.6)$$

$$= \frac{1}{2\pi} \int_{-\infty}^{+\infty} \text{tr} [T_{st}^* T_{st} + T_{ctr}^* T_{ctr}] d\omega \quad (6.7)$$

$$= \frac{1}{2\pi} \int_{-\infty}^{+\infty} \text{tr} [T_{st}^* T_{st}] d\omega + \frac{1}{2\pi} \int_{-\infty}^{+\infty} \text{tr} [T_{ctr}^* T_{ctr}] d\omega \quad (6.8)$$

$$= \|T_{st}\|_2^2 + \|T_{ctr}\|_2^2 \quad (6.9)$$

$$:= \alpha_{st}^2 + \alpha_{ctr}^2 \quad (6.10)$$

With this in mind, we should reexamine our results and look at all three two-norms (we will designate the total two-norm as α_{tot}). To do this, all we have to do is change the C matrix to correspond with the appropriate outputs. MATLAB's μ -Toolbox does this very easily using the SEL (select) command. It takes a *system* matrix ¹ and the appropriate division of Z and forms

¹One way the μ -Toolbox can represent the system. A system is put in this form using the "PCK" (pack) command. It takes the A , B , C and D matrices and packs them together into one matrix with some additional information inside to tell the number of states. It can then determine the number of inputs and outputs.

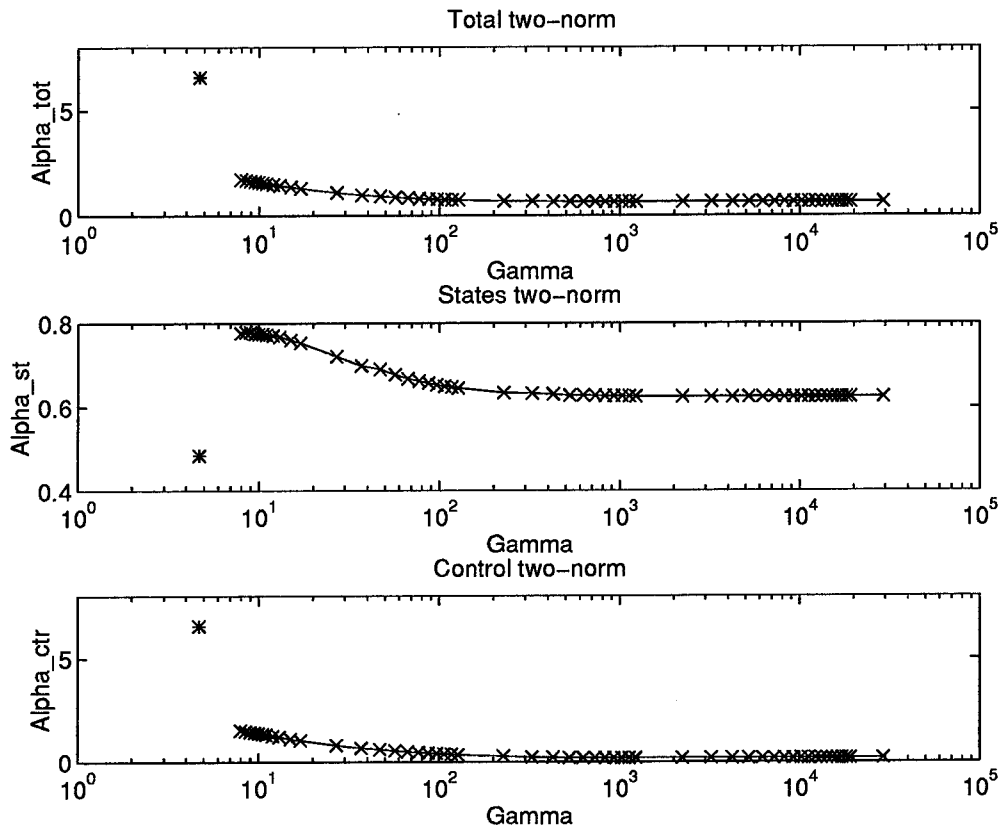


Figure 6.2 γ vs. α curves for the various two-norms using Design A (x), and the μ Controller(*)

the corresponding system matrix for the new system. Table 6.1 shows the final results of the calculations. In fact, we can do this for the whole γ vs. α curve we calculated before. This is found in Figure 6.2.

Table 6.1 Various two-norms for the μ Controller and Mixed Controller A

Controller	α_{tot}	α_{st}	α_{ctr}
μ	6.5668	0.4848	6.5489
Mixed A	2.8271	0.7803	2.7172

After calculating the two-norms of the individual α 's, we see that α_{st} is indeed higher for Controller A than for μ . This corresponds with the time histories we have observed. We also see that α_{ctr} increases as γ decreases. This makes sense in that α_{ctr} is bigger than α_{st} , and therefore

contributes heavily to α_{tot} . Thus, most of the concentration when decreasing α_{tot} is to decrease α_{ctr} . Unfortunately this doesn't correspond with the output we are most concerned about, Z_{states} .

In fact, we can see from Figure 6.2 that we have a problem from the start. At H_2 optimal, we see that we start out at a higher α_{st} than that of μ , so of course the mix will not work well in terms of α_{st} . This is not a good controller from the start.

6.2 Mixed H_2/μ Design B

Let's go back and look at the earlier H_2 design and corresponding controller (from Chapter V) that destabilized the system. Call this H_2 Controller B. Its two-norms are shown in Table 6.2.

Table 6.2 Various two-norms for the μ Controller and H_2 Controller B

Controller	α_{tot}	α_{st}	α_{ctr}
μ	1.120	1.116	0.0894
H_2B	0.4026	0.4021	0.0206

Table 6.3 Change in μ Controller Noise and Wind Effects using H_2 Controller B

state	maximum value	standard deviation	control surface	maximum control deflection
β	-32%	-33%	δ_{DT}	-81%
$\dot{\mu}$	+25%	+21%	δ_{DF}	-81%
n_y	-14%	-8%	δ_R	-71%

Now we are starting out in a good position, with $\alpha_{st}(H_2) < \alpha_{st}(\mu)$. Traditionally, this controller would not have been used in the mixed algorithm since it is not really a good controller by itself (it destabilizes the evaluation model!). However, we will try it anyway in the hopes that the μ controller will extend its robustness characteristics to the mixed controller enough that the mixed controller will stabilize the evaluation model.

For consistency, the summary of the noise and wind responses of H_2 Controller B is found in Table 6.3.

Using H_2 Controller B, the new “end points” are:

$$\mu: \quad \bar{\alpha} = 1.12 \quad \underline{\gamma} = 4.709 \quad 26^{th} order \quad (6.11)$$

$$H_2: \quad \underline{\alpha} = 0.4026 \quad \bar{\gamma} = 3.323e + 5 \quad 9^{th} order \quad (6.12)$$

The γ vs. α curves are found in Figure 6.3. At this point, our main concern is finding an H_2 controller which does better than the μ controller in noise and disturbance rejection. This is where our attention will focus. Thus, we will choose a fairly low α (and subsequently high γ) for our mixed controller. In this way, we hope to determine if our mixed design has potential. The chosen mixed controller (Mixed Controller B) has $\gamma = 18.046$ and $\alpha_{tot} = 0.6228$.

First, let's look at the two-norms. Table 6.4 lists the various two-norms for the “ends” and chosen mixed controller.

Table 6.4 Various two-norms for the μ Controller, H_2 Controller B and Mixed Controller B

Controller	α_{tot}	α_{st}	α_{ctr}
μ	1.120	1.116	0.0894
Mixed B	0.6228	0.6207	0.0514
H_2 B	0.4026	0.4021	0.0206

This looks promising, as $\alpha_{st}(\text{Mixed}) < \alpha_{st}(\mu)$. We also see from Figure 6.4 that Mixed Controller B stabilizes the evaluation model. The μ Controller obviously extended its robustness to this controller. The summary of responses is found in Table 6.5.

Table 6.5 Change in μ Controller Noise and Wind Effects using Mixed Controller B

state	maximum value	standard deviation	control surface	maximum control deflection
β	+50%	+46%	δ_{DT}	-37%
$\dot{\mu}$	+34%	+32%	δ_{DF}	-37%
n_y	+33%	+34%	δ_R	-40%

Again, we are in a quandary. The system's response is worse in all of the 3 states we care about. This is in spite of the fact that $\alpha_{st}(H_2) < \alpha_{st}(\mu)$. We must re-examine the two-norm issue.

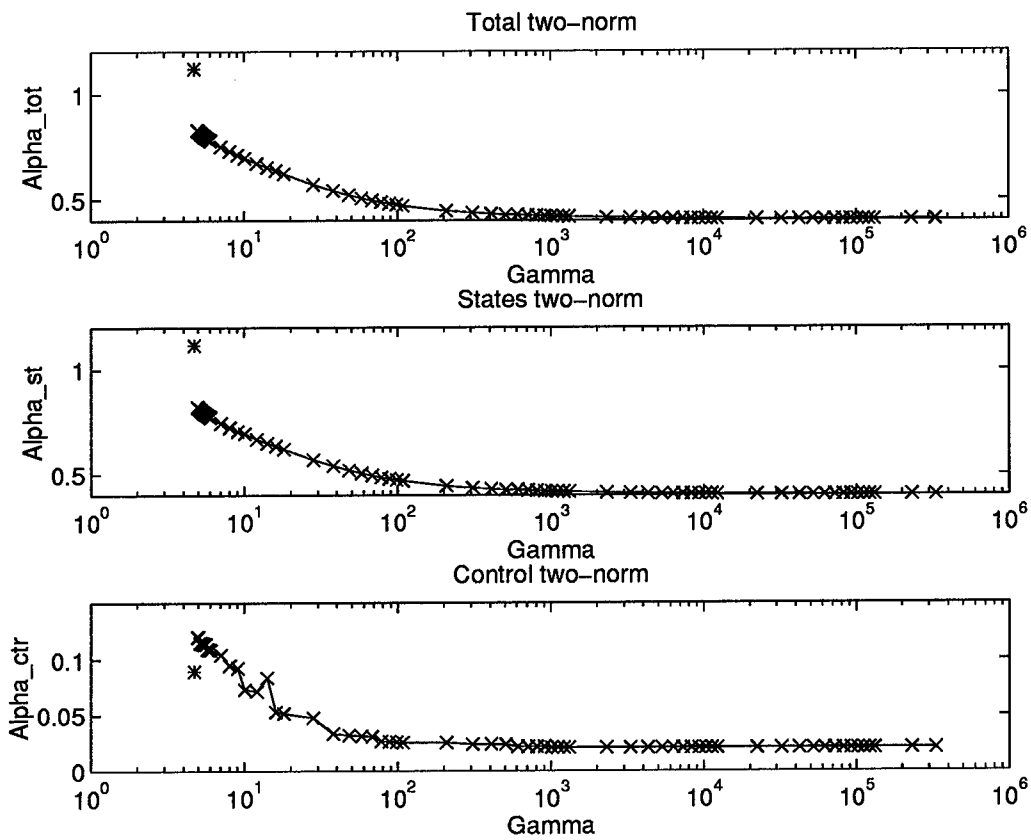


Figure 6.3 γ vs. α curves for the various two-norms using Design B (x) and the μ Controller(*)

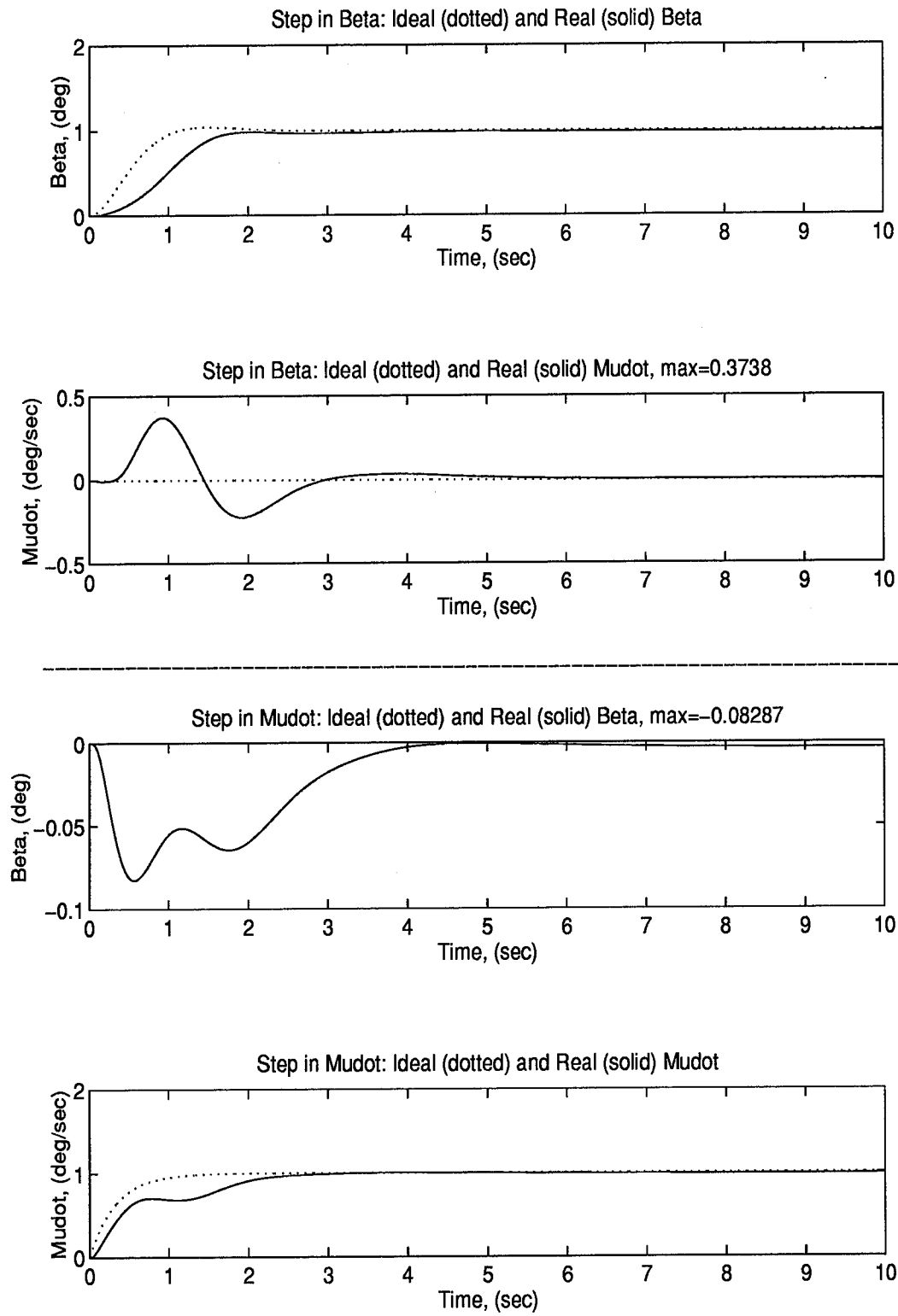


Figure 6.4 System's Response to Steps in β and $\dot{\mu}$, Mixed Controller B

6.3 Yet Another Look at the Two-norm

Let's now look at what Z in (6.2) consists of.

$$z = T_{zw} w = \begin{bmatrix} T_{st} \\ T_{ctr} \end{bmatrix} w = \begin{bmatrix} T_{st} \\ T_{ctr} \end{bmatrix} \begin{bmatrix} w_w \\ w_s \end{bmatrix} \quad (6.13)$$

$$= \begin{bmatrix} T_{st_w} & T_{st_s} \\ T_{ctr_w} & T_{ctr_s} \end{bmatrix} \begin{bmatrix} w_w \\ w_s \end{bmatrix} \quad (6.14)$$

$$T_{zw} = \begin{bmatrix} T_{st_w} & T_{st_s} \\ T_{ctr_w} & T_{ctr_s} \end{bmatrix} \quad (6.15)$$

Now we substitute (6.15) into the definition of the two-norm.

$$\|T_{zw}\|_2^2 := \frac{1}{2\pi} \int_{-\infty}^{+\infty} \text{tr} [T_{zw}^* T_{zw}] d\omega \quad (6.16)$$

$$= \frac{1}{2\pi} \int_{-\infty}^{+\infty} \text{tr} \left\{ \begin{bmatrix} T_{st_w}^* & T_{ctr_w}^* \\ T_{st_s}^* & T_{ctr_s}^* \end{bmatrix} \begin{bmatrix} T_{st_w} & T_{st_s} \\ T_{ctr_w} & T_{ctr_s} \end{bmatrix} \right\} d\omega \quad (6.17)$$

$$= \frac{1}{2\pi} \int_{-\infty}^{+\infty} \text{tr} \{ T_{st_w}^* T_{st_w} + T_{st_s}^* T_{st_s} + T_{ctr_w}^* T_{ctr_w} + T_{ctr_s}^* T_{ctr_s} \} d\omega \quad (6.18)$$

$$= \|T_{st_w}\|_2^2 + \|T_{st_s}\|_2^2 + \|T_{ctr_w}\|_2^2 + \|T_{ctr_s}\|_2^2 \quad (6.19)$$

$$:= \alpha_{st_w}^2 + \alpha_{st_s}^2 + \alpha_{ctr_w}^2 + \alpha_{ctr_s}^2 \quad (6.20)$$

We could extend this even further by breaking up the vectors Z_{st} and Z_{ctr} into their individual signals :

$$Z_{st} = \begin{bmatrix} \beta \\ \dot{\mu} \end{bmatrix}$$

$$Z_{ctr} = \begin{bmatrix} \delta_A \\ \delta_R \end{bmatrix}$$

Hopefully, this will be unnecessary.

Now we can examine the various two-norms of the system we just designed.

Table 6.6 Various two-norms for the μ Controller and Mixed Controller B

Controller	α_{tot}	α_{st}	α_{st_w}	α_{st_s}	α_{ctr}	α_{ctr_w}	α_{ctr_s}
μ	1.1195	1.1160	0.0472	1.1150	0.0894	2.7543e-4	0.0894
Mixed B	0.6228	0.6207	0.0648	0.6173	0.0514	2.4868e-4	0.0514
H_2 B	0.4026	0.4021	0.0597	0.3976	0.0206	6.3648e-5	0.0206

Even though α_{st} is going in the right direction, the bulk of it is composed of α_{st_s} . It should be the sensor noise that is affected the most and in the right direction. To verify this result, the wind in the evaluation model was multiplied by zero to "turn it off". Simulations of the sensor-noise-only response were then completed for both the μ Controller and Mixed Controller B. The maximum magnitude and the standard deviation of the responses were then compared as before. The results of the comparison are in Table 6.7. The plots for Mixed Controller B are shown in Figures 6.5 and 6.6 for later discussion.

Table 6.7 Change in μ Controller Noise Effects Only using Mixed Controller B

state	maximum value	standard deviation	control surface	maximum control deflection
β	-65%	-63%	δ_{DT}	-56%
$\dot{\mu}$	-54%	-48%	δ_{DF}	-56%
n_y	-55%	-50%	δ_R	-53%

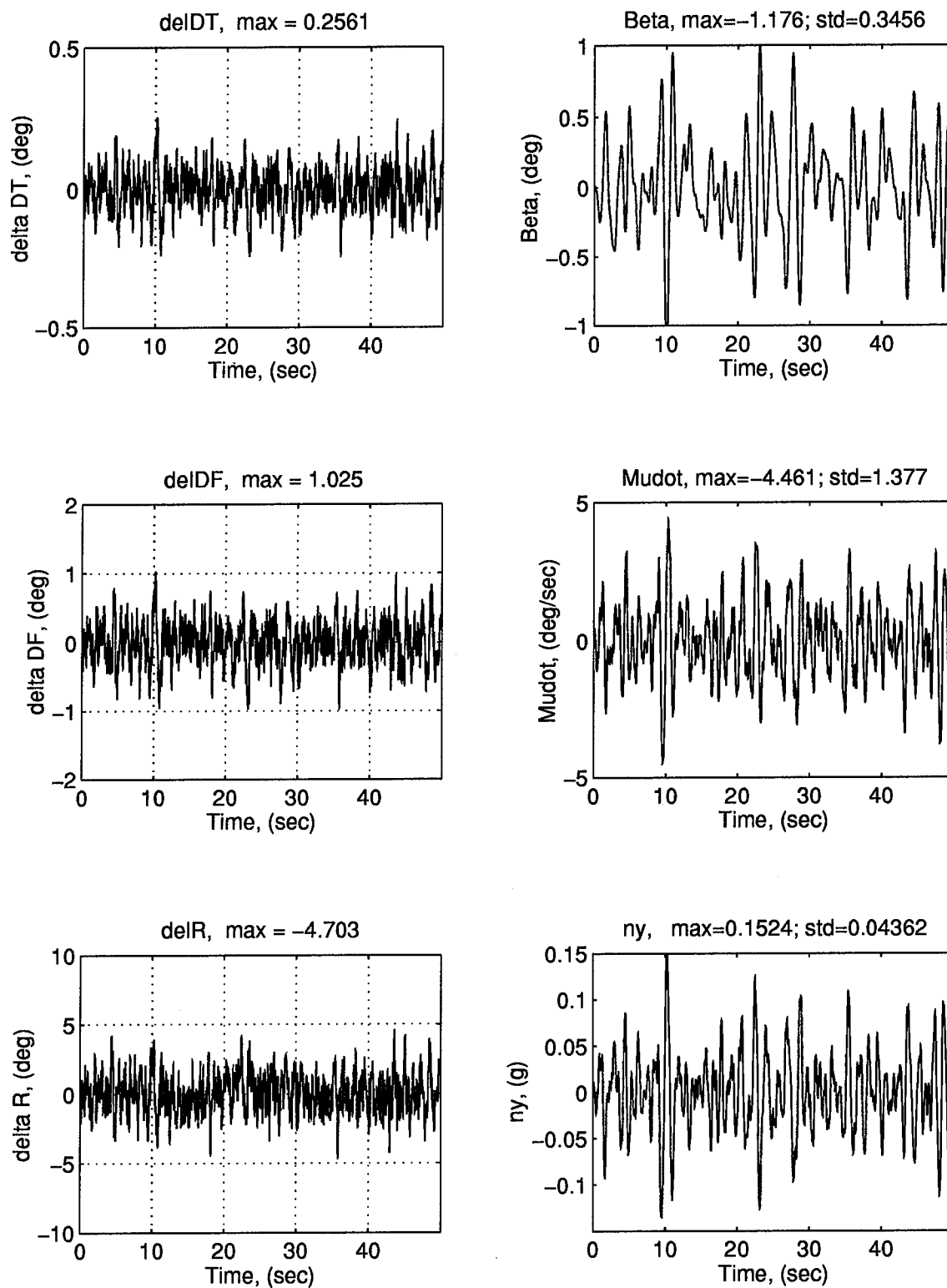


Figure 6.5 System's Response to Wind Gust and Sensor Noise, Mixed Controller B

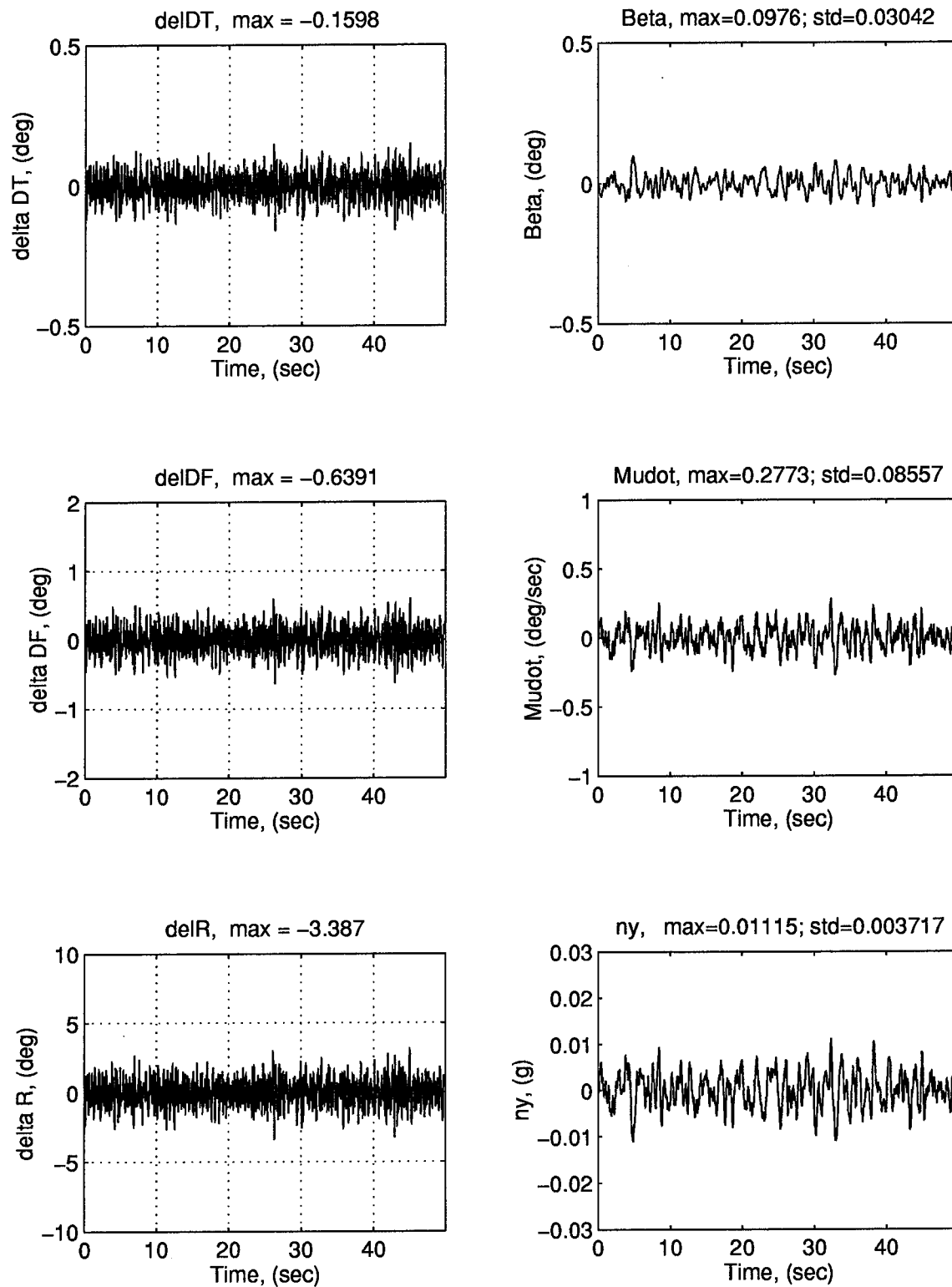


Figure 6.6 System's Response to Sensor Noise only, Mixed Controller B

After comparing Table 6.7 with Table 6.5, we see that the sensor noise was, in fact, affected the most favorably by this controller. We also see when comparing Figure 6.6 to Figure 6.5 that the response to sensor-noise-only is very small compared to the response of wind-and-sensor-noise. Therefore, the majority of the wind-and-sensor-noise response is due to the wind. This corresponds to what we would expect. Thus, it is really α_{st_w} we are trying to decrease as we walk down the curve. We are concerned with α_{st_s} as well, but since the noise response is so small, it would be sufficient if α_{st_s} remains below a certain amount. This sounds like an optimization problem with a (some) constraint(s).

Note also from Table 6.6 that H_2 Controller B has a higher α_{st_w} than the μ Controller. The way the problem is set up, α_{st_w} has to increase. We obviously must have α_{st_w} lower for the anchor than for μ . That, however, is not the end of our problem.

The optimization program we are running tries to produce the optimal curve for that order. Since we are using the μ controller as a reference, we will examine what happens as the curve is traced from the μ controller to the H_2 optimal controller. For the μ controller, we have seen that α_{tot} is made up mostly of α_{st} which is made up mostly of α_{st_s} . In other words, α_{st_s} makes up the majority of α_{tot} . Therefore, as the program forces α_{tot} to decrease (walking down the curve from the μ controller), it is forcing α_{st_s} to decrease. As long as α_{st_s} is decreasing, α_{st_w} could decrease or increase since it is so small. If the H_2 optimal controller had a lower α_{st_w} than the μ controller, but it didn't make up the bulk of α_{st} , there would be nothing to prevent α_{st_w} from getting larger than the corresponding μ value at some point on the curve causing our time responses to get worse.

In fact, we see something similar in α_{st_w} in Table 6.6. There, we see a situation where the mixed controller has a larger α_{st_w} than either the anchor or the μ controller. This brings up the following question: At the optimal curve for that order, are the paths of the smaller two-norms, in fact, allowed to vary at will? Or are they monotonically increasing or decreasing? If the latter is true, then we see from Table 6.6 that we must be at a local minimum. If the former is true, we can

not make such a generalization and may not be able to say anything at all about how the smaller two-norms will behave.

Assuming local minima are not the problem, the answer to our immediate problem lies in finding a weighted H_2 system which will make α_{st} the largest element of α_{tot} and at the same time make α_{stw} the largest element in α_{st} .

6.4 Mixed H_2/μ Design C

We will now attempt to find the weights for our H_2 system which will do two things:

1. Make α_{stw} the largest element in the α array (largest element in α_{tot})
2. Make α_{tot} for the anchor smaller than for the μ controller

We will start our search by varying the weights of H_2 Controller B since it has better time responses when compared to H_2 Controller A. Recall that even though it was destabilizing to the evaluation model, H_2/μ was able to produce a stabilizing controller.

It may be possible to do something similar to the μ weightings, where we use 2 matrices to produce a ΔA

$$\Delta A = \Delta B \Delta C$$

In our case we would produce a matrix of input weightings and a matrix of output weightings which, when combined, would weight Z_{stw} more than the others.

A simpler yet logical choice would be to make the wind weighting, k_g , larger. This could, by the same logic, also make α_{ctrw} larger, which might make α_{ctr} larger than α_{st} . This would be undesirable. However, α_{ctrw} is so small that making it slightly larger shouldn't hurt too much.

The method used was to increase k_g and examine the two-norm array using the resulting H_2 controller as well as the two-norm array using the μ controller. Recall that it is the μ controller with which we will compare. Also recall that the two-norms are of the weighted H_2 part of the

system, so changing the weights changes T_{zw} . Hence, even though the time responses of the μ controller won't change (we are still using the same controller), the two-norms will (we are using the new H_2 system with that controller).

There are several choices available to us as engineers at this point. We could try to get all two-norms of the H_2 controller less than the corresponding two-norms of μ or we could try to get a little more difference between the noise responses of the wind-and-noise for a little bit of loss in the sensor-only response. This would correspond to allowing the percentage difference of α_{st_s} to get smaller so that the percentage difference of α_{st_w} could get larger. This was the choice made. A value of $k_g = 32$ was chosen. A further increase in k_g ($k_g = 64$) produced a situation where the *only* two-norm that decreased relative to μ was α_{st_w} ; all others increased when compared to μ .

The two-norm array for the new H_2 controller (H_2 Controller C) is seen in Table 6.8.

Table 6.8 Various two-norms for the μ Controller and H_2 Controller C

Controller	α_{tot}	α_{st}	α_{st_w}	α_{st_s}	α_{ctr}	α_{ctr_w}	α_{ctr_s}
μ	1.8789	1.8767	1.5096	1.1150	0.0898	8.8139e-3	0.0894
H_2 C	1.4204	1.4105	1.1310	0.8429	0.1668	8.6967e-3	0.1666

The time response plots of the corresponding H_2 optimal controller are found in Figures 6.7 and 6.8. Tables 6.9 and 6.10 summarize the responses.

Table 6.9 Change in μ Controller Noise and Wind Effects using H_2 Controller C

state	maximum value	standard deviation	control surface	maximum control deflection
β	-77%	-74%	δ_{DT}	-71%
$\dot{\mu}$	-22%	-26%	δ_{DF}	-71%
n_y	-46%	-44%	δ_R	-47%

We see that we finally have an H_2 controller which does better than the μ controller in all areas. The closed loop SV plots for Z_{states}/W_g and Z_{states}/W_s are found in Figure 6.9. We see here that we have indeed reduced the gain at the frequency of interest (3.8 rad/sec). An examination of the step response (not included) showed that this controller is destabilizing to the evaluation model.

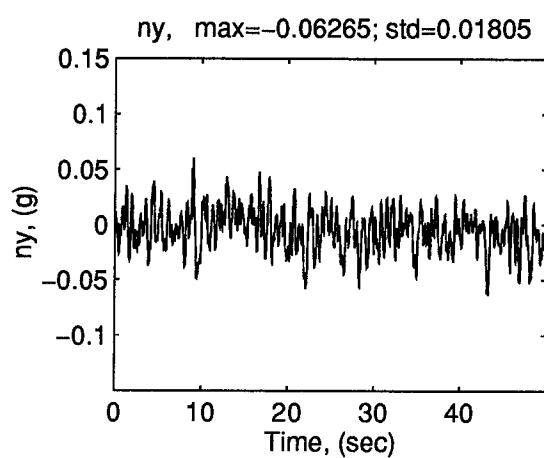
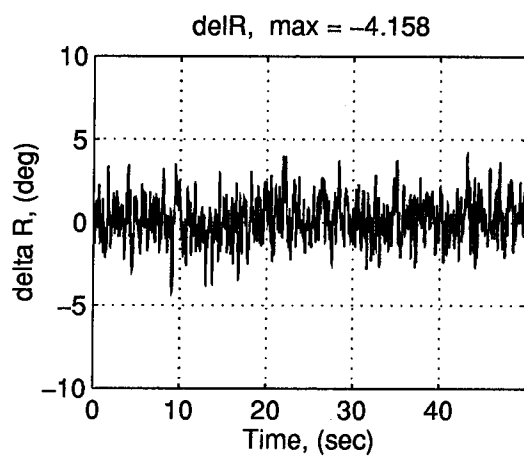
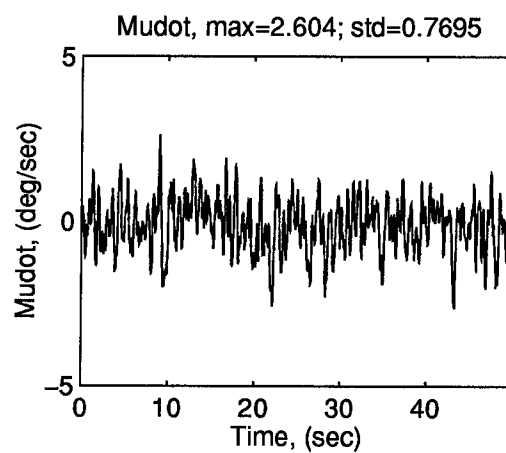
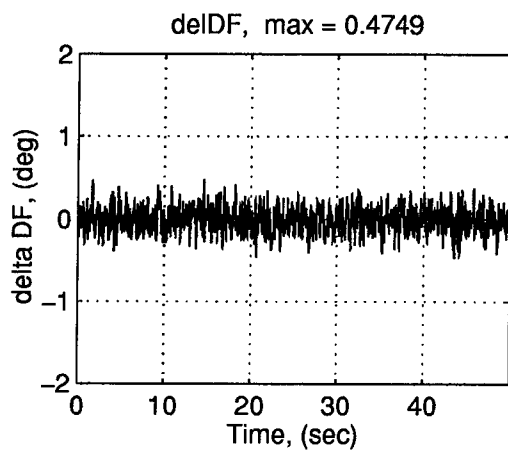
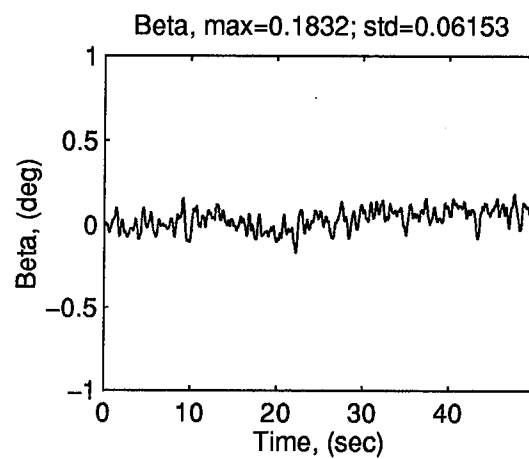
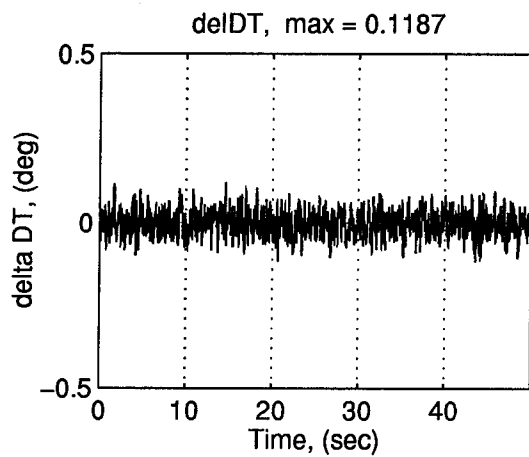


Figure 6.7 System's Response to Wind Gust and Sensor noise, Controller C

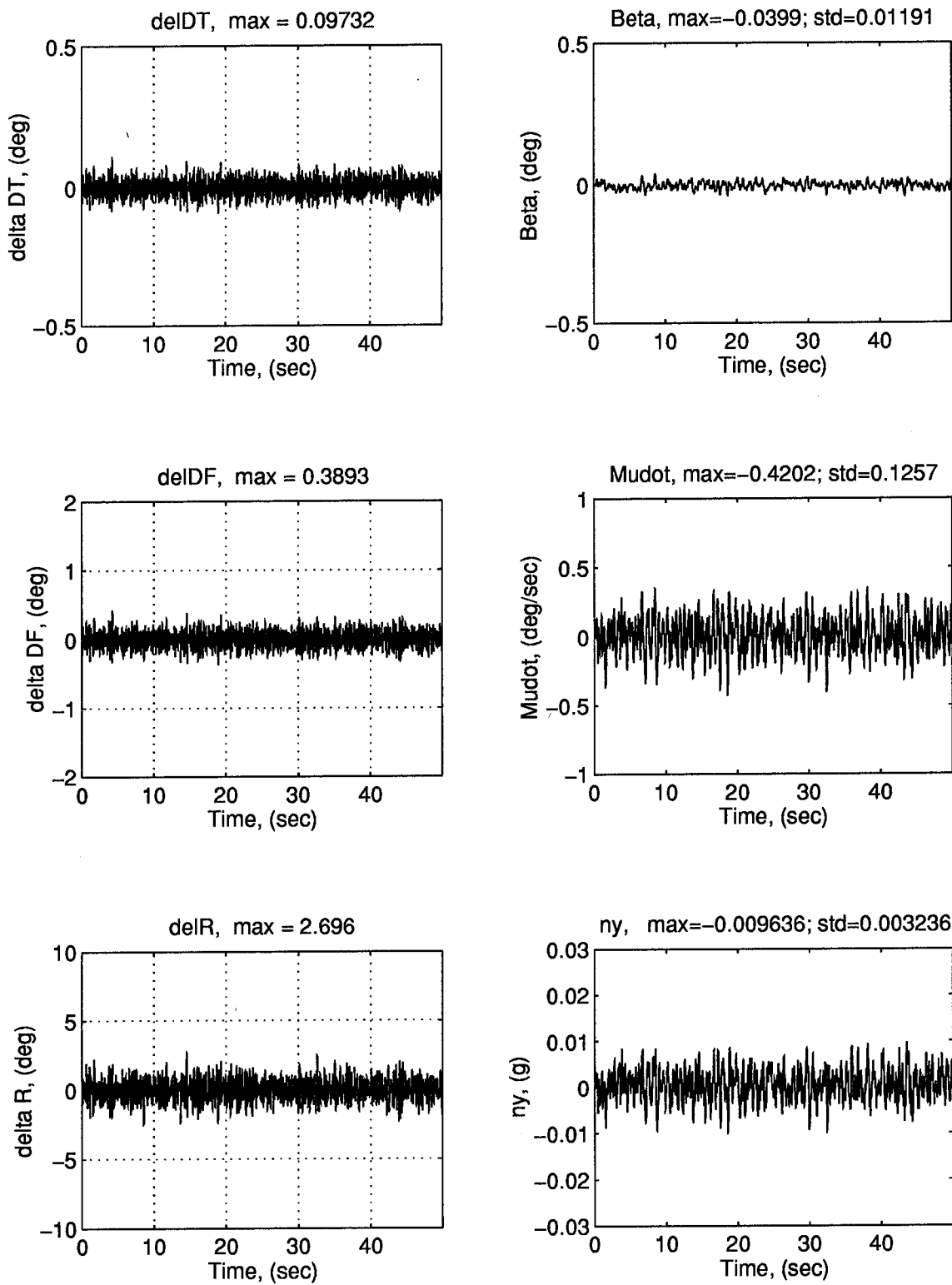


Figure 6.8 System's Response to Sensor noise only, Controller C

Table 6.10 Change in μ Controller Noise Effects Only using H_2 Controller C

state	maximum value	standard deviation	control surface	maximum control deflection
β	-86%	-85%	δ_{DT}	-73%
$\dot{\mu}$	-30%	-23%	δ_{DF}	-73%
n_y	-61%	-56%	δ_R	-62%

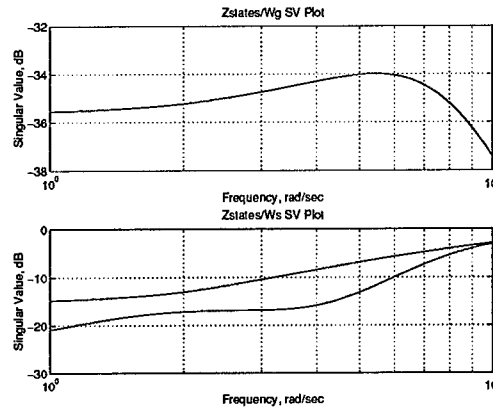


Figure 6.9 Closed loop SV plots for Z_{states} vs. wind gust and sensor noise for Controller C

For later comparison with the mixed controller, Figure 6.10 shows that we have no robustness with our H_2 controller. Our purpose all along has been to incorporate some of μ 's robustness by using the mix and we have seen that μ can also take care of our instability. Both of these things should be taken care of by mixing with μ .

One other point should be brought up before we examine the mixed controller. Note in Table 6.11 that α_{ctr} (and α_{ctr_s}) is larger for H_2 Controller C than for μ , yet the responses show the opposite. The explanation is probably due to the fact that we have been calculating the two-norms using the weighted H_2 system and not the evaluation model.

The resulting γ vs. α curves for mixed H_2/μ with this new (and final) controller is found in Figure 6.11. A mixed controller with $\alpha_{tot} = 1.582$, $\gamma = 7.997$ was chosen as Mixed Controller C. Note that this figure does not plot the whole two-norm array.

The two-norm array is shown in Table 6.11.

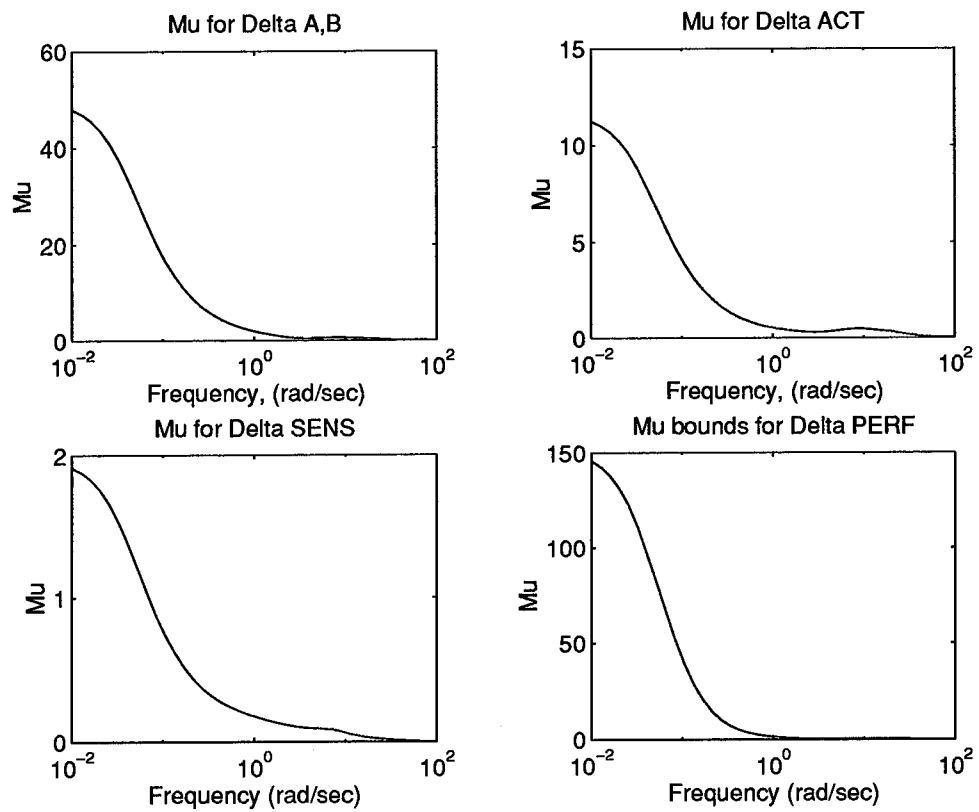


Figure 6.10 μ bounds plot of Controller C

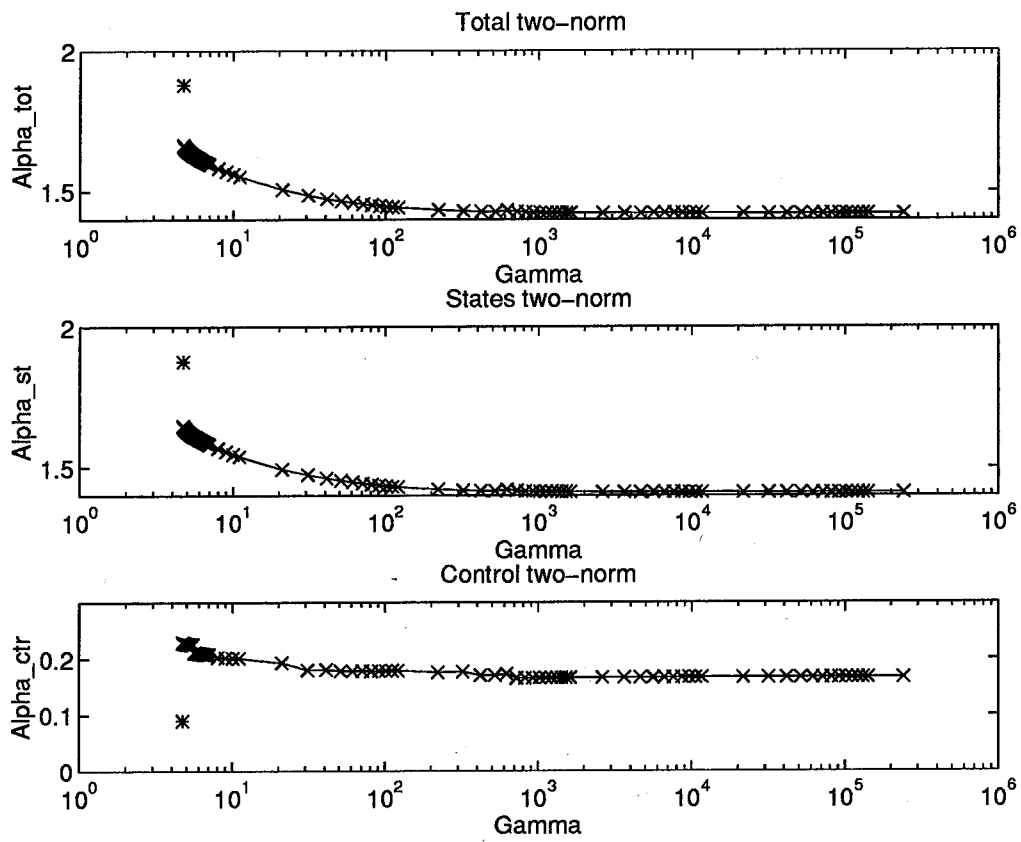


Figure 6.11 γ vs. α curve for the various two-norms using Design C (x) and the μ controller (*)

Table 6.11 Various two-norms for the μ Controller and Mixed and H_2 Controller C

Controller	α_{tot}	α_{st}	α_{st_w}	α_{st_s}	α_{ctr}	α_{ctr_w}	α_{ctr_s}
μ	1.8789	1.8767	1.5096	1.1150	0.0898	8.8139e-3	0.0894
mixed C	1.5819	1.5688	1.1426	1.0750	0.2025	9.3628e-3	0.2023
H_2 C	1.4204	1.4105	1.1310	0.8429	0.1668	8.6967e-3	0.1666

The time response plots of the corresponding mixed controller are found in Figures 6.12 and 6.13. The summary of these responses are found in Tables 6.12 and 6.13. Just as was the case for H_2 Controller C, we see that the time response plots follow the two-norms except for the control usage. This discrepancy, again, may be attributable to the difference between the H_2 design model and the evaluation model.

Table 6.12 Change in μ Controller Noise and Wind Effects using Mixed Controller C

state	maximum value	standard deviation	control surface	maximum control deflection
β	-59%	-54%	δ_{DT}	-30%
$\dot{\mu}$	-24%	-24%	δ_{DF}	-30%
n_y	-43%	-38%	δ_R	-28%

Table 6.13 Change in μ Controller Noise Effects Only using Mixed Controller C

state	maximum value	standard deviation	control surface	maximum control deflection
β	-24%	-24%	δ_{DT}	-28%
$\dot{\mu}$	-6%	+1%	δ_{DF}	-28%
n_y	-20%	-15%	δ_R	-24%

We can see from Figure 6.14 that Mixed Controller C is indeed stabilizing for the evaluation model and provides a fairly good step response. From Figure 6.15 we see that this controller provides robustly stability and robust performance. For comparison purposes, the noisy step response of Mixed Controller C is found in Figure 6.16, the noisy step response of the μ controller is recreated in Figure 6.17. Most of the difference initially is due to the fact that the mixed controller tracks a little worse than the μ controller. After the initial response, though, we can see that the noise response is slightly better for the mixed controller.

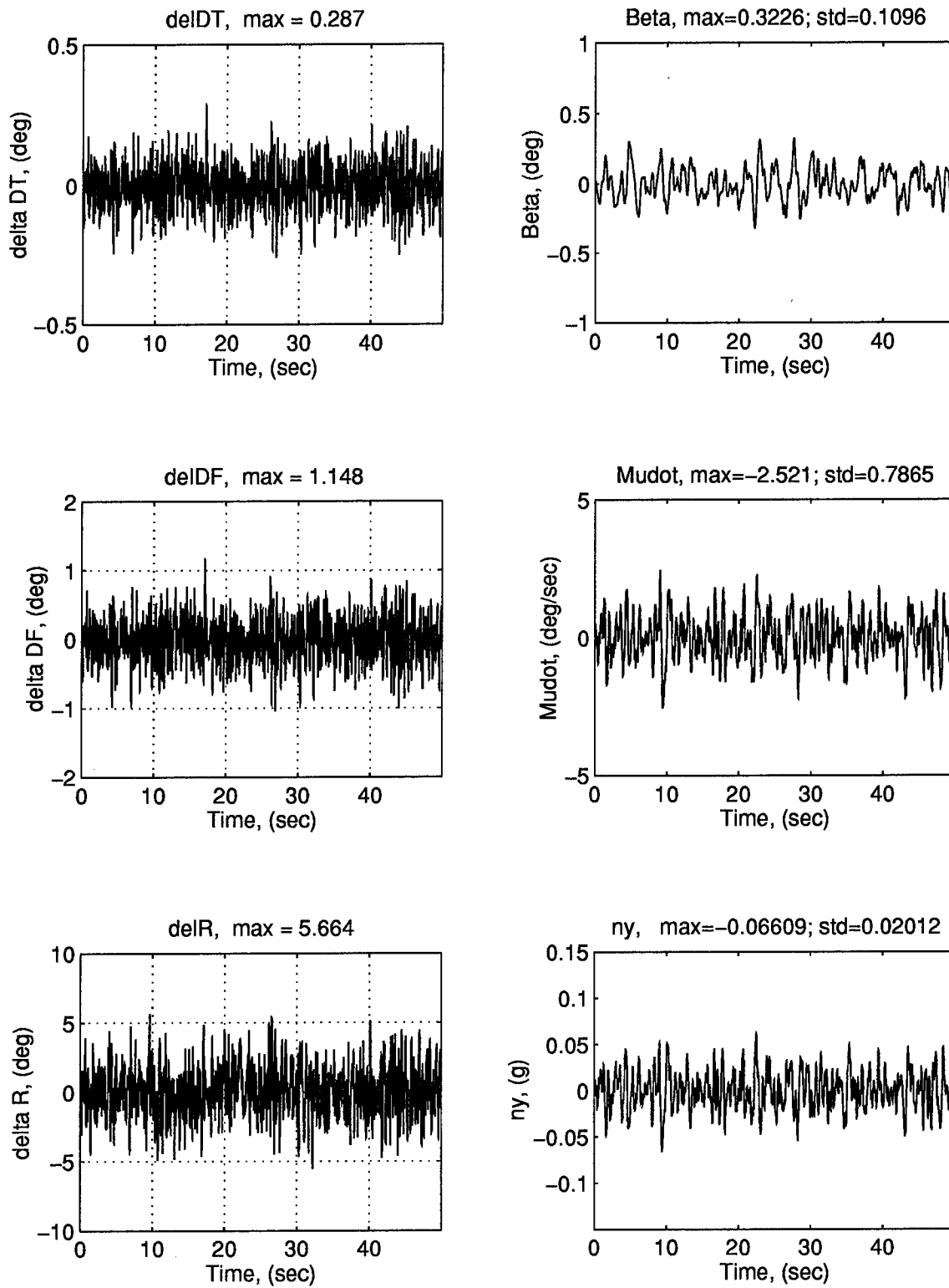


Figure 6.12 System's Response to Wind Gust and Sensor noise, Mixed Controller C

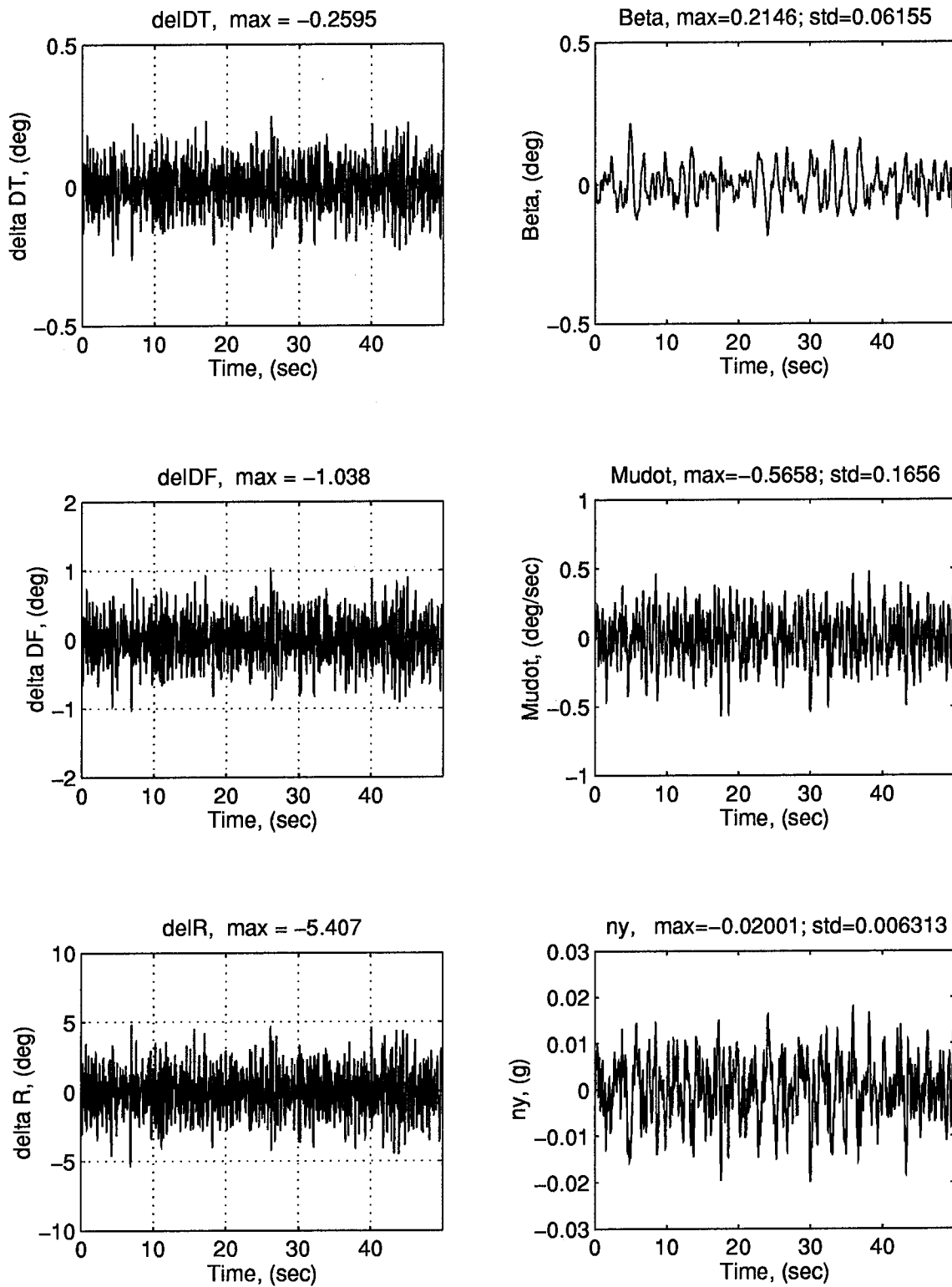


Figure 6.13 System's Response to Sensor noise only, Mixed Controller C

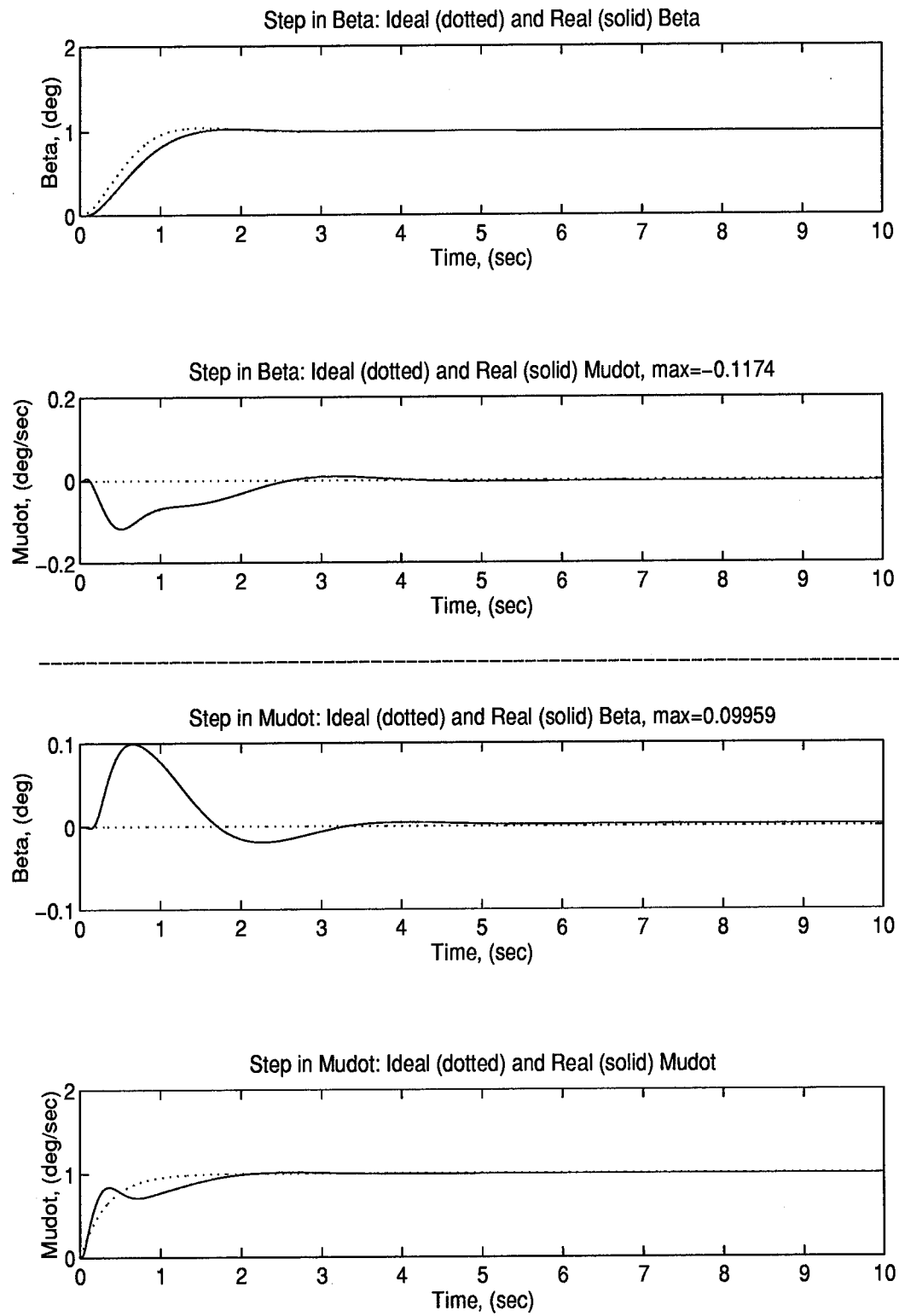


Figure 6.14 Step Response plot of Mixed Controller C

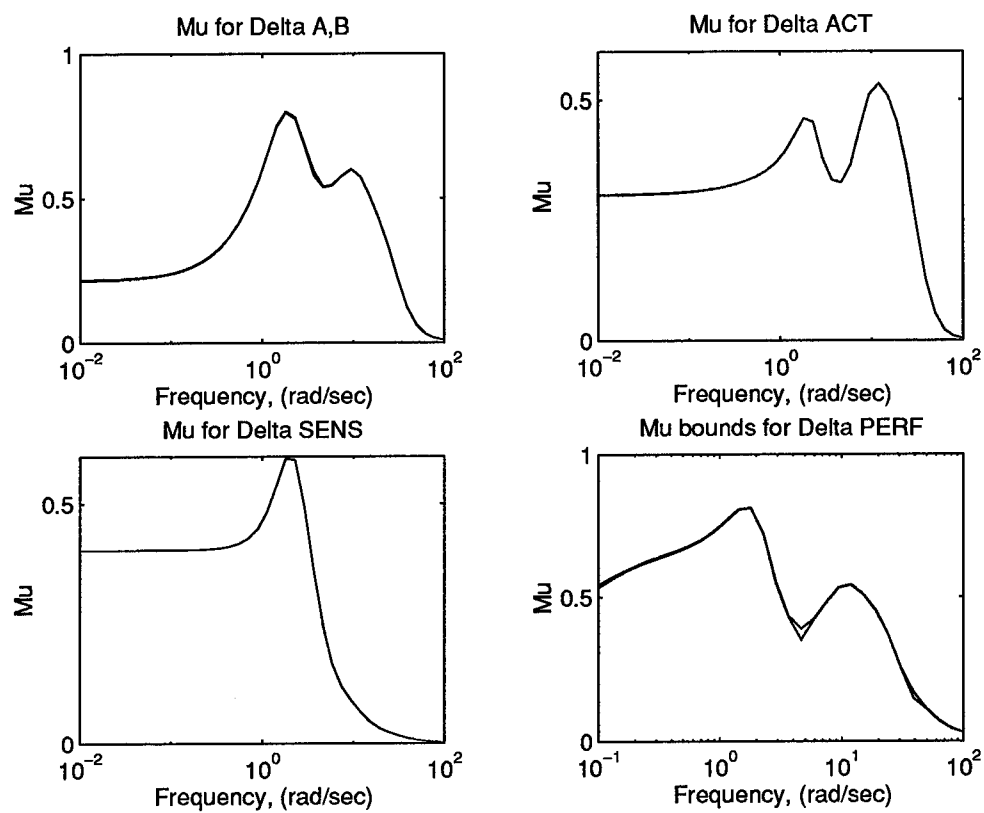


Figure 6.15 μ bounds plot of Mixed Controller C

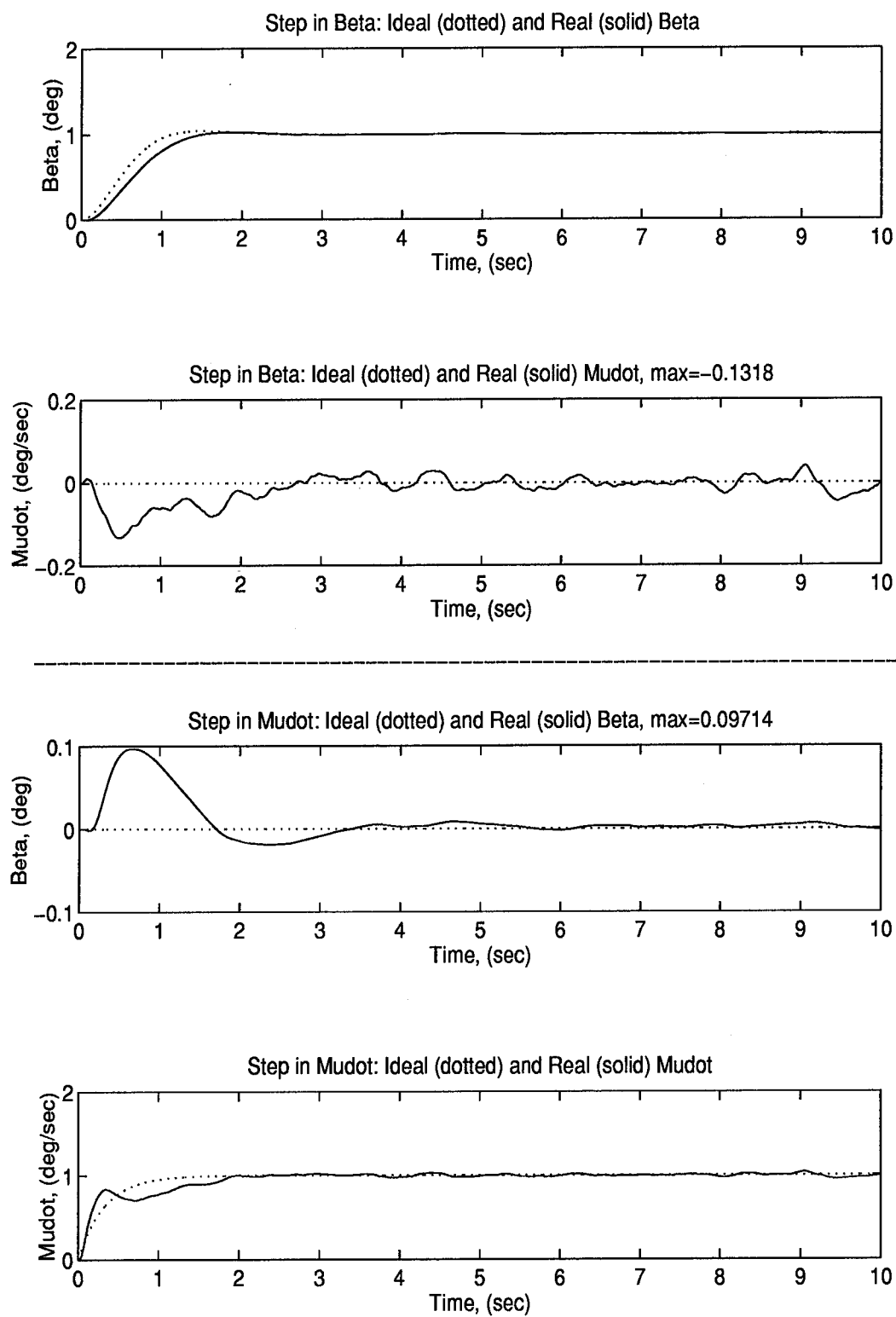


Figure 6.16 Noisy Step Response plot of Mixed Controller C

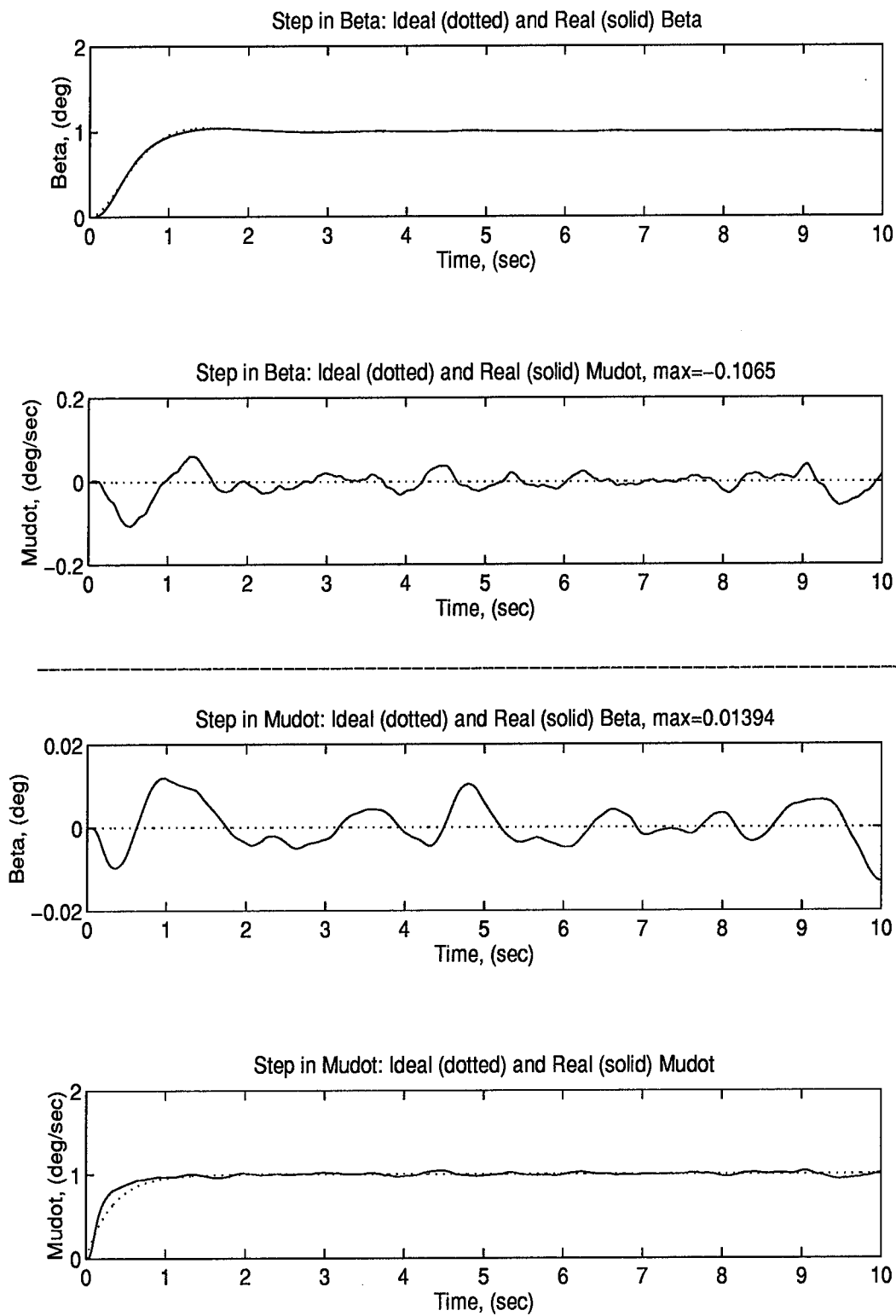


Figure 6.17 Noisy Step Response plot of the μ controller

We finally have a good mixed controller. This mixed H_2/μ controller (Mixed Controller C) incorporates most of the robustness and performance of the μ controller while decreasing the effect of noise and wind gusts on the system. This reduction is fairly significant for the wind-and-noise response and less so for the noise-only response. Note that this improvement is accomplished for a 9th order controller compared to the 26th order μ controller. For these reasons, it is felt that Mixed Controller C is "better" than the μ controller.

VII. Conclusions and Recommendations

7.1 Summary and Conclusions

This thesis examined the mixed H_2/μ problem for a MIMO system. The system chosen was the lateral/directional model of the VISTA F-16. The μ controller proved to be not only very robust with good model following capabilities, but also proved to do reasonably well at noise and disturbance rejection. Due to this, it was difficult to determine the design weightings which would produce an H_2 controller that surpasses μ 's performance in these areas.

In the process of attempting to find just such a controller, several novel techniques were developed to aid in determining the appropriate design weightings for the H_2 system (which would then result in the H_2 controller). The method that was the most successful involved decomposing the two-norm of the system into its constituent elements, the two-norms of the corresponding individual elements of z and w . In this way, we were able to determine the weights which we needed to concentrate on to improve the H_2 noise rejection over the μ controller's. Once we had those, it was a simple matter to improve the H_2 design.

We also found that it was possible to use an H_2 controller which destabilized the evaluation model and still have the resulting mixed H_2/μ controller stabilize the evaluation model. This fact expands the set of controllers which can be used as the "anchor" to the mixed H_2/μ curve (the H_2 optimal point). This may be necessary for the H_2 controller to have better performance than the μ controller.

A 9th order mixed H_2/μ controller was found which improved upon the 26th order μ controller's noise (wind gust and sensor noise) response. This was accomplished while still maintaining acceptable levels of robustness and step response performance.

7.2 Recommendations

- Examine other flight conditions. The design of the inner loop is to force the response of the system to be the same for multiple flight conditions. This thesis analyzed the responses at the *central* flight condition. Other flight conditions should be examined to verify the capability of the inner loop in the mixed H_2/μ problem.
- Use a more accurate model of the VISTA F-16 for the evaluation model. The evaluation model used in this thesis was a simplified, linearized model of the equations of motion. There exists a high fidelity, six degree of freedom, nonlinear simulation model for the VISTA F-16 [ABSB92]. This model should be used to truly evaluate the controller developed in this thesis. This is especially true since the H_2 optimal that was used destabilized the evaluation model. The nonlinear model would be the truth model.
- Examine the discrepancy in the two-norm for control. The two-norms of the control usage terms of the final controller disagreed with the corresponding time responses. There is, as of yet, no explanation for this.
- Attempt to incorporate the constituent two-norms into the optimization routine directly. Now that we know the composition of the two-norm, we can choose the two-norm associated with the item we are most interested in. We could make this two-norm the objective in our optimization routine and treat the other two-norms as constraints. Another possibility would be to make the objective a weighting of some or all of the constituent two-norms and the remaining two-norms left as constraints.
- Study the use of the two-norm decomposition in H_2/H_∞ and H_2/μ . This thesis performed the preliminary investigation. More work is needed. What is the effect, if any, of the ratios between the two-norms? When on the optimal fixed order curve, do the individual two-norms follow a monotonically increasing/decreasing path? If not, is there any way to predict when they would increase or decrease?

Appendix A. Model Data

A.1 Design Model Data

A.1.1 Central Flight Condition. The central flight condition is defined as:

$$Mach = 0.6 \quad h = 20,000 ft \quad \alpha = 4.3 deg \quad \bar{q} = 245.1 psf$$

The state space representation of the central flight condition is:

$$\begin{aligned} A_{central} = & \begin{bmatrix} -1.6885e-01 & 7.5949e-02 & -9.9523e-01 \\ -2.7692e+01 & -2.3750e+00 & 1.7141e-01 \\ 6.6973e+00 & -6.6493e-02 & -3.9717e-01 \end{bmatrix} \end{aligned}$$

$$\begin{aligned} B_{central} = & \begin{bmatrix} 2.3384e-02 & 3.7619e-03 & 2.5281e-02 \\ -2.2464e+01 & -2.9507e+01 & 6.0951e+00 \\ -2.3973e+00 & -5.2764e-01 & -2.6622e+00 \end{bmatrix} \end{aligned}$$

A.1.2 Design Actuator. The actuator model for the design model has the following state space representation:

$$\begin{aligned} A_{act} = & \begin{bmatrix} -1.9700e+01 & 0 \\ 0 & -1.9700e+01 \end{bmatrix} \end{aligned}$$

$$\begin{aligned} B_{act} = & \begin{bmatrix} 1.9700e+01 & 0 \\ 0 & 1.9700e+01 \end{bmatrix} \end{aligned}$$

$$\begin{aligned} C_{act} = & \begin{bmatrix} 1 & 0 \\ 0 & 1 \end{bmatrix} \end{aligned}$$

$$D_{act} = \begin{bmatrix} 0 & 0 \\ 0 & 0 \end{bmatrix}$$

A.1.3 Ideal Model. The IDEAL model has a state space representation of:

$$A_{ideal} = \begin{bmatrix} -4.5576e+00 & -1.0848e+01 & 0 \\ 9.5469e-01 & 2.9759e-01 & 0 \\ 0 & 0 & -3.0303e+00 \end{bmatrix}$$

$$B_{ideal} = \begin{bmatrix} 3.2825e-01 & 0 \\ 0 & 0 \\ 0 & 9.9926e-02 \end{bmatrix}$$

$$C_{ideal} = \begin{bmatrix} 0 & 2.8719e+01 & 0 \\ 0 & 0 & 3.0325e+01 \end{bmatrix}$$

$$D_{ideal} = \begin{bmatrix} 0 & 0 \\ 0 & 0 \end{bmatrix}$$

A.2 Evaluation Model Data

The only difference between the design model data and the evaluation model data is the state space representation of the actuator. The evaluation actuator is a 3×3 transfer function matrix. Each transfer function has 3 states. This produces a 9th order state space representation.

$$A_{act} =$$

Columns 1 through 6

-1.1200e+02	0	0	0	0	6.0433e+03
0	-1.1200e+02	0	0	6.0433e+03	0
0	0	-1.1200e+02	6.0433e+03	0	0
0	0	-1.0000e+00	0	0	0
0	-1.0000e+00	0	0	0	0
-1.0000e+00	0	0	0	0	0
0	0	0	0	0	1.0000e+00
0	0	0	0	1.0000e+00	0
0	0	0	1.0000e+00	0	0

Columns 7 through 9

8.3232e+04	0	0
0	8.3232e+04	0
0	0	8.3232e+04
0	0	0
0	0	0
0	0	0
0	0	0
0	0	0
0	0	0

Bact =

0	0	-1
0	-1	0
-1	0	0
0	0	0
0	0	0
0	0	0
0	0	0
0	0	0
0	0	0

Cact =

Columns 1 through 6

0	0	0	0	0	0
0	0	0	0	0	0
0	0	0	0	0	0

Columns 7 through 9

0	0	8.3232e+04
0	8.3232e+04	0
8.3232e+04	0	0

Dact =

0	0	0
0	0	0
0	0	0

Appendix B. μ Optimal Controller

The state space representation of the controller from μ -synthesis is as follows:

A =

Columns 1 through 6

4.8582e+00	-1.9456e+00	1.9669e+01	-2.3481e+00	1.2155e-01	-2.3579e+00
1.3065e-01	5.8502e-02	-5.9182e-01	1.0984e-01	-5.6868e-03	1.1031e-01
7.2513e-01	-6.1527e-01	4.8747e+00	-1.2647e+00	6.5470e-02	-1.2700e+00
2.9826e+01	1.0654e+01	-2.9648e+01	1.5477e+01	-4.3683e+00	4.0397e+01
-1.3953e+00	-4.9843e-01	1.3870e+00	-3.6609e-01	1.7185e-01	-1.5616e+00
1.6065e+01	5.7384e+00	-1.5969e+01	6.4442e+00	-1.9202e+00	1.6039e+01
4.5564e-04	8.8126e-05	-3.2144e-04	1.4790e-03	3.4164e-05	-4.5169e-04
-2.6293e-03	-1.3881e-04	1.2036e-03	-8.2575e-04	-2.1286e-05	2.9088e-04
-5.4193e-04	-3.2388e-04	7.6824e-04	-6.3265e-03	-1.4483e-04	1.9093e-03
3.4080e-01	-6.7318e-02	7.5323e-01	-1.0525e-01	5.6446e-03	-1.0912e-01
1.3895e+00	4.9458e-01	-1.3781e+00	9.1974e-01	-1.7666e-01	1.6781e+00
2.2246e-05	4.2446e-06	-1.5592e-05	7.0998e-05	1.6404e-06	-2.1690e-05
3.0334e-06	-6.6155e-07	5.9030e-08	-1.6180e-05	-3.6628e-07	4.8108e-06
-2.4485e-05	4.9885e-06	1.4270e-07	1.2327e-04	2.7894e-06	-3.6631e-05
-1.1214e-04	-3.4754e-06	4.7024e-05	1.5755e-05	2.5500e-07	-2.9061e-06
2.4714e-04	-4.9770e-05	-2.4664e-06	-1.2321e-03	-2.7878e-05	3.6609e-04
1.7033e-02	-3.4335e-03	3.8361e-02	-5.4730e-03	2.8331e-04	-5.4957e-03
6.9518e-02	2.4832e-02	-6.9103e-02	4.1782e-02	-9.0803e-03	8.6674e-02
4.1538e-10	5.1919e-11	-2.4297e-10	7.5573e-10	1.7627e-11	-2.3378e-10

1.5949e-09	4.9213e-10	-1.4487e-09	9.0061e-09	2.0694e-10	-2.7313e-09
4.5286e-04	4.0315e-05	-2.3620e-04	4.8430e-04	1.1470e-05	-1.5286e-04
6.0700e-05	4.0767e-06	-2.9322e-05	3.7247e-05	9.0624e-07	-1.2178e-05
-3.5996e-04	-4.7283e-06	1.3962e-04	1.8459e-04	3.8758e-06	-4.9585e-05
4.1138e-04	1.9500e-04	-4.9359e-04	3.7422e-03	8.5753e-05	-1.1308e-03
3.8636e-04	6.3778e-05	-2.5328e-04	1.0258e-03	2.3762e-05	-3.1444e-04
-2.0635e-03	-4.3920e-04	1.5264e-03	-7.5339e-03	-1.7379e-04	2.2967e-03

Columns 7 through 12

2.0401e+02	-2.3482e+02	-1.6917e+01	-5.9330e+00	-1.9665e-01	1.9801e+02
-9.5444e+00	1.0987e+01	7.9154e-01	2.7756e-01	9.2003e-03	-9.2634e+00
1.0988e+02	-1.2648e+02	-9.1122e+00	-3.1956e+00	-1.0592e-01	1.0665e+02
7.8839e+02	-2.3107e+01	-1.1749e+02	-7.9185e-01	-4.3021e+00	-3.3440e+03
-3.6884e+01	1.0855e+00	5.4968e+00	3.7045e-02	2.0127e-01	1.5644e+02
4.2464e+02	-1.2458e+01	-6.3281e+01	-4.2650e-01	-2.3172e+00	-1.8011e+03
-1.7270e-01	1.2036e-01	-9.9271e-01	-1.3263e-05	-3.2333e-05	-2.4697e-02
-2.7694e+01	-3.2048e+00	1.0840e-01	1.0001e+00	2.1172e-05	1.1791e-02
6.6892e+00	6.2683e-03	-3.8784e-01	1.2352e-05	1.0001e+00	1.0683e-01
9.4209e+00	-1.2778e+01	-9.2986e-01	-1.9973e+01	-9.0915e-03	9.0528e+00
3.6012e+01	-7.5940e-01	-5.4279e+00	-3.6918e-02	-1.9900e+01	-1.5517e+02
3.2796e-01	3.1170e-03	1.9463e-04	-6.4843e-07	-1.5527e-06	-4.5588e+00
6.5230e-05	6.4525e-04	5.9521e-05	-1.0780e-07	3.4319e-07	9.5497e-01
-6.1308e-04	9.5917e-02	7.1263e-03	8.6463e-07	-2.6129e-06	-2.1111e-03
-1.0001e+00	-1.8687e-02	-1.4418e-03	3.5486e-06	-1.9076e-07	-3.6151e-04
6.3416e-03	-9.6155e-01	-7.1444e-02	-8.7182e-06	2.6113e-05	2.1102e-02

4.7551e-01	-5.4733e-01	-3.9432e-02	-1.3828e-02	-4.5835e-04	4.6152e-01
1.8376e+00	-5.3873e-02	-2.7384e-01	-1.8456e-03	-1.0027e-02	-7.7941e+00
-9.3358e-10	6.0678e-08	4.2033e-09	-1.2535e-11	-1.6762e-11	-1.2466e-08
-7.1415e-09	3.7468e-08	-2.4585e-09	-4.3556e-11	-1.9534e-10	-1.5139e-07
-8.2717e-04	1.3017e+00	9.8981e-02	-1.3920e-05	-1.0987e-05	-7.8319e-03
1.8792e-03	-1.3570e-02	-1.0470e-03	-1.8866e-06	-8.7896e-07	-5.8059e-04
-6.5465e-03	3.5157e-01	2.6633e-02	1.1492e-05	-3.4879e-06	-3.4331e-03
3.6092e-02	2.6381e-02	-2.8929e-04	-1.0171e-05	-8.0837e-05	-6.3114e-02
-6.3886e-03	6.6590e-02	4.4963e-03	-1.1417e-05	-2.2519e-05	-1.7071e-02
2.0629e-02	-9.8054e-02	-3.1382e-03	5.9439e-05	1.6437e-04	1.2603e-01

Columns 13 through 18

1.5318e+03	6.9288e+03	1.2580e+02	2.9539e+03	-7.3630e+04	6.5496e+02
-7.1664e+01	-3.2414e+02	-5.8855e+00	-1.3818e+02	3.4447e+03	-3.0639e+01
8.2509e+02	3.7319e+03	6.7773e+01	1.5909e+03	-3.9658e+04	3.5277e+02
-2.5429e+04	9.4241e+02	-2.7921e+03	2.7205e+02	-6.6252e+03	-7.6180e+04
1.1896e+03	-4.4071e+01	1.3062e+02	-1.2710e+01	3.0994e+02	3.5639e+03
-1.3696e+04	5.0768e+02	-1.5038e+03	1.4661e+02	-3.5684e+03	-4.1031e+04
-2.9258e-01	-1.1883e-01	-1.3004e-01	-1.2718e-01	-1.4071e-01	-5.6741e-01
1.1398e+00	-6.5303e+00	1.1066e+00	-6.3991e+00	1.0077e+00	3.1989e-01
4.4606e-01	1.3795e+00	-2.9320e-01	1.3759e+00	5.1411e-02	2.4254e+00
7.0158e+01	3.3406e+02	5.8646e+00	1.5125e+02	1.9630e+06	2.9085e+01
-1.1808e+03	4.1955e+01	-1.3050e+02	1.0754e+01	-3.0959e+02	1.9628e+06
-1.0863e+01	-4.8151e-02	-7.8852e-03	-4.8062e-02	-6.9007e-03	-2.7239e-02
2.9670e-01	2.5662e-02	-2.8962e-03	2.5302e-02	-1.5975e-03	6.1969e-03

-5.7195e-04	-3.3187e+00	1.4408e-02	-2.8451e-01	1.2709e-02	-4.7212e-02
2.8781e+01	-2.2124e-01	3.6647e-02	-2.1633e-01	4.4271e-02	-5.8922e-03
7.2176e-04	3.3212e+01	-1.4924e-01	2.8183e+00	-1.2797e-01	4.7189e-01
3.5705e+00	1.6150e+01	2.9326e-01	6.8848e+00	-3.7662e+02	1.5267e+00
-5.9269e+01	2.1970e+00	-6.5077e+00	6.3453e-01	-1.5442e+01	-3.8256e+02
-2.1879e-07	5.4117e-07	-1.3991e-07	5.2607e-07	1.0000e+00	-2.9018e-07
-1.0816e-06	-1.1843e-06	-5.3820e-08	-1.2053e-06	-3.9535e-07	1.0000e+00
-8.3446e-02	9.0659e-01	-3.1604e-02	8.8649e-01	-1.6488e-01	-1.8620e-01
1.7054e-02	2.8010e-01	2.1900e-02	2.7555e-01	-2.2802e-02	-1.4354e-02
-7.9339e-02	-1.8092e+00	-5.8279e-02	-1.7806e+00	1.4551e-01	-7.0275e-02
-2.9959e-01	-3.6735e-01	1.3556e-01	-3.7235e-01	-6.5943e-02	-1.4347e+00
-1.5744e-01	4.8775e-01	-4.3171e-02	4.7381e-01	-1.2511e-01	-3.9365e-01
1.2921e+00	-9.4748e-01	4.5381e-01	-8.9206e-01	6.1605e-01	2.8901e+00

Columns 19 through 24

-5.2433e+06	3.7347e+05	-6.0329e+01	-1.9653e+00	2.4424e+01	-2.0007e+00
2.4530e+05	-1.7472e+04	2.8224e+00	9.1945e-02	-1.1426e+00	9.3602e-02
-2.8241e+06	2.0116e+05	-3.2494e+01	-1.0586e+00	1.3155e+01	-1.0776e+00
1.1304e+04	-7.9079e+06	-8.2243e+00	-1.0608e+00	2.5068e+00	-4.2853e+01
-5.2933e+02	3.6995e+05	3.8475e-01	4.9630e-02	-1.1727e-01	2.0048e+00
6.0905e+03	-4.2593e+06	-4.4297e+00	-5.7139e-01	1.3502e+00	-2.3081e+01
-6.4170e+00	-5.8521e+01	-1.3615e-04	-1.0350e-05	4.8982e-05	-3.2212e-04
6.9676e+01	2.9144e+01	8.3771e-04	3.0711e-05	-3.3559e-04	2.1145e-04
-1.1710e+01	2.5243e+02	1.3109e-04	2.9500e-05	-2.6892e-05	1.3592e-03
3.9139e+07	1.7054e+04	1.6571e+03	7.7562e+01	-8.9288e+02	-9.2484e-02

3.7084e+02	3.9013e+07	-3.8340e-01	-4.9284e-02	1.1704e-01	1.6578e+03
-3.1842e-01	-2.8088e+00	-6.6553e-06	-5.0075e-07	2.3997e-06	-1.5468e-05
-1.5293e-01	6.5213e-01	-1.0821e-06	2.9051e-08	5.0481e-07	3.4172e-06
1.2034e+00	-4.9706e+00	8.6854e-06	-2.0691e-07	-4.0245e-06	-2.6017e-05
3.1874e+00	-7.9730e-01	3.6071e-05	1.1179e-06	-1.4663e-05	-1.8746e-06
-1.2096e+01	4.9685e+01	-8.7585e-05	2.0428e-06	4.0538e-05	2.6001e-04
-1.3221e+04	8.7049e+02	-1.4061e-01	-4.5808e-03	5.6926e-02	-4.6632e-03
2.6350e+01	-1.9431e+04	-1.9169e-02	-2.4726e-03	5.8428e-03	-9.9880e-02
-8.3593e-06	-2.9632e-05	-1.2812e-10	-7.2050e-12	4.8723e-11	-1.6703e-10
-6.2462e-06	-3.5812e-04	-4.5072e-10	-5.0640e-11	1.4516e-10	-1.9458e-09
-1.0552e+01	-1.8712e+01	-1.8319e+02	-8.9283e+00	1.0056e+02	-1.0952e-04
-1.5315e+00	-1.4007e+00	8.9283e+00	3.8518e-01	-4.3763e+00	-8.7675e-06
1.0799e+01	-7.9235e+00	-1.0056e+02	-4.3763e+00	4.8445e+01	-3.4656e-05
4.3991e+00	-1.4918e+02	-1.0667e-04	-1.8403e-05	2.7695e-05	-1.8319e+02
-6.4079e+00	-4.0486e+01	-1.1699e-04	-7.9169e-06	4.3101e-05	8.9281e+00
2.5522e+01	2.9849e+02	6.1095e-04	5.0018e-05	-2.1609e-04	-1.0056e+02

Columns 25 through 26

-1.6216e-01	1.7577e+00
7.5863e-03	-8.2231e-02
-8.7340e-02	9.4672e-01
-5.2461e-01	1.0042e+01
2.4543e-02	-4.6982e-01
-2.8256e-01	5.4090e+00
-4.1141e-06	7.7086e-05

4.4192e-06	-6.6692e-05
1.6341e-05	-3.1573e-04
-7.4568e-03	8.0885e-02
7.7628e+01	-8.9354e+02
-1.9783e-07	3.7042e-06
3.7842e-08	-7.6345e-07
-2.8709e-07	5.8030e-06
6.0716e-08	-3.4396e-07
2.8674e-06	-5.7978e-05
-3.7795e-04	4.0968e-03
-1.2227e-03	2.3407e-02
-2.2654e-12	4.1208e-11
-2.3998e-11	4.5766e-10
-1.6185e-06	2.8267e-05
-1.4760e-07	2.4316e-06
-1.4100e-07	5.4697e-06
-8.9283e+00	1.0056e+02
3.8517e-01	-4.3762e+00
-4.3762e+00	4.8445e+01

B =

-1.4257e-01	1.2333e+00
1.1523e-03	1.5811e-01
-2.6863e-02	-1.8591e-01

-7.0406e-01	3.4795e-02
-5.4630e-02	6.2558e-01
1.7318e-01	-1.2266e+00
-1.6549e+00	4.9913e+00
4.9712e+00	-1.2893e+02
4.5547e-01	1.4696e+01
5.0652e+00	-1.8160e+02
-7.4014e+01	3.1457e+01
3.9740e+01	1.8907e-01
2.2996e-03	1.8393e-01
-6.2455e-02	1.0497e+01
2.7095e-01	-3.2057e+00
6.2868e-01	1.6125e+01
-1.9351e-06	5.4875e-05
3.9842e-05	-2.4799e-05
-1.0435e-06	9.6819e-06
-4.9462e-06	-2.6679e-07
-4.8732e-01	1.6431e+02
2.9340e-01	-5.3829e-01
-1.0554e+00	3.6041e+01
3.3627e+00	1.5712e+00
-1.4190e+00	1.0195e+01
7.6752e+00	-1.5950e+01

C =

Columns 1 through 6

-5.6064e-04	-2.0614e-04	5.9145e-04	-3.4666e-04	7.4780e-05	-7.1552e-04
1.8289e-04	-1.2869e-05	2.7248e-04	-1.9156e-05	-3.2819e-06	8.3916e-06

Columns 7 through 12

6.5613e-03	-6.9979e-04	-1.4817e-02	6.6210e-06	8.2102e-05	6.4322e-02
-3.4428e-03	-3.0469e-03	1.6353e-03	-1.1476e-04	-9.9604e-06	-1.0231e-03

Columns 13 through 18

4.8916e-01	-8.0742e-03	5.3649e-02	-9.6020e-04	6.1684e+01	-8.1863e+02
-7.2792e-03	1.3404e-01	-1.6108e-03	5.6958e-02	8.1867e+02	6.1566e+01

Columns 19 through 24

1.2272e+03	-1.6272e+04	7.0627e-05	1.7485e-05	-1.2838e-05	8.1775e-04
1.6324e+04	1.2307e+03	-1.1671e-03	-3.9164e-05	4.7132e-04	-1.0002e-04

Columns 25 through 26

9.8127e-06	-1.8978e-04
-3.8607e-06	4.8120e-05

D =

0 0

0 0

Appendix C. State Space Representation of H_2 Problem on the Evaluation Model

The H_2 problem on the evaluation model is shown in Figure C.1.

The state space representation of the P in a $P-K$ format for the H_2 problem on the evaluation model is as follows (the control selector is represented as T_c):

$$A_2 = \begin{bmatrix} A_c & B_c C_{act} & \Gamma C_g & 0 \\ B_{act} T_c K_{eq} & A_{act} & 0 & B_{act} T_c K_{eq} C_s \\ 0 & 0 & A_g & 0 \\ 0 & 0 & 0 & A_s \end{bmatrix} \quad (C.1)$$

$$B_w = \begin{bmatrix} \Gamma D_g k_g & 0 \\ 0 & B_{act} T_c K_{eq} D_s K_s \\ B_g k_g & 0 \\ 0 & B_s K_s \end{bmatrix} \quad (C.2)$$

$$B_{u_2} = \begin{bmatrix} 0 \\ B_{act} T_c T_1 \\ 0 \\ 0 \end{bmatrix} \quad (C.3)$$

$$C_z = \begin{bmatrix} T_2 & 0 & 0 & 0 \\ 0 & 0 & 0 & 0 \end{bmatrix} \quad (C.4)$$

$$C_{y_2} = \begin{bmatrix} -T_2 & 0 & 0 & -T_2 C_s \end{bmatrix} \quad (C.5)$$

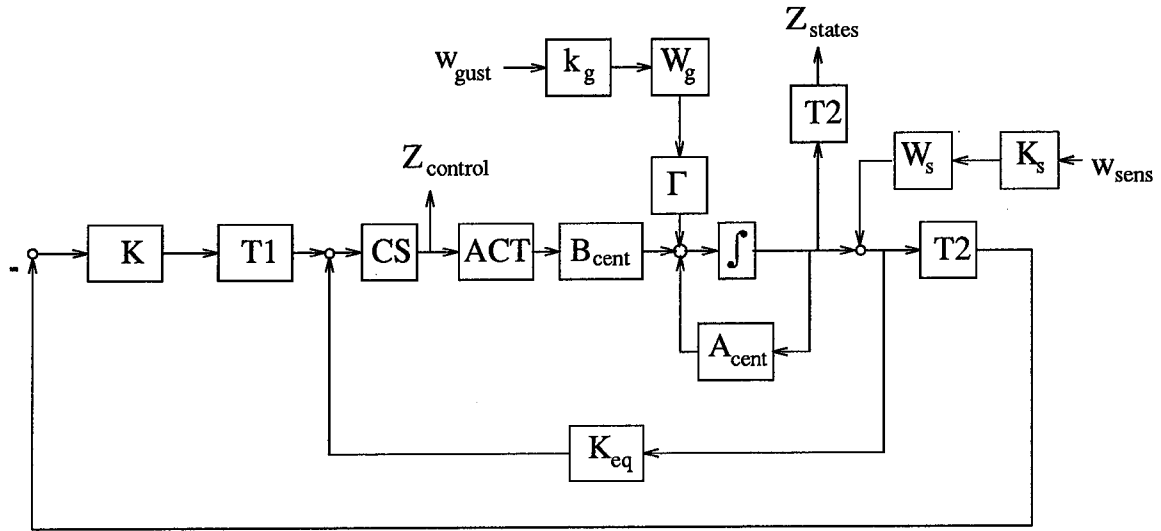


Figure C.1 H_2 Problem on the Evaluation Model

$$D_{zw} = \begin{bmatrix} 0 & 0 \\ 0 & 0 \end{bmatrix} \quad (\text{C.6})$$

$$D_{zu} = \begin{bmatrix} 0 \\ I \end{bmatrix} \quad (\text{C.7})$$

$$D_{yw} = \begin{bmatrix} 0 & -T_2 D_s K_s \end{bmatrix} \quad (\text{C.8})$$

$$D_{yu} = [0] \quad (\text{C.9})$$

Bibliography

- ABSB92. R. J. Adams, J. M. Buffington, A. G. Sparks, and S. S. Banda. *An Introduction to Multivariable Flight Control System Design*. WL-TR-92-3110. USAF, 1992.
- B⁺93. G. J. Balas et al. *μ -Analysis and Synthesis TOOLBOX*. MUSYN Inc., MN, 1993.
- Bai92. J. C. Baird. Strategies for optimal control design of normal acceleration command following on the F-16. Master's thesis, Air Force Institute of Technology, Wright-Patterson AFB, OH 45433, December 1992.
- Dai90. R. L. Dailey. Lecture notes for the workshop on H_∞ and μ methods of robust control. In conjunction with the *American Control Conference*, San Diego, CA., 1990.
- DFT92. J. C. Doyle, B. A. Francis, and A. R. Tannenbaum. *Feedback Control Theory*. Macmillan, New York, 1992.
- LS88. S. H. Lane and R. F. Stengel. Flight control design using non-linear inverse dynamics. *Automatica*, 24:471-483, 1988.
- Mad89. A. N. Madiwale. Reduction of conservatism in mixed H_2/H_∞ design. In *Proceedings of the 28th Conference on Decision and Control*, pages 923-925, Tampa FL, December 1989.
- OS89. A. V. Oppenheim and R. W. Schaffer. *Discrete-Time Signal Processing*. Prentice Hall, 1989.
- PD93. A. Packard and J. Doyle. The complex structured singular value. *Automatica*, 29:71-109, 1993.
- Rid91. D. B. Ridgely. *A Nonconservative Solution to the General Mixed H_2/H_∞ Optimization Problem*. PhD thesis, Massachusetts Institute of Technology, Cambridge, MA, 1991.
- Smi94. L. S. Smith. Improved numerical solution of the general mixed H_2/H_∞ optimization with applications. Master's thesis, AFIT, 1994.
- SZ70. J. Snyders and M. Zakai. On nonnegative solutions of the equation $AD + DA^T = -C^*$. *SIAM Journal of Applied Mathematics*, 18(3):704-714, May 1970.
- Wal94. D. E. Walker. *H_2 Optimal Control with H_∞ , μ , and L_1 Constraints*. PhD thesis, Air Force Institute of Technology, Dayton, OH, 1994.

Vita

Capt Doug Decker was born on 23 June 1963. He graduated from Kansas City Christian High School in 1981 and subsequently attended college at: Cedarville College, Cedarville, OH; Johnson County Community College, Overland Park, KS; and finally finishing his undergraduate education at the University of Kansas, Lawrence, KS in Aerospace Engineering in May 1987. Capt Decker was commissioned in May 1987 and entered Undergraduate Pilot Training in March 1988. After earning his wings in March 1989, he was assigned as an Instructor Pilot at Reese AFB, TX flying the T-37. After a medical grounding, he was assigned as a Satellite Operations/Engineering Officer at Falcon AFB, CO "flying" GPS satellites. Capt Decker entered the Graduate School of Engineering at the Air Force Institute of Technology, WPAFB, OH in May of 1993. Upon completion of his studies, he will be assigned to the 46th Guidance Test Squadron, Holloman AFB, NM working on GPS/INS integration.

Permanent address: POB 116662
Dallas, Texas 75287